FACULTY OF INFORMATION TECHNOLOGY AND ELECTRICAL ENGINEERING
DEGREE PROGRAMME IN ELECTRONICS AND COMMUNICATIONS ENGINEERING

MASTER'S THESIS

Designing Antennas and RF components for Upper Millimeter Frequencies using Advanced Substrate Technology

Author	Muhammad Ibrahim
Supervisor	Dr. Marko E. Leinonen
Second Examiner	Dr. Kimmo Rasilainen

June 2023

Ibrahim M. (2023) Designing Antennas and RF components at D – Band using Advanced Substrate Technology. Faculty of Information Technology and Electrical Engineering, Degree Programme in Electronics and Communications Engineering. Master's Thesis, 79 p.

ABSTRACT

When shifting towards high frequency range, integration in the RF-front end becomes crucial. The ongoing planning of 6G communications systems causes a need to explore the possibilities beyond current 5G systems. To address the compactness and smaller sizes of the RF circuit components, the Integrated Passive Devices (IPD) multilayer technology provides us one solution to this problem. There are options already being tested in terms of implementing on-chip components, especially Antenna-in-Package (AiP) designs with a variety of different substrates. Among these technologies, Low Temperature Co-Fired Ceramic (LTCC) can be seen as a choice offering the freedom of multiple metal layers. IPD can be used for providing AiP solutions, as well as passive components such as baluns, filters, and power dividers.

The main target of this thesis is to explore the possibilities and limitations for high-frequency designs offered by IPD technology developed by (VTT) Technical Research Centre of Finland. The technology has already been tested at 20 GHz, but the focus was to reach the D-band (110–170 GHz) frequency range and subsequently up to even G-band (220–330 GHz). The technology utilizes 3 metal layers and a high resistivity silicon substrate (a lossy material). Starting off with simple transmission line structures (microstrip lines, strip lines and coplanar waveguides), the designs up to 330 GHz, provided information on the possibilities offered by this technology. After that, different AiP options were simulated with frequencies ranging from D- band to G- band. In addition to single elements, also antenna arrays were studied. Additionally, bandpass filters were designed. The dielectric thickness and the width and thickness of 3 the metal layers play a pivotal role in defining the performance of all the RF components designed using this technology. Furthermore, the size and pitch of the RF probe pads used to excite the structures show an impact on the overall behavior of the transmission lines.

Key words: Antenna arrays, Antenna in Package (AiP), D-band, G-band, Integrated Passive Devices (IPD), Low temperature co-fired ceramic (LTCC), RF Front end, 5G band

Ibrahim M. (2023) Antennien ja RF-komponenttien suunnittelu D – kaistalle käyttäen edistynyttä substraattiteknologiaa. Tieto- ja sähkötekniikan tiedekunta, elektroniikan ja tietoliikennetekniikan tutkinto-ohjelma. Diplomityö, 79 p.

TIIVISTELMÄ

Siirryttäessä korkeammille taajuuskaistoille RF-etupään integrointi on entistä tärkeämpää. Käynnissä oleva kuudennen sukupolven (6G) viestintäjärjestelmien suunnittelu edellyttää nykyisiä 5G-järjestelmiä edistyksellisempien teknologisten mahdollisuuksien tarkastelua. Entistä pienempien RF-piirikomponenttien toteuttaminen vaatii uusia teknisiä ratkaisuja, ja yksi mahdollisuus komponenttien pienentämiseen on käyttää integroituihin passiivirakenteisiin (Integrated Passive Devices, IPD) pohjautuvaa monikerrosteknologiaa. Eri vaihtoehtoja on jo testattu sirulle sijoitettavien komponenttien toteuttamiseen eri substraattimateriaaleilla, etenkin paketoitujen antenniratkaisujen (Antenna-in-Package, AiP) suunnittelemiseksi. Eräs vaihtoehto IPD:lle on matalan lämpötilan yhteissintrattava keraamiteknologia (Low Temperature Co-Fired Ceramic, LTCC), joka mahdollistaa useamman metallikerroksen hyödyntämisen suunniteltaessa AiP-rakenteita sekä muita passiivikomponentteja (kuten symmetrointimuuntajia, suodattimia sekä tehonjakajia).

Tämän opinnäytetyön päätavoitteena on tarkastella Valtion teknillisen tutkimuskeskuksen (VTT:n) kehittämän IPD-teknologian mahdollisuuksia ja rajoitteita korkean taajuuden rakenteiden suunnitteluun. IPD-teknologiaa on tähän mennessä testattu 20 GHz:n taajuudelle asti, mutta tässä työssä tarkoituksena on tutkia teknologiaa 110–170 GHz:n taajuuksille (D-kaista) sekä myöhemmin aina 220–330 GHz:iin saakka (G-kaista). Teknologia hyödyntää kolmea metallikerrosta sekä häviöllistä korkean ominaisvastuksen piisubstraattia. Yksinkertaisten siirtojohtorakenteiden (mikroliuskajohto, liuskajohto, koplanaarijohto) suunnittelu aina 330 GHz:n taajuudelle asti antoi tietoa teknologian mahdollisuuksista, minkä jälkeen erilaisia AiP-rakenteita simuloitiin D- ja G-kaistoilla. Yksittäisten antennielementtien ohella tarkasteltiin antenniryhmiä. Työssä suunniteltiin myös kaistanpäästösuodattimia. Käytettävissä olevien metalli- ja substraattikerrosten paksuudella sekä niiden mahdollistamilla liuskanleveyksillä on keskeinen rooli IPD-teknologialla suunniteltujen komponenttien suorituskyvyn kannalta. Lisäksi RF-mittapäiden kontaktikohtien koko ja välimatka vaikuttavat siirtojohtojen ominaisuuksiin.

Avainsanat: Antenniryhmä, D-kaista, G-kaista, integroidut passiivirakenteet (IPD), matalan lämpötilan yhteissintrattavat keraamit (LTCC), paketoidut antenniratkaisut (AiP), RF-etupää, 5G-kaista

TABLE OF CONTENTS

ABSTRACT
TIIVISTELMÄ
TABLE OF CONTENTS
FOREWORD
LIST OF ABBREVIATIONS AND SYMBOLS
INTRODUCTION 9
1........ 9
2 THEORY........ 11
2.1 Transmission Lines 11
2.1.1 Microstrip 12
2.1.2 Strip Line 13
2.1.3 CPW – Coplanar Waveguide........ 14
2.2 Antennas........ 14
2.3 RF Filters........ 16
2.4 S - Scattering Parameters 18
3 Transmission Lines Implementation 20
3.1 Microstrip Line 20
3.1.1 Design Calculations........ 20
3.1.2 Simulation with Ideal Ports 22
3.2 Strip line........ 25
3.2.1 Design Calculations........ 25
3.2.2 Simulation with Ideal Ports 26
3.3 Coplanar Waveguide........ 28
3.3.1 Design Calculations........ 28
3.3.2 Simulation with Ideal Ports 29
3.4 Probe Pads........ 32
3.4.1 Large Size Probe Pads 32
3.4.2 Smaller Probe Pads with 100 µm pitch 33
3.4.3 CST Simulations........ 33
3.5 Transmission Lines Excitation with Probe Pads........ 35
3.5.1 Microstrip 35
3.5.2 Coplanar Waveguide with Ground........ 39
3.5.3 Coplanar Waveguide without Ground........ 41
3.5.4 Via Transition from Microstrip to Coplanar Waveguide (Ungrounded)... 43
3.5.5 Transmission lines performance comparisons........ 45
3.6 DRC – Design Rule Check 46
3.6.1 Microstrip Structure........ 47
3.6.2 CPW with Ground Structure 48
3.6.3 Ungrounded CPW Structure........ 49

3.6.4 Via Transition Structure 49
4 Antennas 51
4.1 Single Patch Antennas 51
4.1.1 D-Band Antenna 51
4.1.2 G-Band Antennas 55
4.1.3 Antennas comparisons 62
4.2 Multiple Elements Antenna Array 63
4.2.1 D-Band Antenna Array 63
4.2.2 G-Band Antenna Array 65
4.2.3 DRC – Design Rule Check (Antenna Structures) 66
4.2.4 Antenna arrays observations 68
5 RF Filters 69
5.1 Edge-Coupled Bandpass Filters 69
5.1.1 DRC runs for filters 72
5.1.2 Observations in filters simulated 73
6 SUMMARY 75
7 REFERENCES 76

FOREWORD

This work has been done at CWC-RT (center for wireless communications – radio technologies), University of Oulu, as thesis research project to qualify for the degree of masters in Wireless communications engineering – RF.

I would like to express my gratitude to Prof. Aarno Pärssinen, for providing me an opportunity to work on this interesting topic, with his guidance throughout the process made this work useful. I am extremely grateful to my supervisors: Dr. Marko Leinonen and Dr. Kimmo Rasilainen for their continuous support and putting me on a right track. This research wouldn't have been executed successfully without their help.

I am thankful to all the staff members and my co-workers at CWC-RT for their contribution in the completion of my thesis. Specially, I want to mention Jiangcheng Chen and Dr. Janne Aikio as I found them really helpful.

As a final word, I would like to dedicate this work and all of my academic journey till now to my parents and teachers.

Oulu, June 09, 2023

Muhammad Ibrahim

LIST OF ABBREVIATIONS, UNITS AND SYMBOLS

β	propagation constant
Δ	fractional bandwidth
ΔL	effective length
ε_r	relative dielectric constant
ε_{reff}	effective dielectric constant
$\tan \delta$	dielectric loss tangent
v_p	phase velocity
µm	micrometer
λ	wavelength
a	incident wave
a_z	acceleration in z-direction
b	reflected wave
c	speed of light [m/s]
C	capacitance [F]
D	largest dimension of the antenna [m]
D	directivity [dBi]
E	electric field [V/m]
f_r	resonance frequency [Hz]
G	gain [dBi]
g	gap
g_n	low-pass prototype values
H	magnetic field [A/m]
h	height [m]
I_z	current in z-direction [A]
J_n	admittance inverter constant
k	extension co-efficient
k_o	wave number
l	length of the conductor [m]
L	inductance [H]
L	length
mm	millimeter
m^2	square meter
P_{in}	incident power [W]
P_{rad}	radiated power [W]
q	electric charge [columb]
Q	quality factor
R_o	reference impedance [Ω]
S	scattering
S_{11}	input reflection coefficient
S_{12}	output reflection coefficient
S_{21}	forward transmission coefficient

S_{22}	reverse transmission coefficient
U	radiation intensity
U_o	radiation intensity of isotropic source
W	power
W	width
w	width
Z_{ant}	input impedance of the antenna [Ω]
Z_0	characteristic impedance of the transmission line [Ω]
Z_{0e}	even mode impedance [Ω]
Z_{0o}	odd mode impedance [Ω]

AiP	antenna in package
ADS	advanced design system
BAW	bulk acoustic wave
BCB	Benzocyclobutene
CST	computer simulation technology
CPW	coplanar waveguide
CWC-RT	center for wireless communications – radio technologies
DRC	design rule check
EM	electromagnetic
FBW	fractional bandwidth
FNBW	first null beamwidth
GDSii	geometric data stream
GSG	ground-signal-ground
HPBW	half power beamwidth
IC	integrated circuit
IF	intermediate frequency
IPD	integrated passive devices
ISM	industrial, scientific and medical
LNA	low noise amplifier
LTCC	low temperature co-fired ceramics substrates
LTE	long-term evolution
MMIC	monolithic microwave integrated circuit
PA	power amplifier
PCB	printed circuit board
RF	radio frequency
SAW	surface acoustic wave
SiP	system in package
TEM	transverse electromagnetic mode
VTT	Technical Research Centre of Finland

1 INTRODUCTION

With the growing demand of high data rates, low latency, broader bandwidth with good energy efficiency, there comes a need for ongoing improvement for telecommunication devices – especially wireless systems to be more efficient. 5G demands variety in scalability, power consumption and other constraints in different scenarios: like the need for a base station to meet the specific needs of user equipment. The RF – radio frequency front end comes up with so many possibilities to be explored. The main problem to be catered is to have a high level of compactness to avoid losses, and more integration. The integrated passive devices (IPD) technology is a good approach to address these desired needs. There are different options available by different vendors to implement IPD technology varying in aspect of substrates for example. A comparison – as an example shown in the Figure 1 is portraying that how IPD technology is impactful when it comes to area reduction and less power losses as compared to discrete elements – an area reduction of approximately 70.8 mm^2 is possible as result of switching from discretes to IPD [1]:

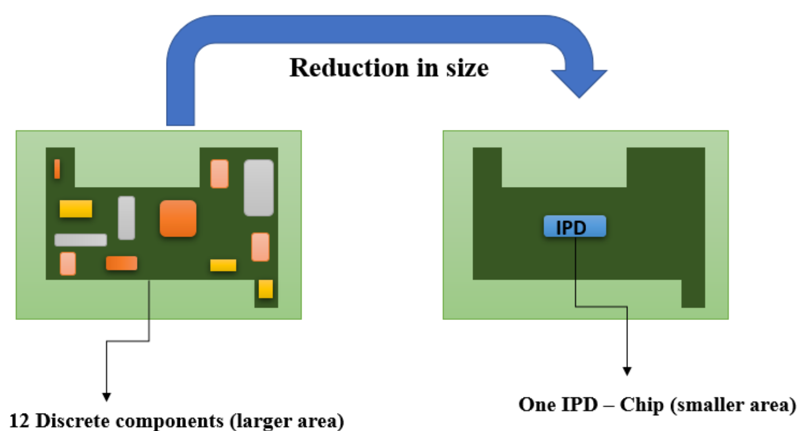

Figure 1. Compactness of IPD vs discrete passive devices

With this IPD technology, there comes the option to have antennas in package (AiP), because at high frequency antenna size becomes – comparable to wavelength, so fitting that into package substrate becomes more practical. Also, with AiP the interconnections between RFIC - radio-frequency integrated circuit and AiP become smaller resulting in low losses and high efficiency [1]. The main aim of this thesis is to test the ongoing, under developing technology by VTT (Technical Research Centre of Finland). Available option other than IPD is low-temperature cofired ceramic (LTCC), which has been tested for 60 GHz, the major positive aspects of this technology can be regarded in terms of increased number of metal layers and lower dielectric tangent loss (tan δ) but signal routing density within different layers becomes low and also there comes some size scalability issues with this technology [2]. Comparison between IPD, LTCC, and discrete elements in terms of different aspects is represented in Table 1 [1].

Table 1. IPD vs other technologies

Specifications	IPD	LTCC	Discrete elements
Integration	Very good	Good	Bad
Flexibility	Very good	Low	Very Good
Thickness	Very good	Good	Medium
Simplification	Very good	Good	Low
Space coverage	Good	Medium	Bad
Performance (in terms of losses)	Very good	Good	Low
Standardity	Medium	Very good	Very good

The essence of this research work lies on utilization of IPD technology (that is being developed further) by VTT. This has been carried out by starting off with basic structures: Microstrip, strip line, coplanar waveguides etc. To route the signals or excite the antenna, the transmission lines play a vital role. The first structure to be tested was microstrip line aiming to be 50-ohm line, and then the other transmission lines come. The transmission lines were tested by using simulations with CST software at mm-Wave frequencies. Exciting the structures on chip need some based on µm level to probe it, so ground-signal-ground (GSG) configuration for probe pads was used. The lossy, with larger area standard probe pads were used initially and then minimum allowed area was used.

Other implementation of this technology was to test it with the AiP solutions, so designs ranging from single patch antennas to arrays were tested. The initial frequency band was D-band but later, the research was extended till G-band. Other than that, filters were being implemented.

2 THEORY

2.1 Transmission Lines

Transferring power from generation point to where it is needed is a fundamental feature for all electrical devices. The main concern about the power and signal transfer is that the electrical signal remains at minimum level of power loss and signal integrity remains intact. The term "transmission line" is quite diverse, but in RF engineering the only band is to be catered is the RF band itself: 30 – 300 GHz. Initially, the waveguides and coaxial cables remain popular type of transmission of RF signals depending upon the application. The waveguide serves its purpose of high-power handling and low losses [3] whereas, a coaxial cable is limited to the ease of its usage in different scenarios. The thing which is common between all the transmission lines used mostly is the use of two conductors insulated by some dielectric.

Planar type of transmission lines are widely used in RF and microwave devices nowadays, but they did not see any major developments until the 1950s [3]. The strip line (being regarded as planar coaxial cable) remained more relevant than microstrip lines until some thinner substrates were being used [3]. Required characteristics of a planar transmission line are the propagation constant, attenuation constant and characteristic impedance of the line. The other factors which are kept in mind while dealing with planar type of transmission lines are the propagation modes they offer, transverse electromagnetic (TEM) mode being offered only in the transmission lines involving two conductors, which waveguides cannot provide.

Wavelength dependency is what to be kept in mind while defining a transmission line for a specific frequency or range of frequencies. The main purpose of an RF transmission line is to carry electromagnetic (EM) field and its effects. The EM energy is being transferred through circuit modelling of the transmission line, the main three components for defining the electromagnetic energy is through an inductance (defined by the metallic parts itself and for magnetic energy storage), the other thing is done through capacitance (defined by the type of insulator being used in between conductors and for storing electrical energy), the third and main component is the resistance part, the inherent part of the electrical devices to represent losses [4]. The resistance, inductance, and capacitance (RLC) equivalent circuit of a planar transmission line for example is shown in the Figure 2 below [5], where L, R, C, and G are inductance, resistance, capacitance and conductance per unit length respectively:

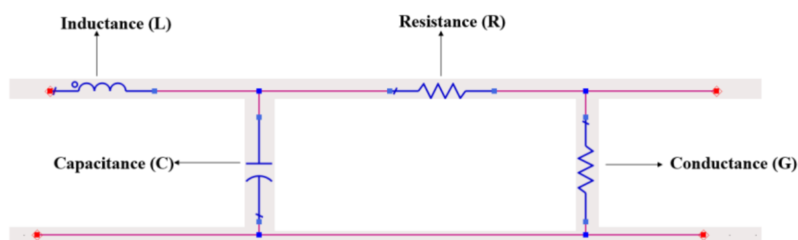

Figure 2. Equivalent circuit of planar transmission line

The starting point to check a technology and its feasibility over a certain frequency range is to check with the transmission lines because they are the power routing elements which can be

used to excite or route the electrical signals to any of the more complex or useful RF elements, for example an antenna or an RF filter.

2.1.1 Microstrip

Easy to fabricate, compact and with the flexibility to fit in many planar structures, microstrip comes up to be a famous choice. The structure is defined by two metallic conductors unlike a strip line which involves three metals, separated by a dielectric defined by dielectric coefficient and loss tangent. Determining parameters for a microstrip is the width (W), thickness (t) of the top metal which is exposed to air as another medium apart from the main insulator. The other factor is the thickness of the insulator which can be defined as (d) and relative permittivity ($\mathcal{E}_r$). The other main deciding factor is the characteristic impedance (Z_o) of the line which is defined by the parameters W, d, t and $\mathcal{E}_r$.

The EM field becomes complex in defining of a microstrip because of the absence of the top metal like in a strip line which provides shielding above and below of the central conductor. Thus the mode in this type of line is called the quasi-TEM mode, which is not a TEM mode, this type of behavior arrives because of the air presence [3]. Due to this fact the phase velocity which is in the air is different from phase velocity in the dielectric medium [3]. So, the phase velocity (v_p) and propagation constant (β) can be defined as, where (k_o) is wave number:

$$v_p = \frac{c}{\sqrt{\mathcal{E}e}} \tag{1}$$

$$\beta = k_o\sqrt{\mathcal{E}e} \tag{2}$$

Whereas $\mathcal{E}_e$ (effective dielectric constant) is between 1 and $\mathcal{E}_r$ because of the interaction between air and dielectric material defined by $\mathcal{E}_r$ [3].

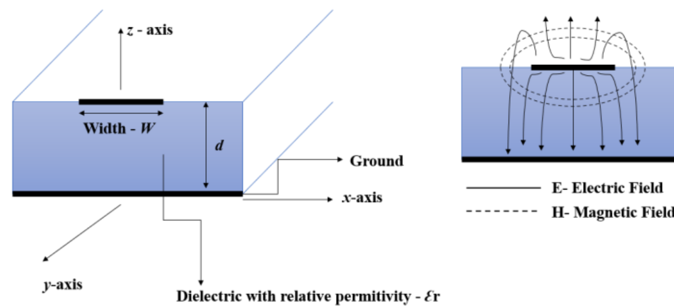

Figure 3. Electric (E) and magnetic (H) field distribution in microstrip

The above shown Figure 3 shows the basic structure of the microstrip and how the field lines (electric and magnetic) appear around the central signal line and the ground metal. There are some variations and possibilities of how a microstrip must be implemented with different applications: a microstrip can be a buried in a dielectric or it can be sandwiched in between two different dielectrics defined by $\mathcal{E}_{r1}$ and $\mathcal{E}_{r2}$, as seen in Figure 4.

Figure 4. Embedded microstrip line

2.1.2 Strip Line

A strip line, shown in Figure 5 can be comparable to a coaxial line with the structural difference that it is flattened and planar. The central conductor is shielded by upper and lower conductor through a dielectric medium. The three main design parameters are width (*W*) of the central conductor, the separation between upper and lower conductor (*b*) and the relative dielectric constant ($\mathcal{E}_r$) from which the characteristic impedance Z_o of the strip line is dependent and defined. The central medium can be replaced by air if low losses are required [3].

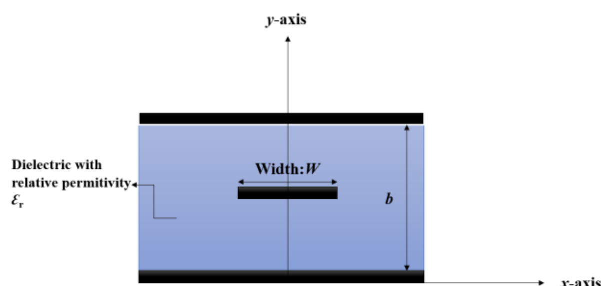

Figure 5. A strip line of Width (W)

There are certain other possibilities as well while defining a strip line which can be in homogeneously filled with different dielectrics having $\mathcal{E}_{r1}$ and $\mathcal{E}_{r2}$. The main mode which is present in strip line structure is the TEM mode; there is a possibility of higher order modes as well in a strip line [3]. The electric and magnetic field distribution in a strip line is shown in Figure 6.

E- Electric Field
H- Magnetic Field

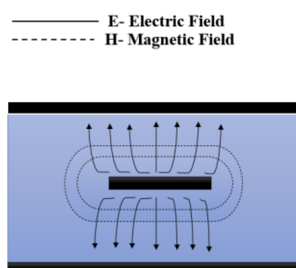

Figure 6. Electric and magnetic fields distribution (Strip Line)

Strip line being TEM mode supportive, its phase velocity (v_p) and propagation constant (β) can be defined by the equations below:

$$v_p = \frac{c}{\sqrt{\varepsilon r}} \tag{3}$$

$$\beta = k_o\sqrt{\varepsilon r} \tag{4}$$

2.1.3 CPW – Coplanar Waveguide

Unlike the former two lines: microstrip and strip line, coplanar waveguide (CPW) is an alternative invented by Cheng. P Wen in 1969 [5]. A coplanar waveguide places ground and the signal line on the same plane as a slot line having a signal in between [3]. The elimination of via holes for connecting the signal line to ground and due to grounds on both sides of signal line there comes a reduction in cross talks as well [6]. The field is majorly concentrated within the dielectric unlike other two lines it is not as dispersive as other lines. This line supports quasi-TEM modes but at higher frequencies it starts acting like TE mode supportive [5]. Figure 7 shows the basic structure (without having a ground backing) and EM field distribution of CPW.

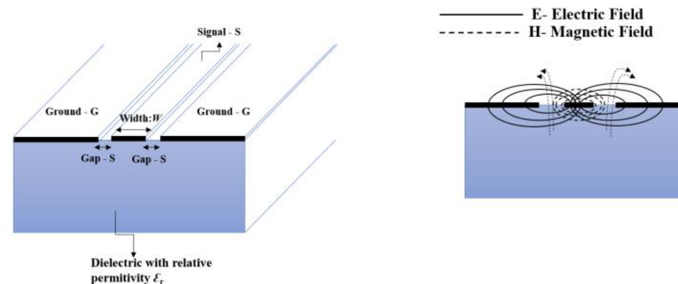

Figure 7. GSG CPW & E, H fields distribution in CPW

There can be addition of a ground (a metallic structure) below the upper plane, which is regarded as CPW with ground. This sort of structure acts like a microstrip but with better grounding structure, it is less dispersive in nature and provides increased isolation [5]. The magnetic field tends to be elliptically polarized due to the discontinuity in displacement current density, which arises because of the gap between signal line and adjacent grounds [7]. The characteristic impedance Z_o for CPW can be given defined and dependent on these factors: Width (W), gap (S), relative permittivity ε_r, and height (h) of substrate.

2.2 Antennas

Not all the RF power / signal propagation needs to be wired, there must a solution to propagate EM energy wirelessly. The antennas are way to send or receive the EM power or waves wirelessly. The basic mechanism to have a detached EM wave

transmission or reception is to have an oscillating source producing accelerated or decelerated currents, considering a thin (zero radius) wire, the current I_z in the wire can be given by the equation from [8]:

$$I_z = ql.v_z \quad (5)$$

where ql is the charge per unit length and v_z is the velocity of the charges. Now when the I_z is changing with time in a wire of length l, we can get the accelerated charges by differentiation of the above equation 5, which provides the basic antenna propagation requirement:

$$l\frac{d(Iz)}{d(t)} = l.ql.\frac{d(v_z)}{dt} = l.ql.a_z \quad (6)$$

The fundamental antenna structure consists of three basic elements: An oscillating generator, a transmission line to deliver the power to the radiating element, and a radiating element. The pivotal factor which determines the antennas characteristics, and its performance is the matching between load (radiating part) and generator: if not matched properly, the energy will not reach to the antenna (load) [8]. The E-field radiation mechanism in an antenna is shown in Figure 8.

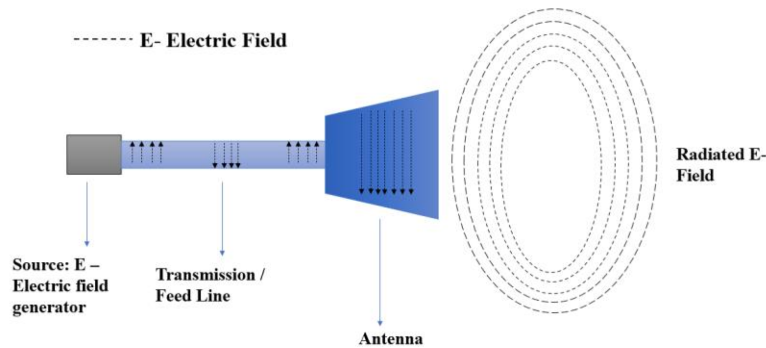

Figure 8. E – field leaving antenna to propagate

Antennas can be found in various shapes depending on the application: helical, wire, Yagi-Uda, horn or even planar. Antennas can be classified or distinguished on basis of various properties but out of these, usually the main important factors are gain, directivity, efficiency, bandwidth and beamwidth. The directivity firstly can be defined as the ratio of the radiation intensity specified in a certain direction to the radiation intensity radiated over all directions [8] or the radiation intensity in a certain directional antenna relative to an isotropic antenna, the equation 7 is given as:

$$D = \frac{U}{Uo} = \frac{4\pi.U_{max}}{P_{rad}} \quad (7)$$

U is radiation intensity (W/unit solid angle), U_o is radiation intensity of isotropic source (W/unit solid angle), and P_{rad} represents total radiated power (W). Related to directivity, the term gain is to be used to define directivity combined with efficiency. The definition of gain is the ratio of the intensity, in a given direction, to the radiation intensity that would be obtained if the power accepted by the antenna were radiated isotropically [8]. Usually, the gain's direction is defined in terms of the maximum radiation. The gain can be represented mathematically as equation 8:

$$G = 4\pi . \frac{U(\theta,\varphi)}{P_{in}} \quad (8)$$

Excluding constants, the numerator in the above equation is radiation intensity and P_{in} is the input power to an antenna.

Beamwidth (HPBW – half power beamwidth and FNBW – first null beamwidth) shown in Figure 9 of an antenna is another important term which is crucial in defining any type of antenna specially where a directive application is needed and defines the resolution capabilities of an antenna. It is defined in terms of angular perspective, the separation between two similar points on the opposite sides of maximum radiation pattern lobe (relative to side lobes) [8]. Mostly, the HPBW is a matter of concern which is defined by IEEE: In a plane containing the direction of the maximum of a beam, the angle between the two directions in which the radiation intensity is one-half value of the beam [8].

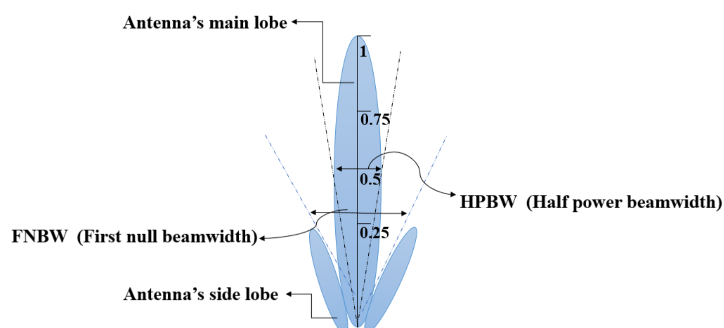

Figure 9. 2D Representation of radiation pattern defining HPBW and FNBW

2.3 RF Filters

RF range is roughly from 30 kHz to 300 GHz, so defining RF filters is quite a broad term. There is hardly any telecommunication circuit or application where filters are not used. The variety can be based on the frequency band and application (can be a lowpass, high pass, bandpass or band stop). A filter can be a lumped element filter usually at lower frequencies, but distributed elements become relevant when shifting towards higher frequencies. A simplified representation of a satellite

downlink [10] showing microwave band pass filters (BPF) as a part of the RF front end can be seen in Figure 10:

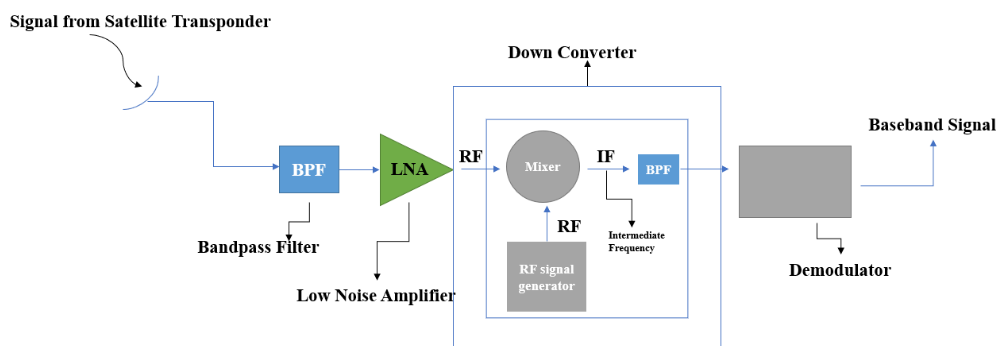

Figure 10. Block diagram of a satellite downlink system

The likely 5G band varies from roughly from 3.5 GHz to 71 GHz [9]. With this increased frequency range and bandwidths, the number of filters also demand an increase in a mobile device for example. The Long-Term Evolution (LTE) technology allows more than 30 bands in a device, so going beyond the LTE will accumulate bands exceeding 30 bands [9]. The surface acoustic wave (SAW) and bulk acoustic wave (BAW) filters are already in use, but their performance can be limited going above 6 GHz [9]. Testing the ability of a filter can be realized in terms of quality factor Q, the low insertion loss and high return loss. The technologies like LTCC and IPD open the horizons to check up for filter applications. For IPD technology, the starting point can be a planar type of filter for example an edge coupled filter using microstrip lines. Based on bandwidth, these types of filters are quite limited to 20 % [3]. The theory is based on even and odd mode excitation of single quarter wave line [3], but when extended to higher number of lines based on the order of the filter, it can be implemented as bandpass filter. Figure 11 illustrates an edge-coupled filter.

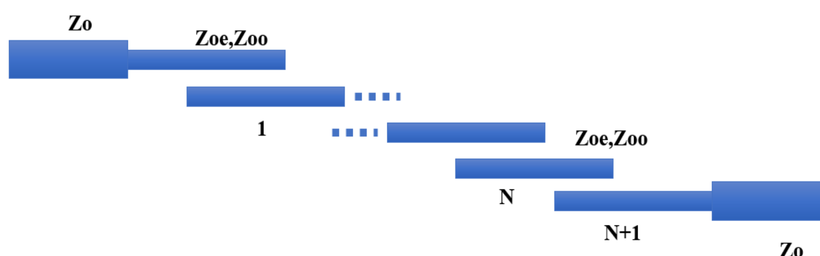

Figure 11. Edge coupling using even and odd mode impedances

Each line of the above-mentioned structure is based on even (Z_{oe}) and odd (Z_{oo}) mode impedances, which in return determines the physical length of each section based on phase shift.

2.4 S - Scattering Parameters

S parameters get their name from scattering of either voltage, current or power while transferring electrical signal from one side of a device to another. The electrical signal can be seen as a wave while dealing in higher frequencies, the behavior of a device under test or a two-port network device becomes highly dependent on varying frequency with smaller wavelengths [12].

Two port device under test is excited by a voltage source V_{s1} having a reference impedance R_o which is typically taken as 50 ohm standard. The voltage V_1 at the input of the device is result of the transmitted and reflected voltage combined [11]. Energy transfer from input to output point (can be seen as port 1) to be realized in terms of a_1 which is the energy transferred in case when input impedance of the device is exactly in accordance with reference impedance. If this does not happen, then the parameter b_1 shows how much energy is being reflected by mismatch [13]. Similarly, these definitions of a and b can be applied from output side taken as port 2 as shown in Figure 12, the generic form for a and b can be defined by the equations:

$$a_1 = \frac{V_{1i}}{\sqrt{R_o}} = \sqrt{R_o}.I_{1i} \quad (9)$$

$$a_2 = \frac{V_{2i}}{\sqrt{R_o}} = \sqrt{R_o}.I_{2i} \quad (10)$$

$$b_1 = \frac{V_{1r}}{\sqrt{R_o}} = \sqrt{R_o}.I_{1r} \quad (11)$$

$$b_2 = \frac{V_{2r}}{\sqrt{R_o}} = \sqrt{R_o}.I_{2r} \quad (12)$$

The above equations (9)-(12) are then usually interpreted or related to each other in terms of a matrix (which is more meaningful way) for a two-port network for example, defining the S parameters:

$$\begin{bmatrix} b_1 \\ b_2 \end{bmatrix} = \begin{bmatrix} S_{11} & S_{12} \\ S_{21} & S_{22} \end{bmatrix} . \begin{bmatrix} a_1 \\ a_2 \end{bmatrix}$$

From the above matrix, S parameters for a two-port network can be defined with a condition having a_2=0 (which means no signal excitation at the port 2 side or output side) [13], then we can write:

$$S_{11} = \frac{b_1}{a_1} \quad (13)$$

$$S_{21} = \frac{b_2}{a_1} \quad (14)$$

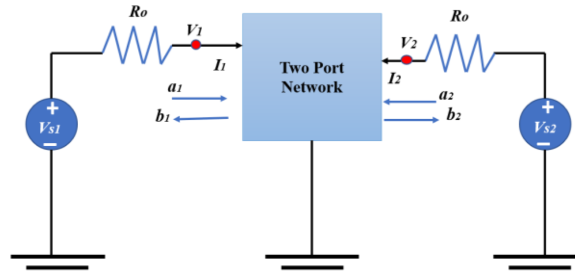

Figure 12. Two port network device

The S-parameters are not limited to only two port networks but can be extended to any number of ports as an N-port network. Scattering parameters not only define losses or gain but also provides information about phase changes in a signal. These parameters are highly dependent on frequency, the reference impedance, and the device itself. In RF engineering, S_{11} or S_{21} plays always an important to check the performance of any RF device.

3 Transmission Lines Implementation

3.1 Microstrip Line

Starting off to implement a microstrip structure in the IPD with not so many choices but three metal layers. The allowed metal layers are metal 1, metal 2 and metal 3, of which metal 3 is the topmost and thickest one. From accessibility point of view, top metal layer 3 would be the preferred layer to implement a microstrip. The definition of ground plane can vary between metal 1 or metal 2 having a separation by oxidation layer. The following Figure 13 shows an example of 3 metals layered IPD stack with dielectric layers:

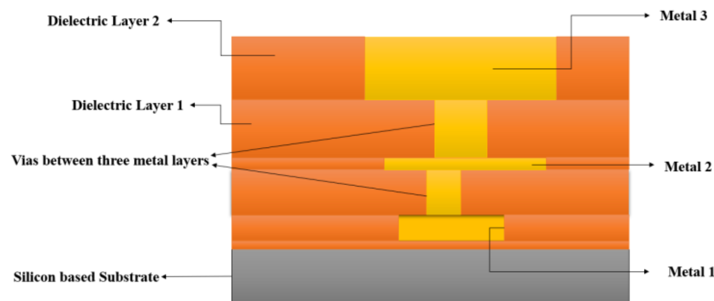

Figure 13. IPD Stack

We can see how much we have freedom to design any passive element in this defined set of rules, whether we want to have capacitive or inductive effect. The Figure 13 shows an example of planar cutting without via 3 which can used to connect the top metal either with solder bumps or probe pads. The microstrip structure initially was simulated without any probe pads or bumps.

3.1.1 Design Calculations

While designing the line, the three main factors defining the microstrip are: Width (*W*) of microstrip, dielectric constant of substrate / dielectric material $\mathcal{E}_r$ which then contributes to effective dielectric constant $\mathcal{E}_e$, and the thickness of dielectric *d*. The basic design equations taken from [4] based on the characteristic impedance of the line Z_o we want are:

$$\frac{W}{d} = 8e^{A}/e^{2A-2} \quad (15)$$

for *W/d* <2

$$\frac{W}{d} = 2/\pi[B - 1 - \ln(2B - 1) + \varepsilon_r\text{-}1/2\,\varepsilon_r\{\ln(B\text{-}1) + 0.39\text{-}0.61/\varepsilon_r\}] \quad (16)$$

for *W/d* >2

Where A and B can be defined as:

$$A = \frac{Z_o}{60}.\sqrt{\varepsilon_r + 1/2} + \varepsilon_r - 1/\varepsilon_r + 1(0.23 + 0.11/\ \varepsilon_r) \quad (17)$$

$$B = 377\pi/2Z_o.\sqrt{\varepsilon_r} \quad (18)$$

The equations are based on assumptions that microstrip line has zero thickness and is not immersed in dielectric. But the IPD technology by the definition of its stack, comes up with a situation in which not only the top metal 3 has nonzero thickness but also submerged partially in the dielectric can be seen from Figure 13. The microstrip structures possibilities are many but the defined case is unique combining two scenarios, where there no two dielectrics involved but a partial air / dielectric interaction is involved having top microstrip exposed to air but buried from sideways. An embedded microstrip with different height distribution of dielectric can be visualised in the following Figure 14.

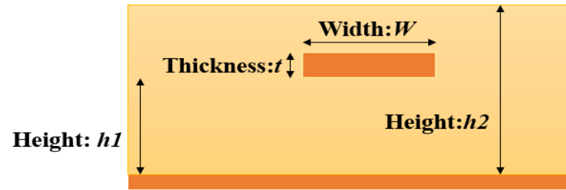

Figure 14. Uneven dielectric layer around Microstrip

With the defined case, first the *W/d* ratio was found for 50-ohm impedance, from the graph which is can be found in the book [13]. The ratio found was based on $\mathcal{E}_r$ for polyimide which is: 3.36, then based on this ratio Z_o which is for this partially buried case, can be found by the equation:

$$Z_o = Z_{o,\text{microstrip}}\sqrt{\varepsilon_{e(microstrip)}}/\sqrt{\varepsilon_{e(buried)}} \quad (19)$$

And $\mathcal{E}_{e\,(\text{microstrip})}$ is defined as:

$$\varepsilon_e = \frac{\varepsilon_r + 1}{2} + \frac{\varepsilon_r - 1}{2}.(1)/\sqrt{1 + 12.d/W} \quad (20)$$

While $\mathcal{E}_{e(\text{buried})}$ is:

$$\varepsilon_{e(buried)} = \varepsilon_e{}^{(-2.0.b/h)} + \varepsilon_r[1.0\text{-}e^{(-2.0.b/h)}] \quad (21)$$

where *b* and *h* being as buried depth and height of the substrate. With these equations, after calculations for 50-ohm line the *W* width from *W/d* ratio turns out to be 30 µm. This theoretical value gives a basis for a start to get the desired impedance.

3.1.2 Simulation with Ideal Ports

The first structure – Microstrip with the high resistivity silicon based IPD was simulated in CST. Microstrip being thickest is made on top layer metal 3. For ground to microstrip, metal layer 2 was selected. Metal 2 layer is separated by silicon substrate through Silicon Oxide - SiO_2, followed by SiO_2 there is a polyimide layer 1 and then top dielectric with metal 3 is polyimide layer 2. The whole stack with dielectrics and all the metals – only 3 and 2 constructed in CST is shown in different views in Figures 15, 16 and 17.

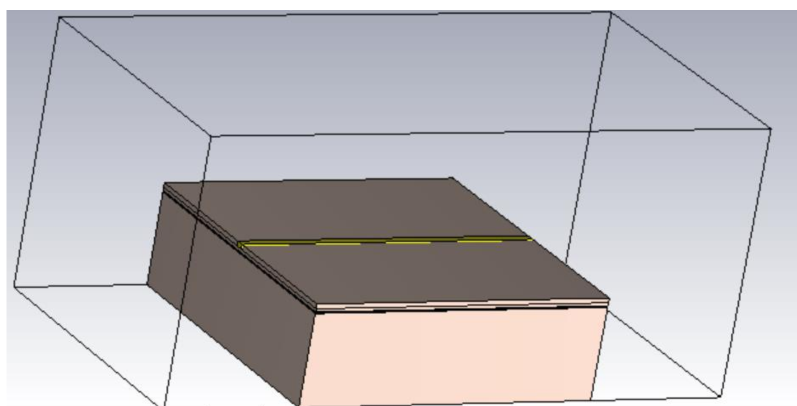

Figure 15. Microstrip CST (Perspective View)

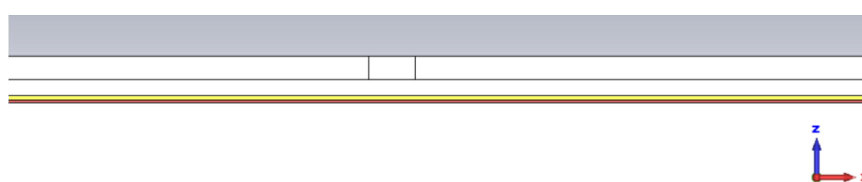

Figure 16. Microstrip CST (Side View)

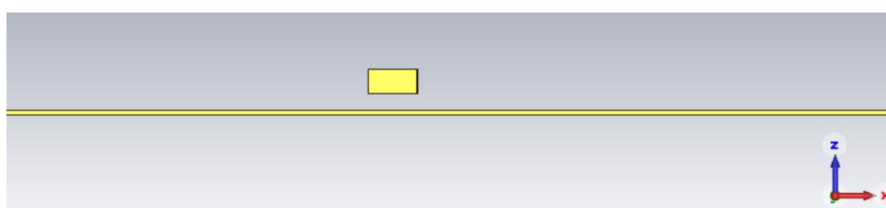

Figure 17. Microstrip CST (only metals: metal 3 and metal 2 as ground)

The length and width of the stack were initially taken as 1 *mm* x 1 *mm* size, because the losses in terms of S_{21} are typically defined per mm or cm but later the size was updated to 0.5 *mm* x 1 *mm* for all transmission lines. The ideal ports were used to excite the structure: they are defined in CST through the solver by the definition of port extension coefficient k. To have the dimensions for ideal waveguide port, the solver in CST was used which can also construct the ports through k. The solver for the case 30 µm wide microstrip is shown below in Figure 18.

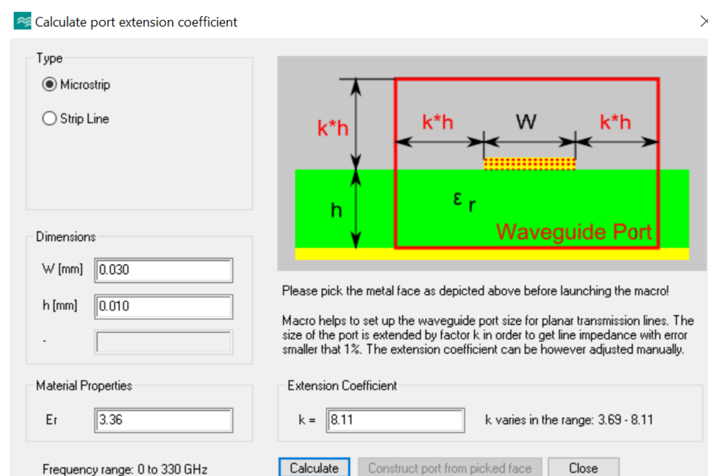

Figure 18. Extension coefficient calculator

$\mathcal{E}_r$ for polyimide is 3.36 and *W*, *h* being Width of the microstrip and height of the dielectric respectively in mm. From this calculated k, we can construct ports for excitation. After creation of ports, boundary conditions were set to generic open conditions in all directions except for the direction *-z* which represents beneath the silicon substrate to be electric. In an actual measurement setup, there is some metal aluminum or steel beneath silicon substrate. The simulation was done across a frequency range of DC to 330 GHz. The test structure and ports 1 and 2 along with boundary conditions defined is shown below in Figure 19.

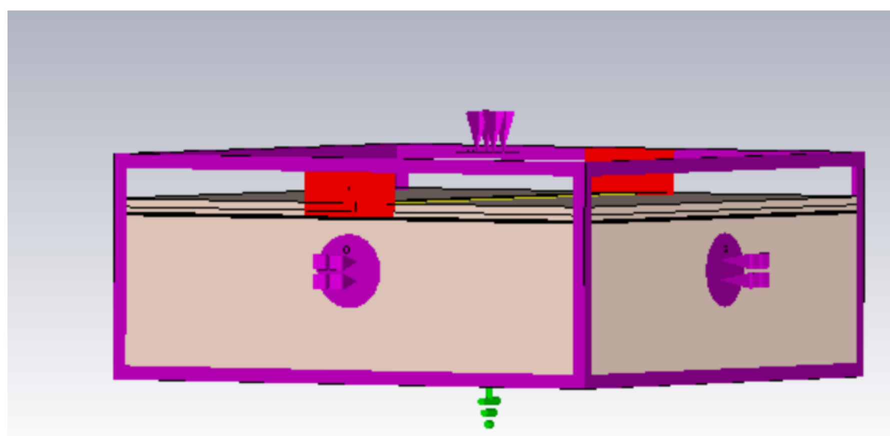

Figure 19. Boundary conditions

Just at the start of simulation, the port information gets accessible, and we can see the line impedance. When this structure was simulated, the line impedance was 32 ohms, which was not what it has to be calculated theoretically. Later on, two approaches were being used, first as rough estimate to see the trend of width with line impedance, the width was doubled and the second approach was to have a structure with a thinner width. The trend observed was that the impedance gets closer to standard 50 ohm, as we go towards the narrowermetal 3. Different impedances with thicknesses are shown in Table 2. The test structure with a width of 30 µm but same stack size and boundary conditions is shown in Figure 20.

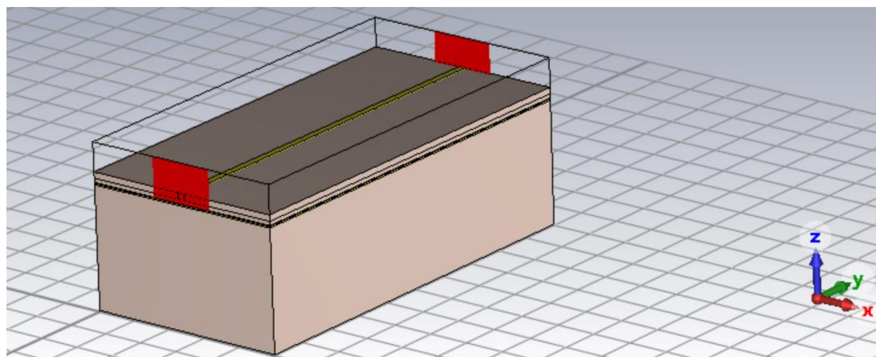

Figure 20. Microstrip (excited with ideal ports)

Table 2. Different Microstrip Widths

Metal Width (Metal 3)	**Line Impedance**
30 µm	32 ohms
50 µm	24 ohms
17 µm	42 ohms

The E-field after simulation at port 1 is shown at 165 GHz in Figure 21 below. Simulation results, got from simulating a 17 µm wide microstrip excited with ideal ports were then renormalized to the 50-ohm standard and the simulation results can be visualized in terms of S_{11} and S_{21} parameters by looking at Figures 22 and 23.

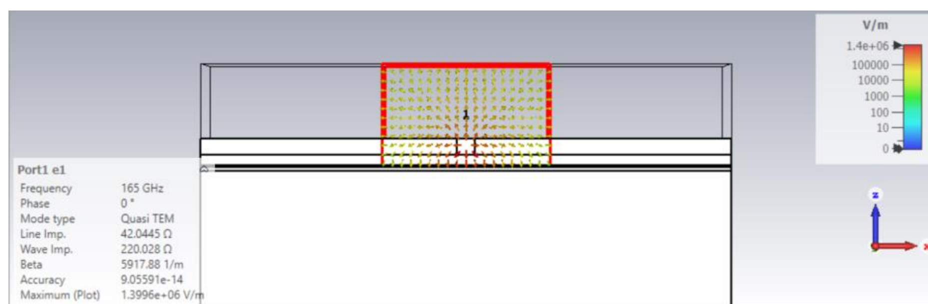

Figure 21. *E*-Field at port 1

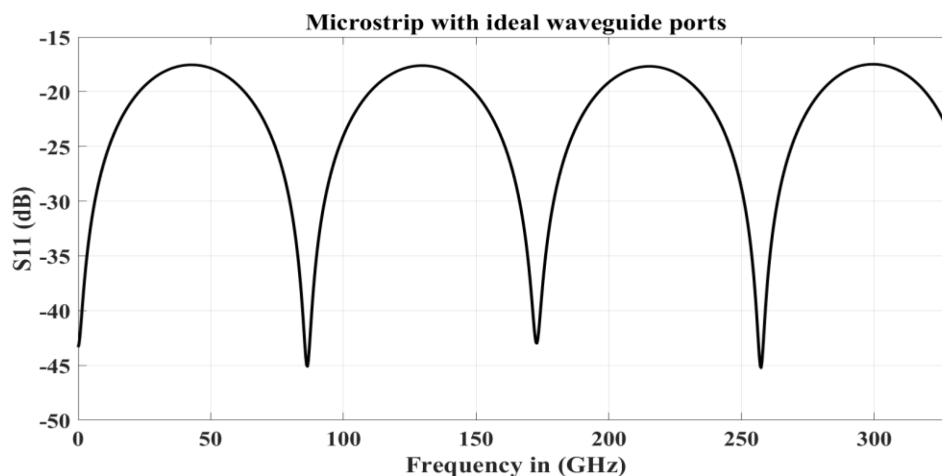

Figure 22. S_{11} (dB) – 0 to 330 GHz Microstrip

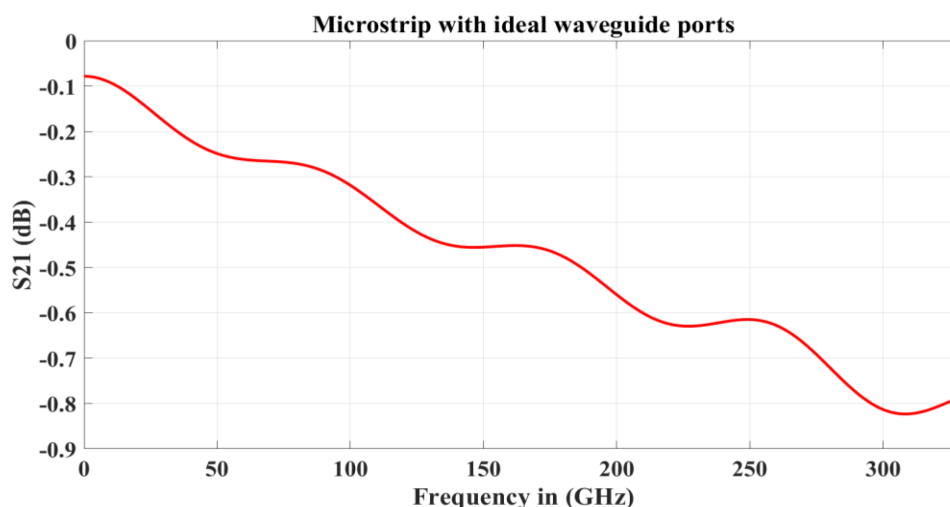

Figure 23. S_{21} (dB) – 0 to 330 GHz Microstrip

3.2 Strip line

Second structure to be tested was a strip line which utilised all 3 metal layers, metal 2 being sandwiched between metal 1 and 3. Unlike the microstrip, the strip line has its own usage and can be utilised to implement more sophisticated and complex structure with this IPD. The other reason to have this structure was trying to get 50-ohm line which was not possible in the microstrip case. The design calculations along with the structures and results are discussed in the following sections.

3.2.1 Design Calculations

Based on the results obtained from hand calculations for microstrip and what we get from analytical line calculator from CST, the calculations from CST calculator give some realistic and more practical results than hand calculations. So, to have the dimensions for a strip line with the given stack case: a strip line with uneven distribution of dielectric around it, the CST's analytical line impedance calculator was used, the calculator is based on [14]. The '*t/h'* ratio defined in the calculator (asymmetric thick strip line case) was found to be too large and didn't

give any estimation for the expected line impedance. Then, as a rough estimation the height '*h2*' was taken as 5 μm.

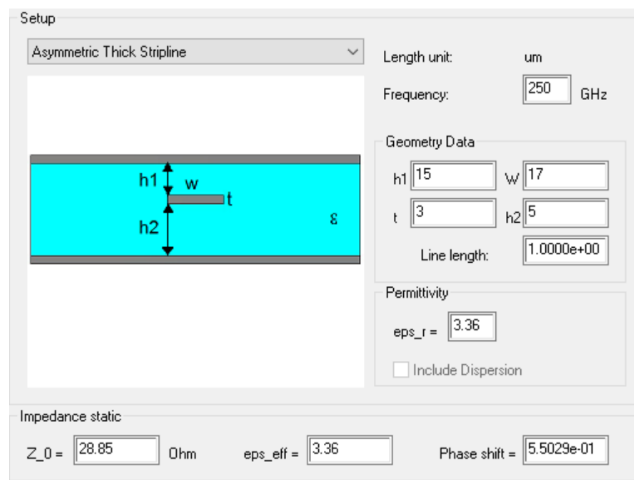

Figure 24. Asymmetric strip line calculator

3.2.2 Simulation with Ideal Ports

Strip line's width was taken as 17 μm, the separation between metal 1 and metal 3 can be realized by polyimide layer and having metal 2 acting as strip line, the visual depiction in terms of only metals in the form of cross-sectional view from CST model (Metal's thicknesses being in the direction of +*z* axis) is represented in Figure 25.

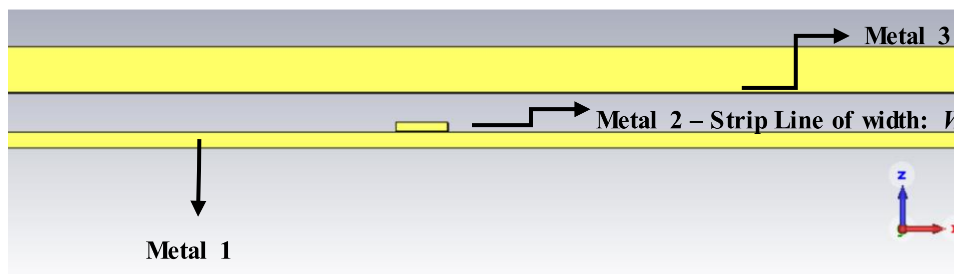

Figure 25. Cross-sectional view (metals only)

To excite the strip line structure, the waveguide port excitation was utilized, which is shown in the Figure 26. The waveguide port definition requires the value of 'k' extension coefficient to have correct dimensions in terms of defining ideal waveguide port in CST. For calculation of 'k', the solver in port definition of CST was used, which gives the value of 'k' for the situation of strip line's dimensions as k = 1.31.

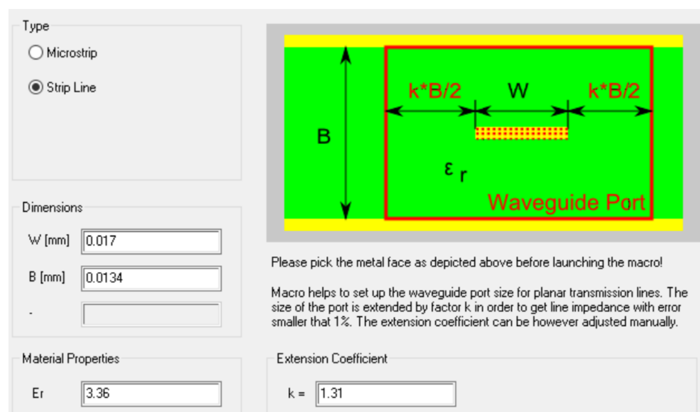

Figure 26. Port Extension Coefficient calculator

Taking up the value for 'k', the ports were defined for the strip line. The boundary conditions were kept same as the microstrip case, and the frequency range was also similar with microstrip structure for simulation. The strip line structure with ports is visible in Figure 27.

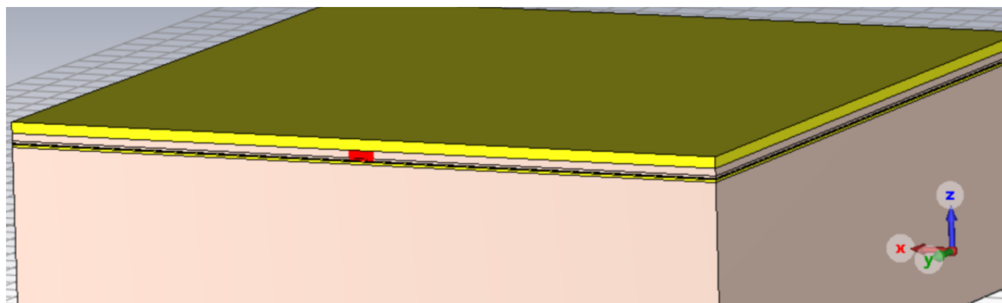

Figure 27. Strip line excitation with ideal waveguide ports

Results in terms of line impedance for strip line were not really promising, the line impedance which can be seen from port information was 3.85 ohm for the simulated structure. This impedance was really low, the only dimension which can be varied was the '*W*' width of strip line, which was then changed to a wider width. The main impedance defining or improving factor was the distance between metal 2 and metal 1 which is quite narrow according to the IPD technology, so increasing the width '*W*' even worsened the impedance which gets lower to value of 2.25 ohm as compared to 3.85 ohm for the case of thin strip line.

Limited by the IPD technology, there was no way out to get a line impedance closer to 50 ohm for strip line. Any further proceeding with strip line structure was discarded opposite to other structures which were then simulate with probe pads, discussed in the following sections of this document.

3.3 Coplanar Waveguide

Third transmission line CPW has two cases, where it is firstly defined by the case in which there is no ground backing of the ground-signal-ground metallic structure and other one is the case in which there is some other metal layer involved providing a ground beneath or above the ground-signal-ground metal layer (based on the specific application). Two of the cases: CPW without ground (defined in terms of metal 3 and metal 1) and with a ground (metal 2) beneath metal 3 as top layer. These two types of CPW were simulated in CST with ideal ports.

3.3.1 Design Calculations

Following the trend in the earlier section of strip line to calculate dimensions to achieve a line impedance of 50 ohm, the same calculator from CST software was used, the screenshot taken from CST's calculator can be seen in Figure 28.

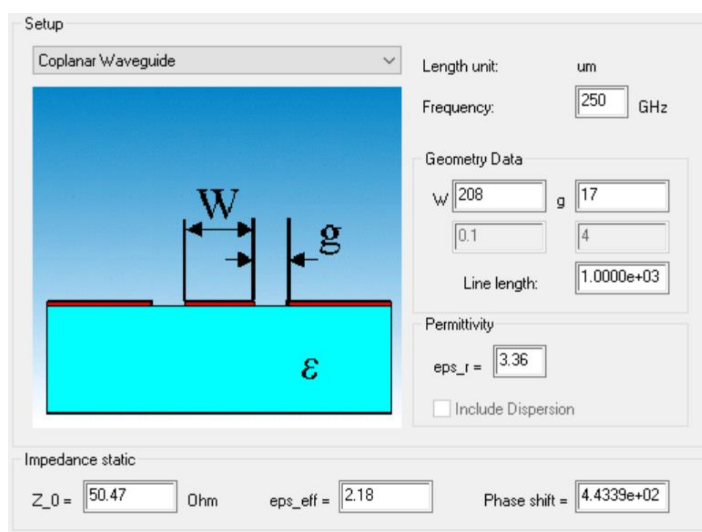

Figure 28. CPW without ground (dimensions)

Defining the frequency as 250 GHz and having metal 3 on top level give us the values of 'g' and '*W*' for CPW to get line impedance of 50 ohm. The calculator calculates these values based on equations from [15]. The CPW with ground's dimensions with CST calculator can also be seen in the following Figure 29.

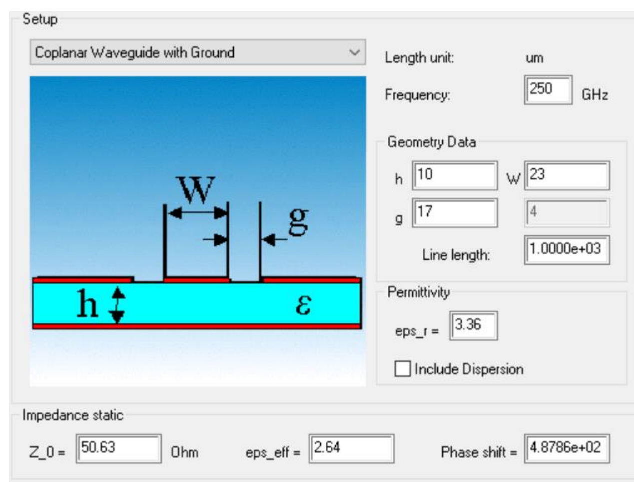

Figure 29. CPW with ground (dimensions)

3.3.2 Simulation with Ideal Ports

Both the structures, one with ground and other without ground for CPW were simulated in CST with ideal waveguide ports to give a validation for calculated dimensions from CST solver, in order to get a line impedance of 50 ohm. Figure 30 shows an ungrounded CPW excited with ideal ports.

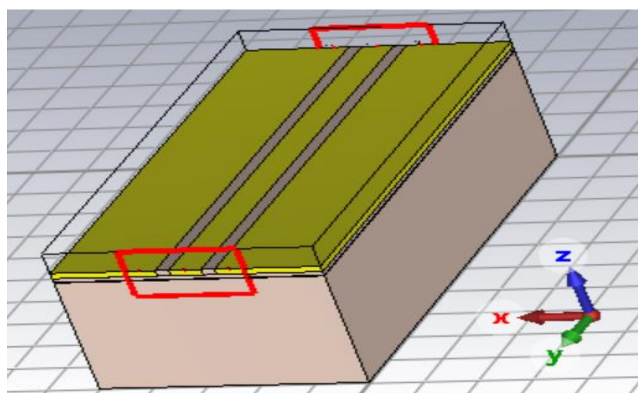

Figure 30. CPW Ungrounded CST Stack

The boundary conditions set for microstrip were repeated for CPW as well. Ports definition was done with defined polarity of GSG – ground signal ground case (negative - positive - negative) and dimensions of ideal ports were set from CST's definition shown in Figure 31.

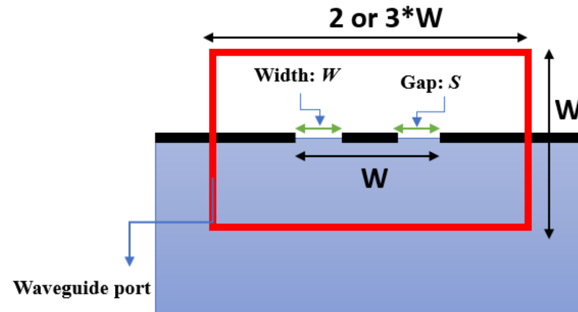

Figure 31. Waveguide port definition for ungrounded CPW

The line impedance for ungrounded CPW after simulation comes out to be 32.5 ohm, which was not what was expected. An approach to get 50-ohm line, a thinner width for large area probe pads were tried out in order to avoid tapering from probe pads to the signal line of CPW. Values of '*W*' and '*g*', after few simulations for ungrounded CPW case are shown in Table 3.

Table 3. Ungrounded CPW's line impedance being function of *W* and *g*

Ungrounded CPW (Width W)	**Ungrounded CPW (Gap g)**	**Line Impedance**
17 µm	208 µm	32.5 ohm
25 µm	60 µm	50 ohm

CPW with ground when simulated with all the conditions for grounded CPW not changed, we get the line impedance 32.5 ohm, so to have higher impedance than 32 ohm, a number of simulations were made. After tuning, we get some increase in line impedance but not closer to 50 ohm. With some simulations, the possibility to get a line impedance similar to microstrip, and the tuned dimensions are shown in Table 4. With the increase in gap there was an increment in the line impedance, but as the gap increases the CPW starts behaving almost like a microstrip. The effect of ground in the lateral direction becomes irrelevant and non-dominant, the grounded CPW E-field simulation showing its behavior like a CPW (comparison in terms of varying E-field with gap 'g') is given in Figure 32, while Figure 33 shows the CST's port definition for grounded CPW.

Table 4. Grounded CPW Line Impedance

Grounded CPW (W)	**Grounded CPW (g)**	**Line Impedance**
23 µm	17 µm	32.5 ohm
17 µm	17 µm	37 ohm
17 µm	36 µm	42 ohm

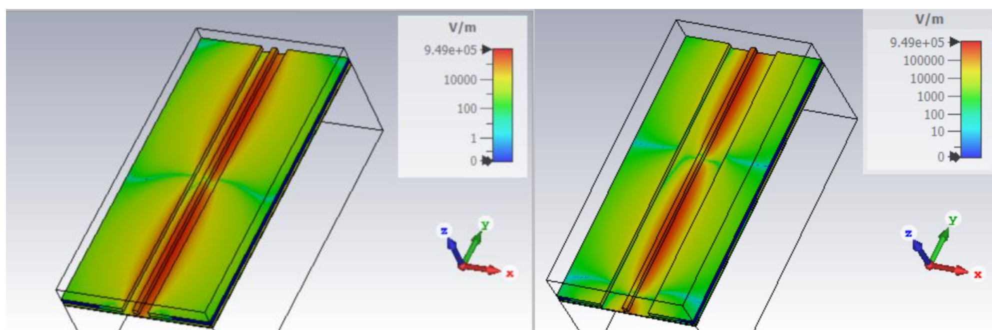

Figure 32. *E*-field animation at 165 GHz (*g*-36 μm vs wider gap)

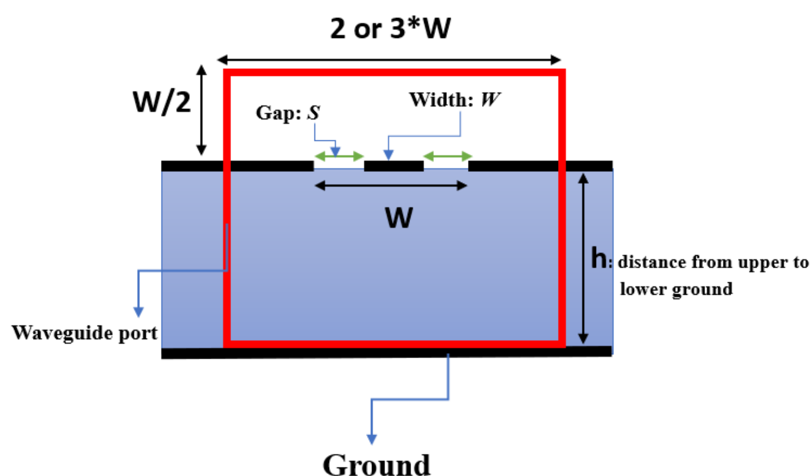

Figure 33. Waveguide port definition for grounded CPW

The comparison of the performance between ungrounded and grounded CPW with the selected dimensions having 50 and 42 ohms line impedances respectively, can be made in terms of S-parameters. For both structures after simulations with ideal ports, the reference impedances were re-normalized to 50 ohm, and the plots in terms of S_{11} and S_{21} parameters are given in the following Figures 34 and 35.

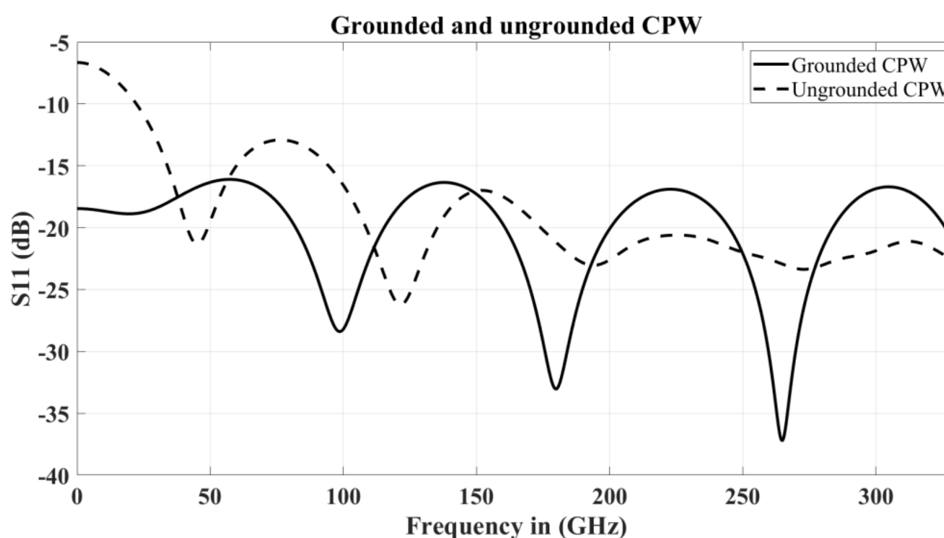

Figure 34. S_{11} (dB) Grounded and ungrounded CPW

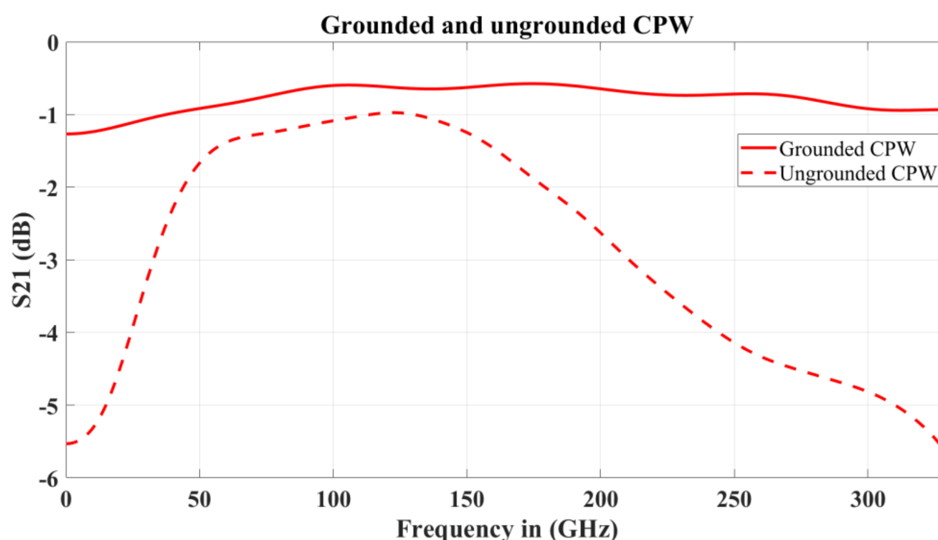

Figure 35. S_{21} (dB) Grounded and ungrounded CPW

3.4 Probe Pads

Measuring some parameters, to test a device or for any other purpose at wafer level, the RF probes plays a very important part. The three main advantages for using probe pads over semi-rigid RF cables can be categorized into: necessity, accuracy, and productivity [16], as they offer practicality to measure the micro level circuits with accuracy in a short period of time. Probe pads have made it a reality to measure above 500 °C, with a lower limit to 4 K, high power handling capacity (60 W), and a THz frequency range: up to 750 GHz [17]. Among different variations in terms of probe pad configuration, the most common one is GSG (ground-signal-ground) configuration.

3.4.1 Large Size Probe Pads

VTT's IPD technology offers both larger and smaller GSG - ground signal ground configuration for probe pads. The pitch for these types of pads varies from 100 µm to a wider one according to the measuring setup of probe station. Taken as an example of different sizes, the width for signal pad can be small, while the ground pads may be wider having the same length as signal pad. These dimensions and an example of this large probe pad configuration is presented below in Figure 36.

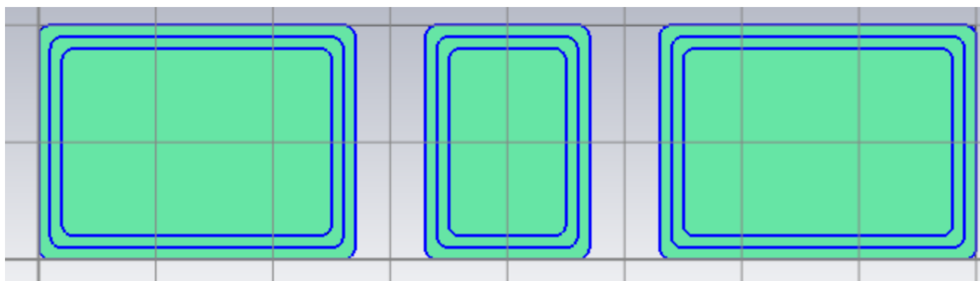

Figure 36. Large GSG probe pads

3.4.2 Smaller Probe Pads with 100 µm pitch

Another permissible set of pad dimensions were smaller than the larger pads, and both the width and length were shrunk as compared to larger area probe pads. The configuration and the pitch size may vary for the desired application. EMC- electromagnetic compatibility lab at CWC-RT (center for wireless communications – radio technologies) has the facility of a probe station with 100 µm probe pitch as the actual measurement setup. So, the 100-µm pitch can be selected for probe pads with GSG configuration.

3.4.3 CST Simulations

In CST, both probe pads (the larger and the smaller ones) were modelled and simulated across a frequency range up to 330 GHz. First, wider probe pads were simulated and then the pads smaller in size with 100 µm pitch were simulated. The comparison can be made between these two types of variations in terms of line impedance they offer and the performance in terms of return and insertion losses. The modelling was done in accordance with pitch size, the CST model (with and without dielectric) for wider pads is shown in Figure 37:

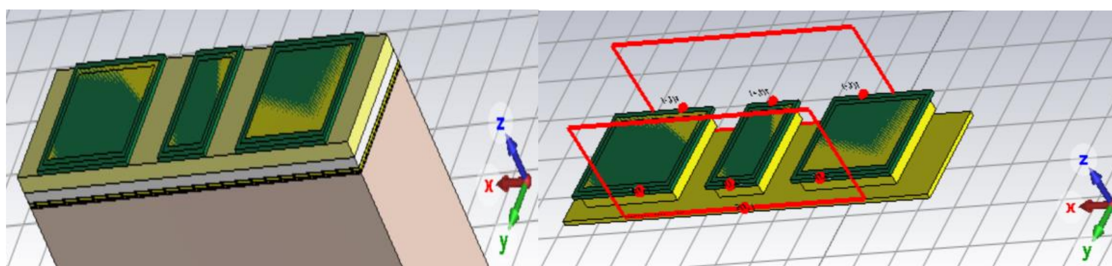

Figure 37. Full stack and only metals with waveguide port

Similarly, the modelling was done for smaller pads in CST. In both models, the simulations were carried out with vias 2 and 1 under the probe pad metal area shown in Figure 38. For both cases (larger and smaller), the waveguide port with polarities (positive and negative) was defined to excite the probe pads, as they have same structure as a coplanar waveguide. The boundary conditions and frequency range were same as used for microstrip, and coplanar waveguides.

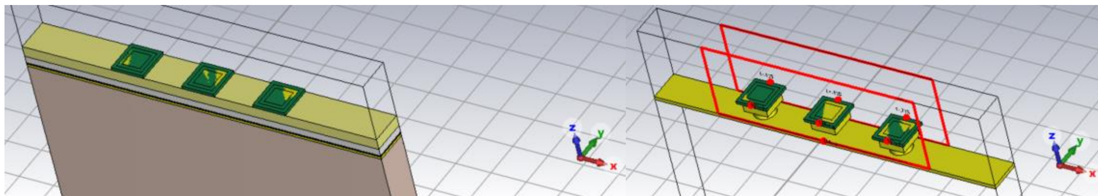

Figure 38. Full stack & Only metals with waveguide port

After simulations, the impedance was re-normalized to 50-ohm standard. The results in terms of S-parameters can be seen in Figures 39 and 40. Table 5 shows the impedance variations when varying the probe pad area.

Table 5. Probe Pads comparison

Probe Pads	**Line Impedance**
Large in area (150 µm - Pitch)	43 ohms
Smaller area (100 µm - Pitch)	56 ohms

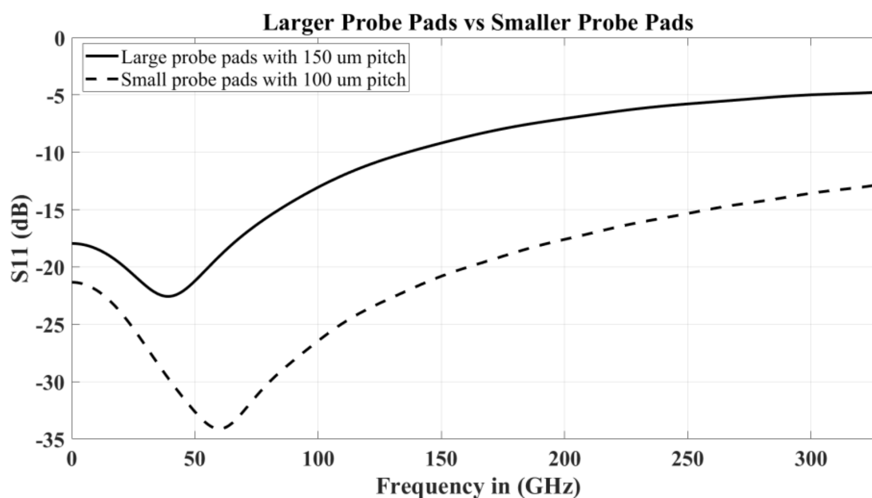

Figure 39. Comparative S_{11} (dB) - smaller and larger probe pads

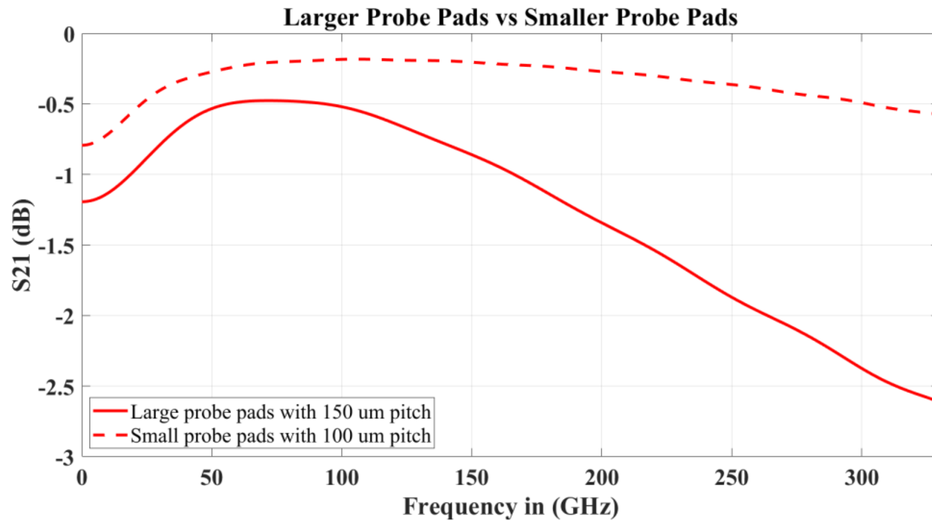

Figure 40. Comparative S_{21} (dB) - smaller and larger probe pads

By looking the above graphs from Figures 39 and 40 in a comparative way, it looks obvious that the performance of the pads in terms of either line impedance or in terms insertion & return loss improved with smaller pads. With larger area and pitch, probe pads were limiting the performance in terms of all aspects, as they have restrictive effect in term of S_{11}, stopping it at around 135 GHz. Through the, S_{21} graph (Figure 40), we can say that there is significant amount of improvement when shifting to smaller pads. The insertion loss realized in terms of S_{21} parameters gets worse after 100 GHz.

3.5 Transmission Lines Excitation with Probe Pads

In the actual measurement setup, all the passive structures constructed and simulated based on the IPD technology must be excited by probe pads and not with the ideal waveguide ports. To proceed further, after comparison made based on sizes and pitch for probe pads, smaller probe pads were chosen to have simulations with all the 3 structures: Microstrip, Coplanar Waveguide (Grounded), and CPW (Ungrounded). Along with these lines, a transitional structure from microstrip to ungrounded CPW was made and simulated.

3.5.1 Microstrip

Except for the dielectrics, the changes were made for metals in order to use probe pads instead of ideal waveguide ports. With 100 µm pitch size, GSG configured probe pads were landed on the microstrip having signal line of pads aligned with microstrip. Signal line of the pads was found to be wider than microstrip, and later on tapering was done. After trying angle sweeps: from 10 degrees to 100 degrees, the best possible angle selected was 45°, which can be seen in Figure 41.

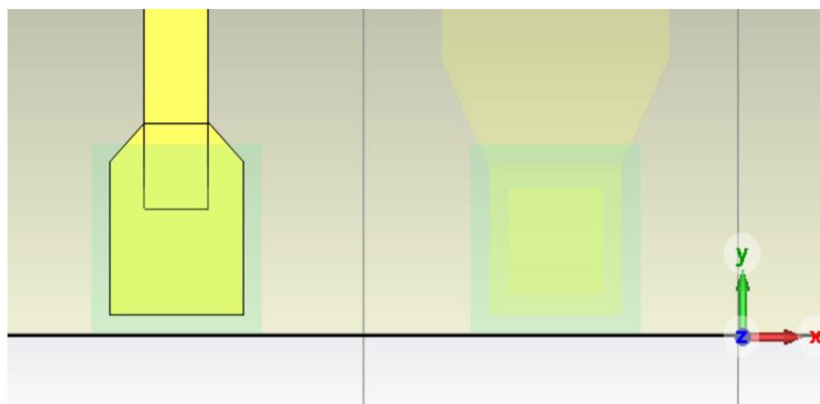

Figure 41. Tapering for metal 3

The other changes made were to slide the metal 3 away from probe pads, and the tapering was also done from pads to metal 3 providing ground to metal 1 through vias 1 and 2. There were other simulations done with the probe pads having 150 µm pitch shown in Figure 43 but the results were not as promising as they are with smaller ones, the ground implementation through metal 3 is shown in Figure 42.

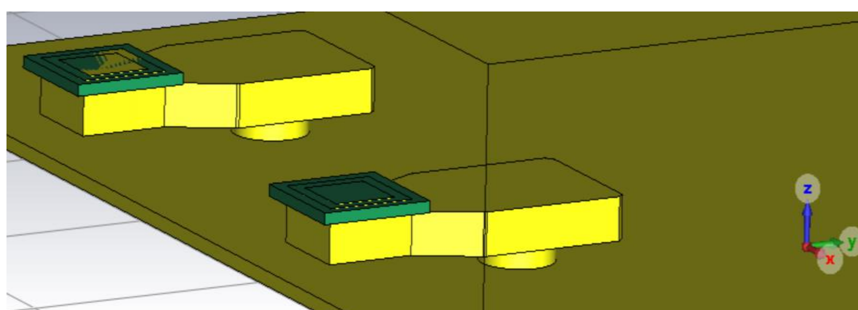

Figure 42. Probe pads grounding implementation

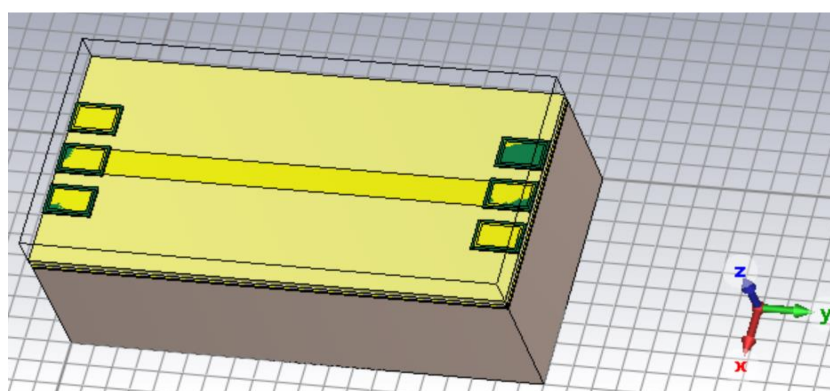

Figure 43. Microstrip excitation with larger probe pads

The S-parameters for microstrip with smaller pads are re-normalized to 50 ohms, and also the de-embedding of ports was done from the center of probe pads, where usually the probe are

landed for actual measurements. The results can be seen with these modifications in Figures 44 and 45 showing S_{11} and S_{21} respectively.

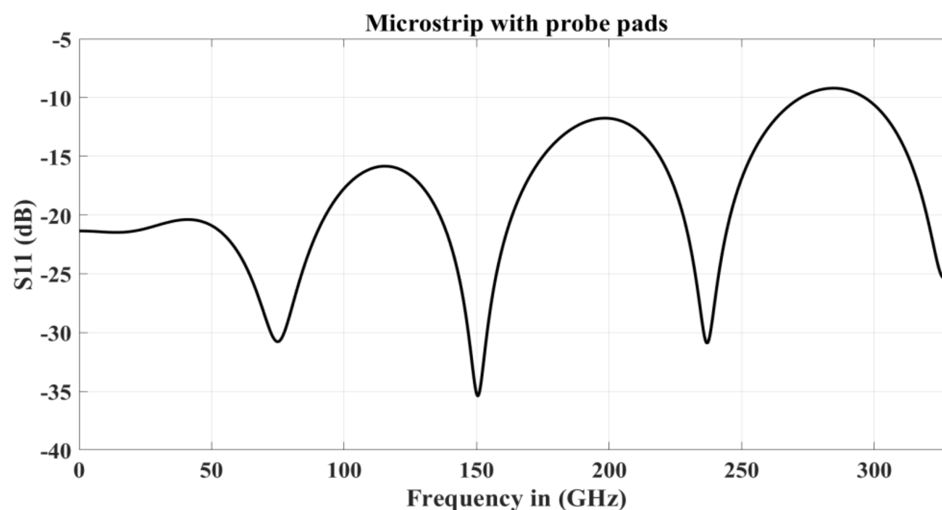

Figure 44. S_{11} (dB) Microstrip

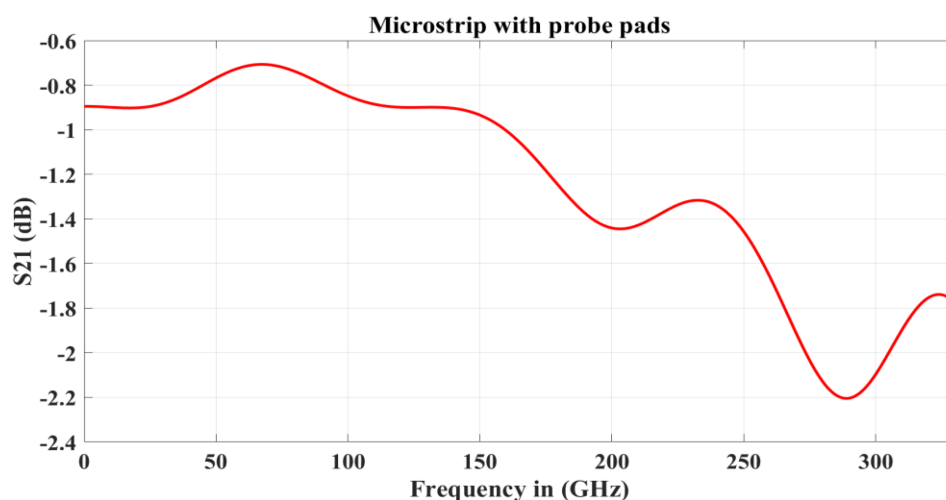

Figure 45. S_{21} (dB) Microstrip

With the shift from metallic / ceramic-based electronics packages to plastics-based packaging, the passivation layer on top metal layer usually copper is an essential part of almost every integrated circuit (IC) design in order to avoid corrosion [18] and oxidation of copper. Apart from these factors it gives some mechanical and thermal support to dielectric and copper interconnects beneath passivation layer [19].

While all the simulations were done without a passivation layer on top metal, there must be some passivation over the copper layer and consequently the simulation must be made. A thick polyimide layer on top of metal 3 along + *z*- axis is shown in Figure 46.

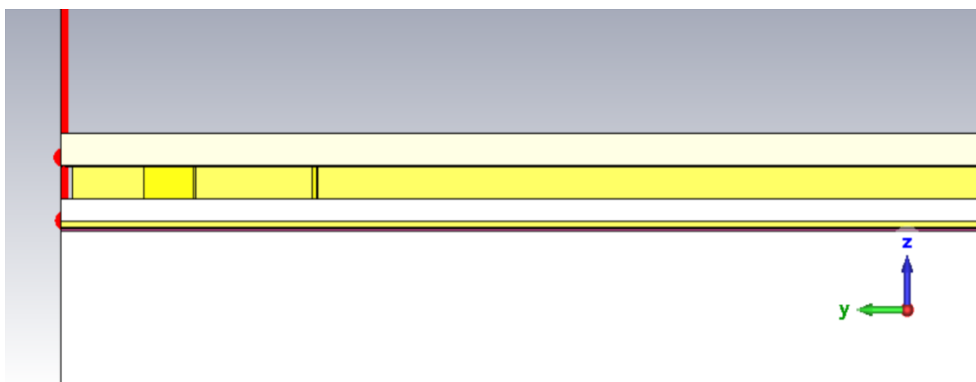

Figure 46. Passivation layer on top of metal 3

Simulation results show us the effect of passivation layer, the results in terms of S_{11} and S_{21} parameters are represented in Figures 47 and 48, respectively. By looking at the plots, we can see the effect of passivation: there is an increased mismatch as compared to non-passivated microstrip till 50 GHz frequency in terms of S_{11} but with increasing frequency, the matching coincides with the non-passivated microstrip. In terms of S_{21}, the difference can be roughly estimated as 0.2 dB difference (increment) as compared to simulation when top copper layer is exposed to air. These results / comparisons give us an idea of passivation affecting the simulation results when metallic structures are not covered with polyimide.

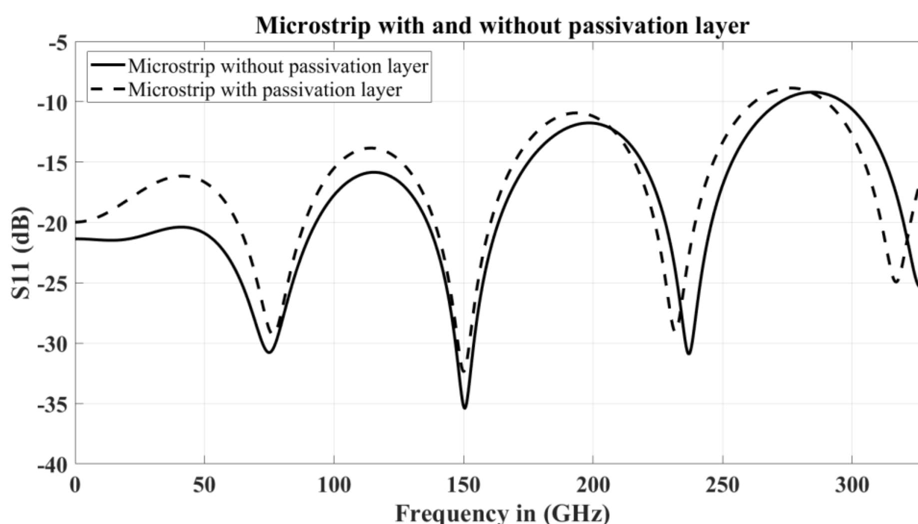

Figure 47. S_{11} (dB) Microstrip with passivation layer

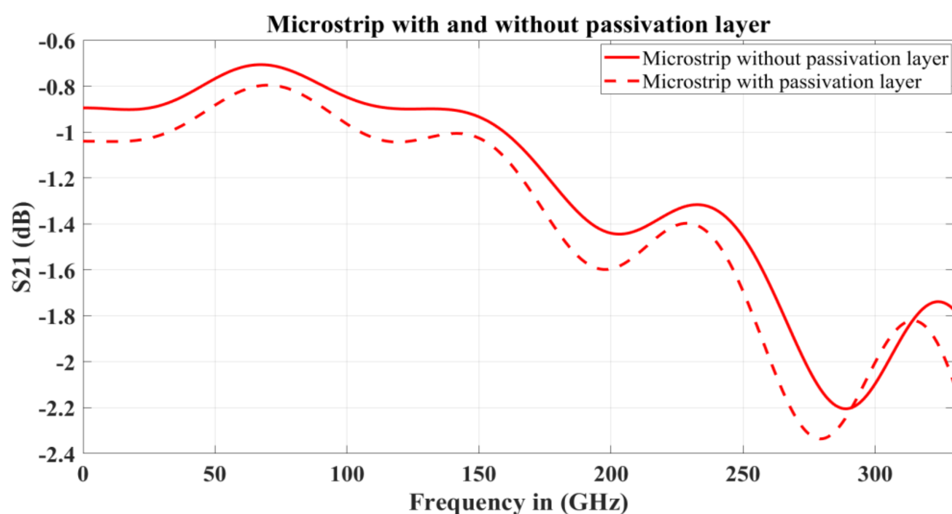

Figure 48. S_{21} (dB) Microstrip with passivation layer

3.5.2 Coplanar Waveguide with Ground

Transmission line to be simulated after microstrip with probe pads was CPW with ground. The dimensions used for ideal waveguide port excitation and the stack size in terms of width and length remain the same along with boundary conditions. The difference lies in the transition from wider probe pads to thin signal line of CPW. Not only signal for signal, but the tapering was also required from ground pads to grounds of CPW. Tapering was done to make its effect as small as possible, so that the CPW acts like its characteristic behaviour; otherwise it may behave as a microstrip. The tapering for CPW case is shown in Figure 49.

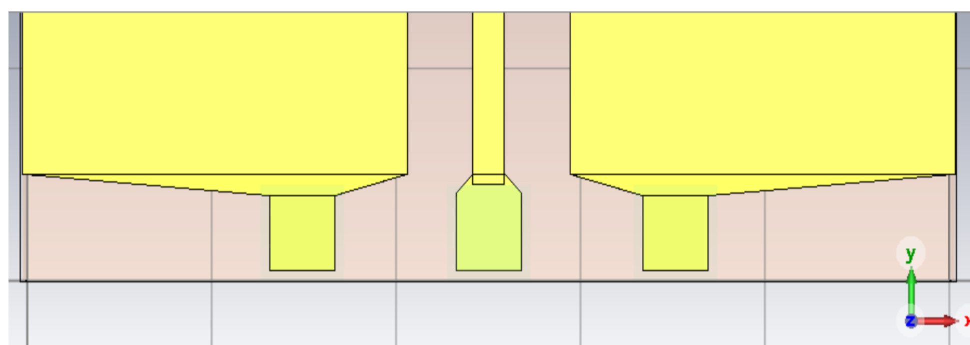

Figure 49. Tapering for GSG pads to CPW (Metal 3)

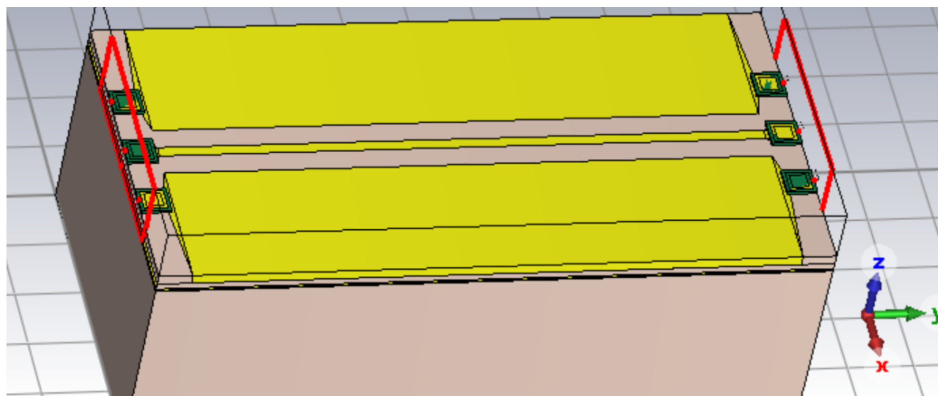

Figure 50. CPW without via fencing

In addition to 42-ohm CPW line without via-fence visible in Figure 50, there was another structure with via fencing on the grounds around signal line was simulated. The via fencing serves various purposes like: higher orde mode suppression, increase in bandwidth or even it turns out to be a cost effective method in decreasing the number of layers in PCB (printed circuit board) [24]. The vias introduced, total 18 vias: via 2 from metal 3 to ground lines to see the behaviour of via fencing, as shown in Figure 51.

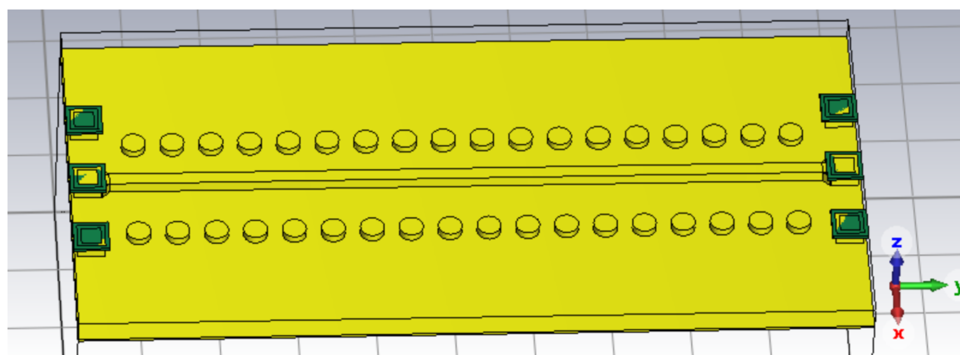

Figure 51. CPW with via fencing

For the CPW with and without via fencing, the simulation results with probe pads over the same frequency range and conditions provide an estimate to see how the fencing creates a difference in terms of either insertion loss or return losses, the results were re-normalized to 50 ohms. The parameters to be compared are S-parameters, which can be plotted together for two cases, and with the addition of extra vias the impedance may vary, which will consequently effects both S_{21} and S_{11} as compared to CPW without fencing as shown in Figures 52 and 53.

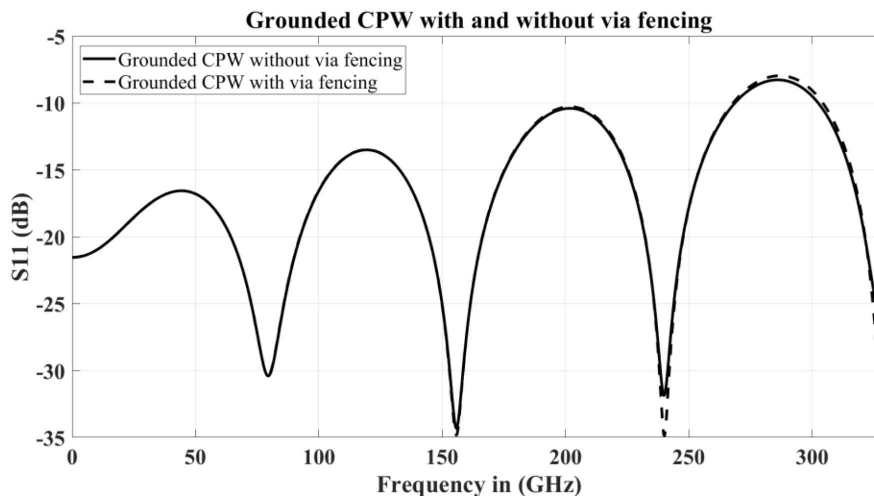

Figure 52. S_{11} (dB) Effect of via fence

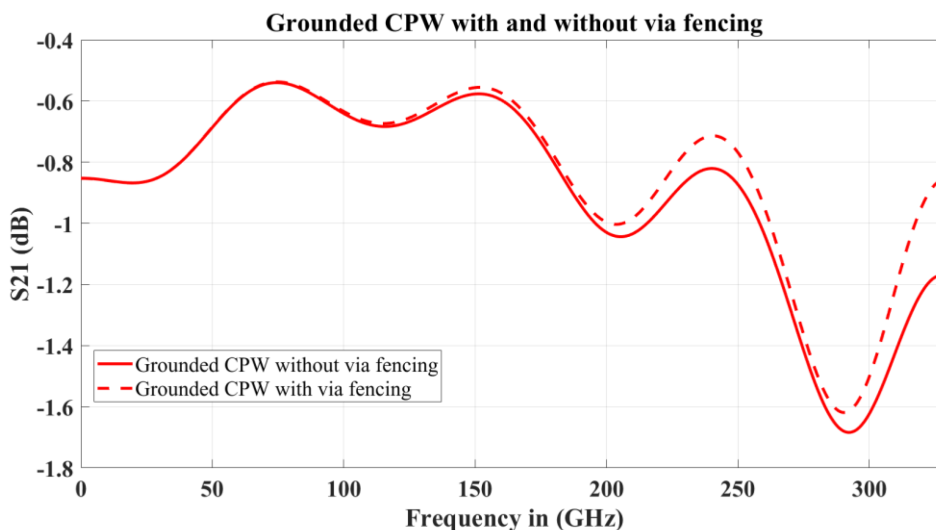

Figure 53. S_{21} (dB) Effect of via fence

3.5.3 Coplanar Waveguide without Ground

Probe pads simulation for ungrounded CPW also needed to be done, in a similar way as it was simulated for the ground backed CPW case. The dimensions were different contrary to grounded CPW case, but the tapering need to be done from pads to metal 3 GSG line. The minimum amount of distance was taken into account from thinner pads to wider GSG lines, the chamfering was done with 45° angle shown in Figure 54.

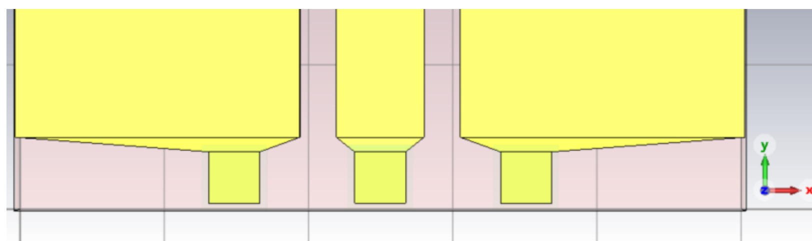

Figure 54. Metal 3 tapering – GSG (Probe Pads) to GSG (CPW)

The same boundary conditions, frequency range, stack size and waveguide port which was defined for ideal port excitation were used also with the probe pads. The probe pads excited structure was simulated, the expectation was to define the probe pads as CPW without ground as per CST port definition the stack along with ports is shown in the following Figure 55.

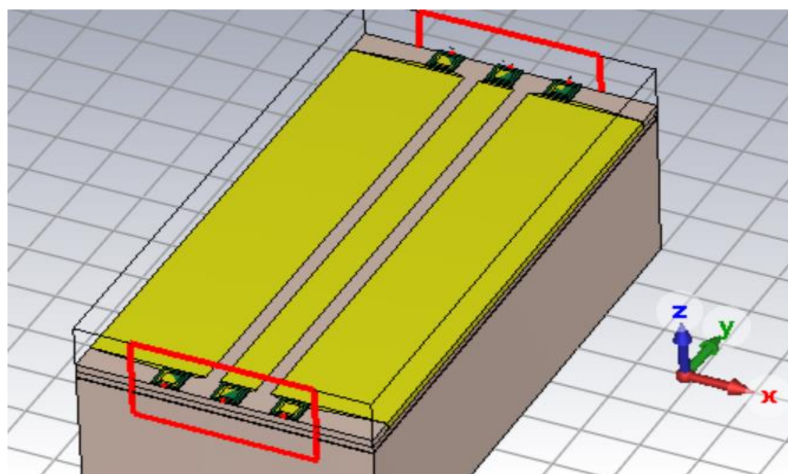

Figure 55. Ungrounded high impedance CPW

After simulation, re-normalization to 50 ohms from high impedance ungrounded case, gives us the S-parameters. Another factor after simulation was de-embedding the ports: 1 and 2, there was de-embedding done from the center of probe pads to have similar scenario with the actual measurement environment. The insertion loss S_{21} or return loss in terms of S_{11} plotting can be then visualized from the following Figures 56 and 57.

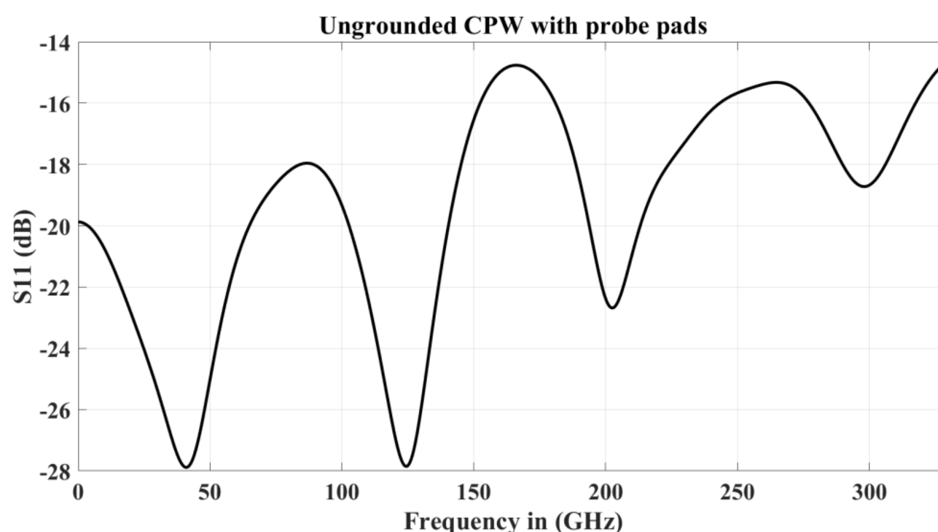

Figure 56. S_{11} (dB) Ungrounded CPW

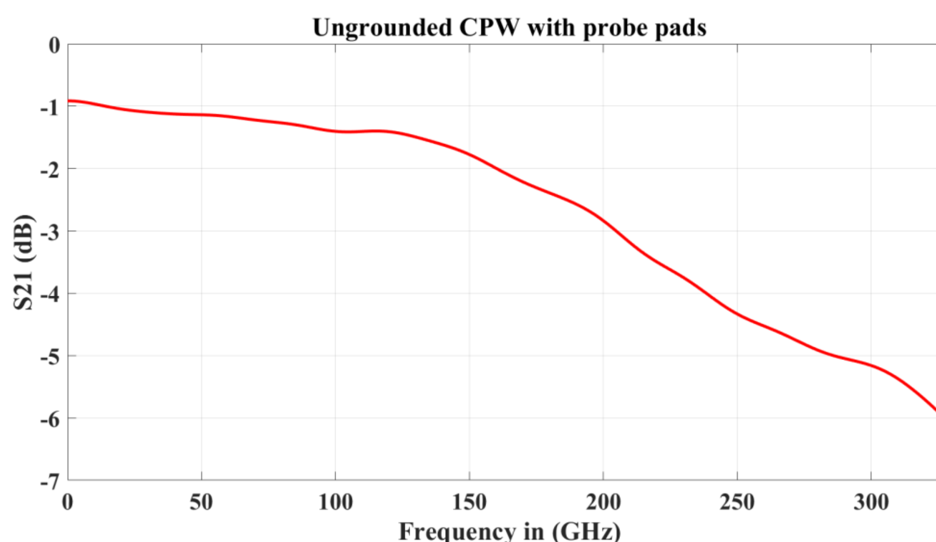

Figure 57. S_{21} (dB) Ungrounded CPW

3.5.4 Via Transition from Microstrip to Coplanar Waveguide (Ungrounded)

In addition to microstrip, and CPW, a via based transition from microstrip to ungrounded CPW was simulated. Looking into the past, in 1970s for monolithic microwave integrated circuit (MMIC) on-wafer measurements, the transition from probe pads - CPW structure to a microstrip becomes one of the prominent reasons for this type of integration or transition [20]. With ongoing advancements in wireless communications systems, the compactness become a substantial part for RF/Microwave circuits. In Multi-layer Integrated circuit (MIC), the transitions from one passive structure to another passive structure which may co-exist on the same layer or may lie on another layer, becomes important specially at higher frequencies [21]. The transition in such situations can be judged in terms of insertion loss and how a circuit can be useful with a via transition. Based on the broad band or any other specific requirement the transition from a microstrip to a CPW (taken as example), can be done through bond wire, via holes, and a vialess structure (through electromagnetic coupling) [22].

In this thesis work, the transition's effect from microstrip on metal 3 to lower metal 2 ungrounded CPW was simulated. The transition was via based using via 2 from metal 3 to metal 2 and only one via was used for such transition in a back-to-back case excited using 2 ports from port 1 to port 2. In terms of length, both the passive structures – microstrip and CPW were divided equally in 500 µm (for a total length of 1 mm). The tapering for via 2- larger in terms of diameter as compared to microstrip was done. Stack width, frequency range, boundary conditions and meshing remain same as it was used for previously simulated passive elements, shown in Figure 58.

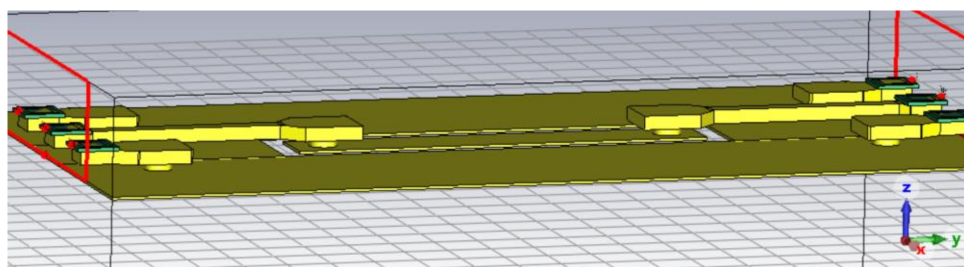

Figure 58. Via Transition Microstrip to CPW (Metal 3 to Metal 2)

After simulation, the effect can be visualized by E-field animation in CST at 165 GHz in Figure 59. The line impedances for both ports were re-normalized and later we can see the S_{11} and S_{21} parameters. The plots for insertion and return loss for the transitional case are presented in Figures 60 and 61.

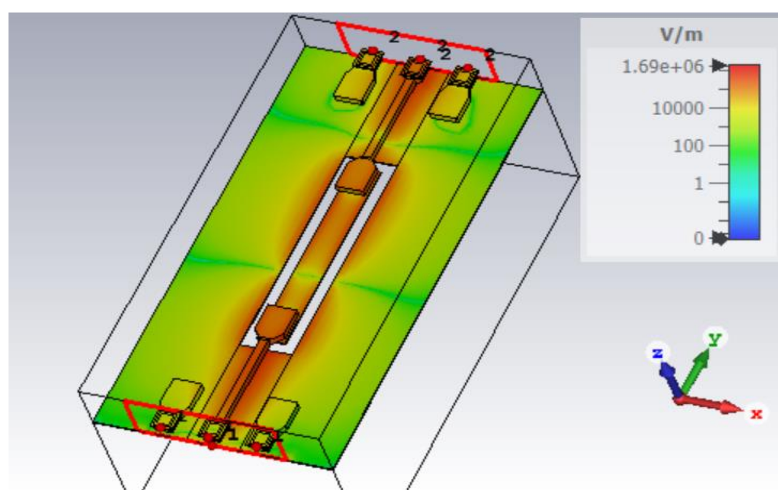

Figure 59. *E*-field animation at 165 GHz

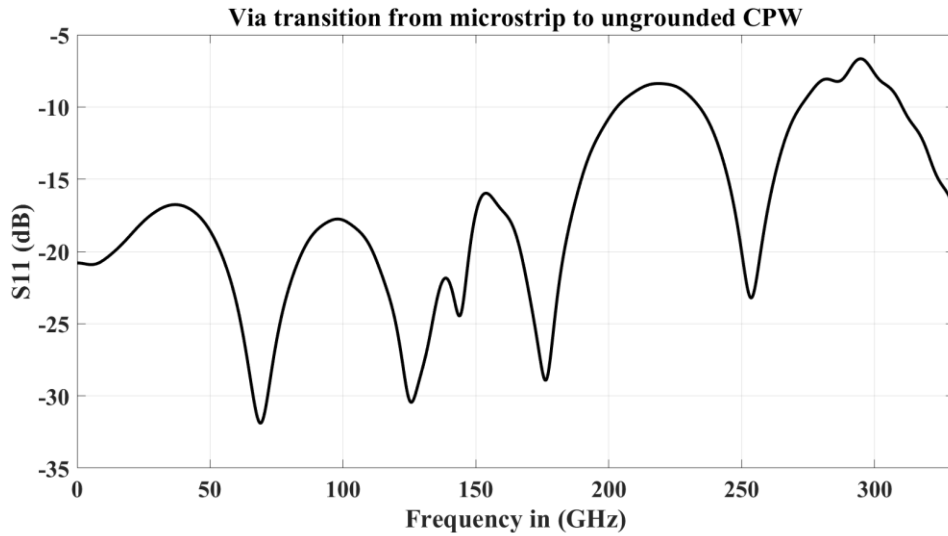

Figure 60. S_{11} (dB) Via Transition

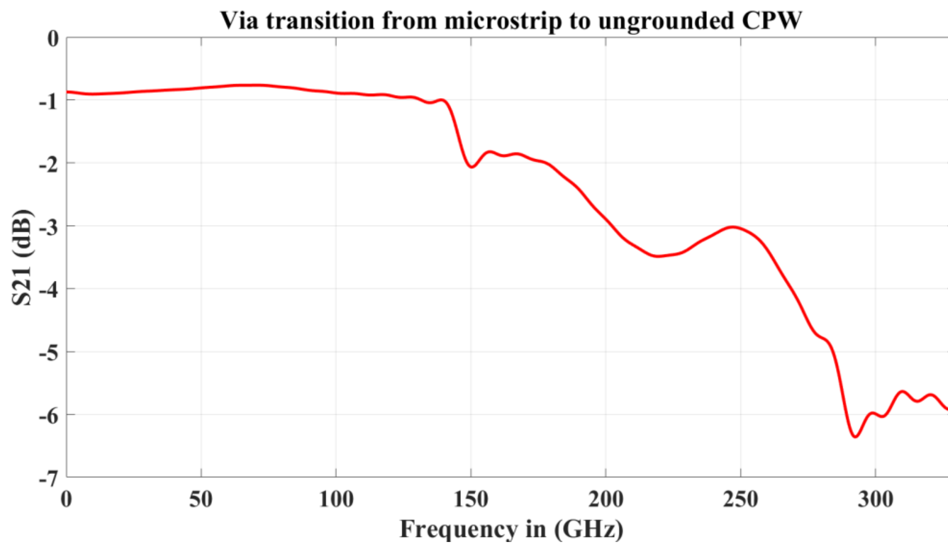

Figure 61. S_{21} (dB) Via Transition

3.5.5 Transmission lines performance comparisons

From delivering power to an antenna to implementing any other passive device like a filter, the transmission lines simulations provide us an estimation towards a direction up to which extent this IPD technology can be utilized. With three lines: microstrip, grounded and ungrounded CPW simulated with probe pads in CST, we can make comparisons and draw conclusions based on the results we obtained. Table 6 shows a comparison based on the same silicon substrate with a length of 1 mm for all three mentioned transmission lines. Performances in terms of insertion loss for a 100 µm thick glass substrate ($\mathcal{E}_r$:4.9 and tanδ:0.0056) laminated with a 15 µm polymer layer ($\mathcal{E}_r$:3.2 and tanδ:0.0045) can be mentioned as: 3.5 mm long microstrip shows an insertion loss of 0.23 dB/mm at 110 GHz and an ungrounded CPW shows 0.21 dB/mm at 110 GHz and 0.27 dB/mm at 170 GHz respectively [23]

Table 6. Transmission Lines in a comparative way

Transmission Line	**S_{21} (dB)**	**Frequency defining S_{21} (GHz)**	**Line Z_0 (ohm)**
Microstrip	-1.5	250	42
Ungrounded Microstrip	-1.5	130	50
Grounded Microstrip (Via fenced)	-1.5	280	42.5

Beside the above-mentioned factors, the return loss can also be included in the comparison. An ungrounded CPW offers better return loss with high impedance closer to 50 ohms but with high insertion loss (by looking at the plots in Figures 56 and 57). Among grounded CPW and microstrip, a better choice can be made to proceed further for more complex structures implementation, as both have almost identical return loss but CPW offers less insertion loss. But for a CPW as compared to microstrip it might become a challenge for using it for example in an antenna application because various technology-related restrictions. Then a microstrip comes up to simpler in implementation to have the simplest form of microstrip patch antenna as to be tested.

3.6 DRC – Design Rule Check

Ongoing reduction in chip size (nanometer technology) with the increase in frequency range approaching THz ranges has increased the emphasis on Electronic Design Automation (EDA) to check for post layout verifications [25]. The DRC is what we can call it the conformity of a chip design with the certain set of rules by the chip manufacturer. DRC plays an important role in chip designing and manufacturing, so that it doesn't become a waste of time and resources [26]. Specially below 45 nm the complexity and importance of DRC becomes a challenge, which may require or apply new definitions with multidimensional layers DRC [27]. The DRC can be some constraints within one plane or a layer, but it can also be a restriction within multilayered structures. Mostly the DRC concerns are related to minimum spacing, widths and metal cuttings allowed [28], an example of different types of DRC restrictions is shown in Figure 62 within one metal layer:.

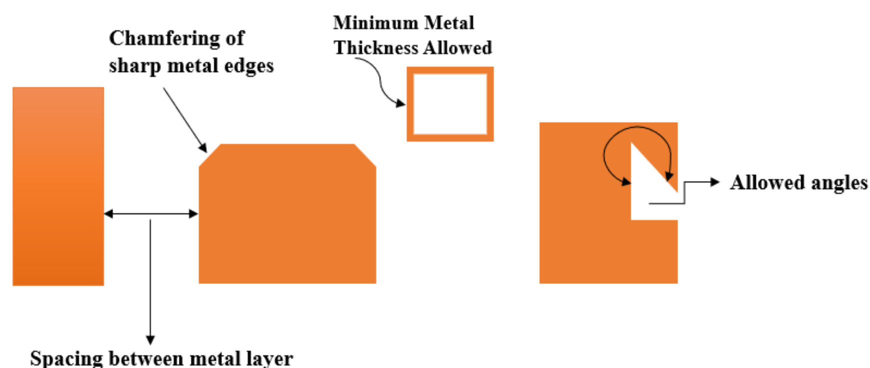

Figure 62. DRC within one layer

For this IPD technology by VTT, the DRC check was done using a tool kit for the software KLayout. After doing simulations in CST for transmission lines, there was an obvious need to check all the structures for DRC. These structures were checked for DRC individually before putting them on the chip as final layout.

3.6.1 Microstrip Structure

First structure to be checked in KLayout was microstrip. To have a layout in the DRC software, there was a need to convert the microstrip's metallic parts into a GDSii - Geometric Data Stream format. The 3D model in CST allows us to have a GDSii file containing multiple layers, while exporting GDSii file, the major hurdle was to have all the metal layers, vias, and probe pad metal to be on separate layers and not included into a single layer. 3D model in CST simulated was made on metal layers contact through vias, where a separation can't be created but to have a GDSii file, there must be an adequate separation between all the vias and metals to have a multilayered GDSii file shown in Figure 63. Otherwise CST exports it as a single layer.

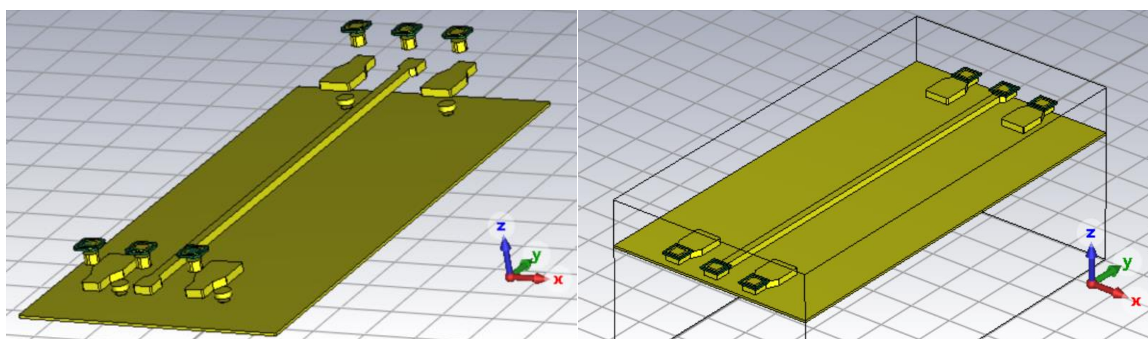

Figure 63. Separated vias and metals vs simulated microstrip

The simulations cannot be done with all the rounding and cuttings for probe pads, it was restricted by the meshing in CST. The homogeneity must remain there within the first three mesh cells. Due to this reason the proper rounding – blending in CST for metals was done later in only creation of GDSii file shown in Figure 64.

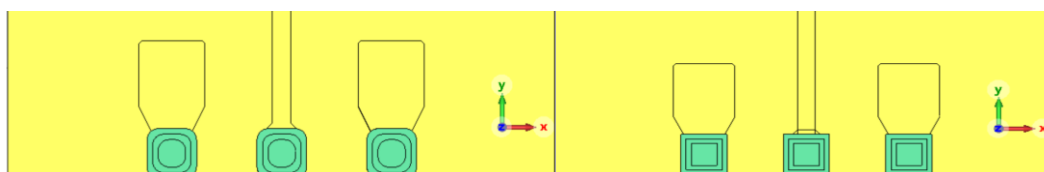

Figure 64. Probe pads with sharp edges (for meshing) & rounded probe pads

In KLayout, the GDSii file from CST can be imported but it does not give the metal layers code or layer specification and after importing it takes it as default layered structure. The layers specifications were done through editor in KLayout exactly as defined in the design rules. Later, after running the DRC code, we can have the errors if any in the form of different animations, but for the designed microstrip after DRC run, no error was found. A DRC clean microstrip is shown in Figure 65.

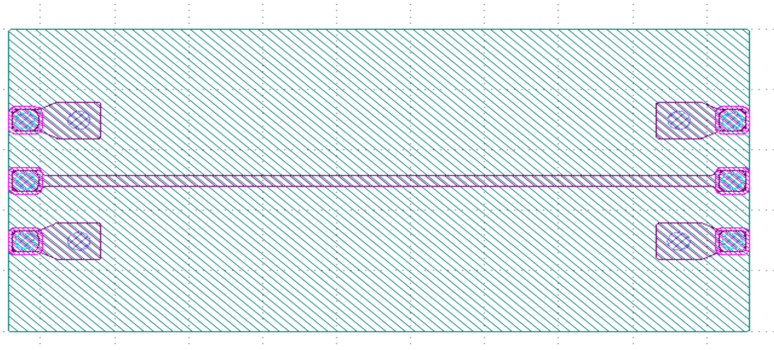

Figure 65. DRC check for microstrip (KLayout)

3.6.2 CPW with Ground Structure

Previously explained steps for DRC (microstrip), were considered for CPW. The simulated CPW was separated and a GDSii – multilayered shown in Figure 66 was created. Unlike microstrip, there was some more tapering involved and all the roundings and chamfering was done accordingly. Just like with the microstrip, the layers and vias mapping was defined in KLayout, and DRC run was done. There were also no errors found in this case, and a DRC clean structure is shown in Figure 67.

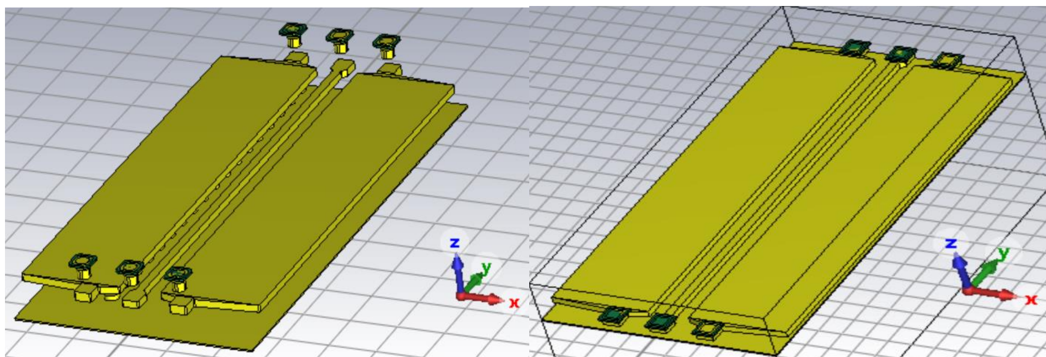

Figure 66. Separated vias and metals vs simulated grounded CPW

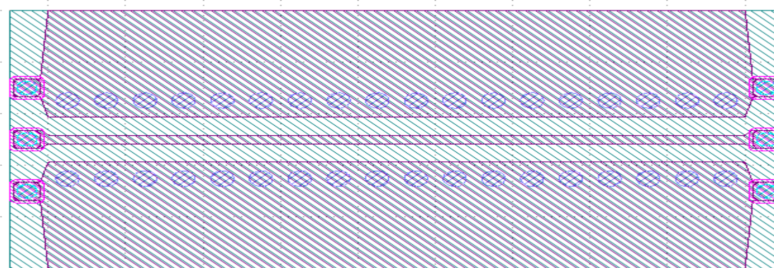

Figure 67. DRC check for grounded and via fenced CPW (KLayout)

3.6.3 Ungrounded CPW Structure

Variations occur between ungrounded CPW and grounded CPW, since there is no ground in this case as can be seen in Figure 68. The other variation was the width of the central signal line and the gap between ground and signal line. After separating the different metal layers, vias and probe pads, the GDSii was exported to KLayout. Factors affecting the geometry of any passive element were mostly distances within a layer, and sharp cutting edges. KLayout takes all the metal layers as polygons and the errors may be define in terms of convex or concave angles. But no errors were found so we had an error free structure shown in Figure 69.

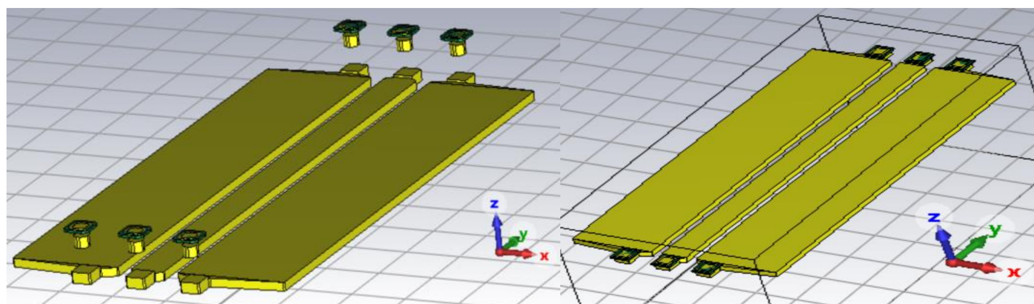

Figure 68. Separated vias and metals vs simulated ungrounded CPW

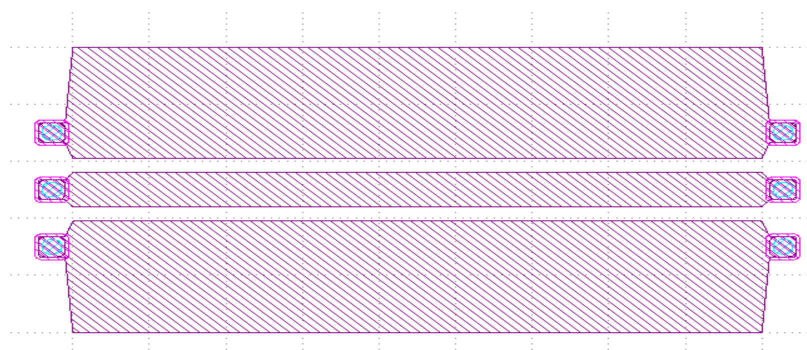

Figure 69. DRC check for ungrounded CPW (KLayout)

3.6.4 Via Transition Structure

Via transition involved some more geometric shapes in comparison with other structures. Major layer involving tapering was the metal 3 layer. All the transitions within a metal or to cross metals were rounded and tapered not to have any conflicts with the DRC. The separated different metal layers, vias, and pads are shown in Figure 70 as compared to what we had in the simulation case. When imported to KLayout, the layers were mapped again for design rules conformity and definition of the metal structures. After running DRC check, no violation was detected, and the structure can be considered as DRC clean visible in Figure 71.

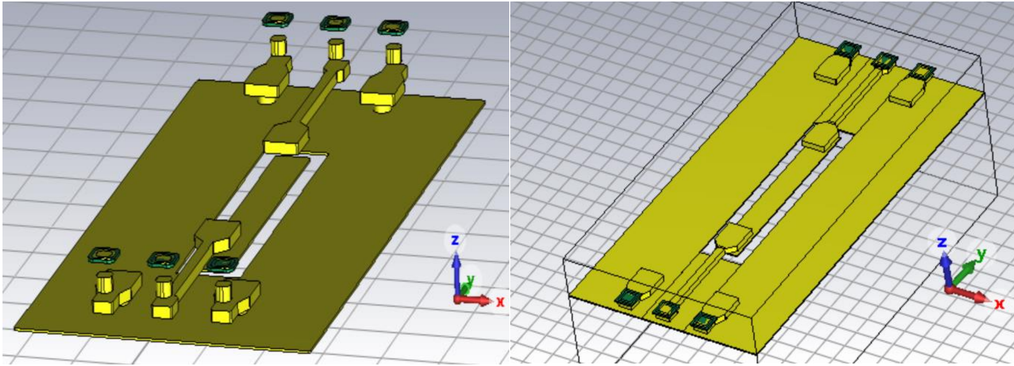

Figure 70. Separated vias and metals vs transition structure

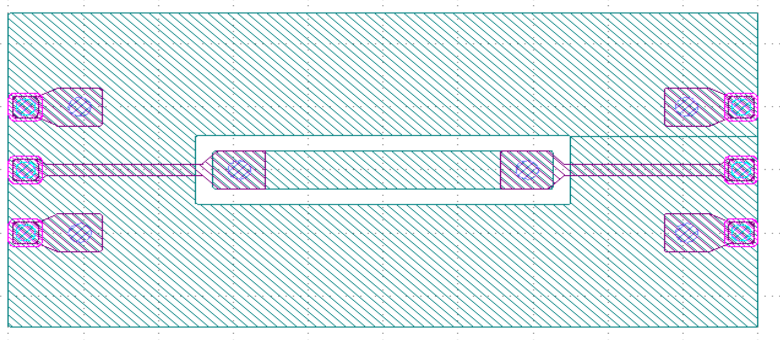

Figure 71. DRC check for microstrip to ungrounded CPW transition (KLayout)

4 Antennas

Using IPD technology, antennas can be implemented as two-dimensional planar antennas. Planar antennas offer the benefits like low profile, lighter weight, lower in cost, easy integration with other electrical circuits and they are also versatile in many aspects like (varying in shapes, resonant frequency, impedance, and polarization etc.) [29]. On the other side they still have limitations such as narrower bandwidth, low gain, and limited power handling capacity [30].

In wireless communications with the ongoing push towards higher frequency range, the importance of electrically small antennas is becoming important and can be found everywhere in a wireless communications system, and planar antennas provide us their applicability in various wireless systems. One of their versatilities is their reconfigurability in terms of operating frequency, type of polarization and switching from one type of radiation pattern to another [31].

4.1 Single Patch Antennas

Planar antennas can be microstrip patch antennas, slot antennas, suspended plate antennas, sheet monopoles and dipoles etc. [32]. For a single patch element to be made as a starting point, a microstrip patch antenna with a single feed can be selected. Basic structure of a microstrip patch antennas consists of a feeding line, a radiating patch, substrate and ground beneath the radiating patch. Depending upon the required gain or bandwidth, the microstrip patch antennas can be a rectangular shaped, circular one, triangular or even an elliptical shaped shown in Figure 72:.

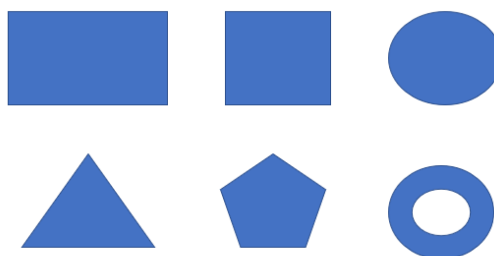

Figure 72. Different shapes of patch antennas

Microstrip patch antennas form a basis for implementing arrays which in return find their application in mm-wave radar, sensing and in wireless communications systems. With the current day automotive radar application till 60 GHz, the microwave imaging at 94 GHz, the frequency above 100 GHz is of special interest in research [33].

4.1.1 D-Band Antenna

Frequency band of 110-170 GHz, being the core targeted band in this thesis was selected as AiP implementation's starting range. AiP in system in package (SiP) doesn't only address the problem of putting low noise amplifiers (LNAs), power amplifiers (PAs), transceivers and filters with antennas in RF front end but also provides us with better signal integrity, lesser signal attenuation and cope up with propagation problems at high frequencies [34]. Achieving high end frequency range in different wireless applications like in 5G mobile networks (Ka band 26.5 to 40 GHz), in ISM (industrial, scientific and medical applications), for some sensing

devices 60 GHz has been achieved. In automotive industry, 77 GHz radar performed better than 24 GHz band (better accuracy and resolution) [35].

With an increasing trend in the frequency range specially going beyond 100 GHz and above, the next important band is the D-band. This band provides us with improved data-rates over short range communications, may give us the upcoming solutions for implementing highly dense networks for beyond 5G [36], the applicability of this band shows it potential over longer – 60 km range communications in the form of radar transceiver at 122 GHz [37]. The sub band (130-150 GHz) of D-Band offers lower atmospheric absorption which results in lowering path loss, this range looks suitable for long range wireless applications [38].

For the first rectangular patch antenna, the frequency selected was 150 GHz. In a rectangular patch antenna design, given with the three terms: f_r – resonance frequency, $\mathcal{E}_r$, and h – height of the substrate, L and W (length and width of patch) being important parameters based on the factors which include: $\mathcal{E}_{reff}$ and ΔL (effective length) of the patch, can be calculated using the equations 22 -25 from [9]:

$$W = \frac{v_o}{2f_r}\sqrt{\frac{2}{\varepsilon_r+1}} \qquad (22)$$

Where v_o is the free space velocity on the above equation 22,

$$\varepsilon_{reff} = \frac{\varepsilon_r+1}{2} + \frac{\varepsilon_r-1}{2}\left[1 + 12\frac{h}{W}\right]^{-1/2} \qquad (23),$$

for $W/h > 1$,

$$\frac{\Delta L}{h} = 0.412\frac{\left(\varepsilon_{reff}+0.3\right)\left(\frac{W}{h}+0.264\right)}{\left(\varepsilon_{reff}-0.258\right)\left(\frac{W}{h}+0.8\right)} \qquad (24)$$

$$L = \frac{\lambda}{2} - 2\Delta L \qquad (25)$$

With the above-mentioned equations, we can find the antenna's patch basic dimensions L and W, the other values in the rectangular patch which cannot be neglected are the inset feed y_0 and inset feed gap. The latter two factors help us to achieve the desired resonance at a certain frequency. The rectangular patch antenna's example with the all the mentioned dimensions is presented in Figure 73.

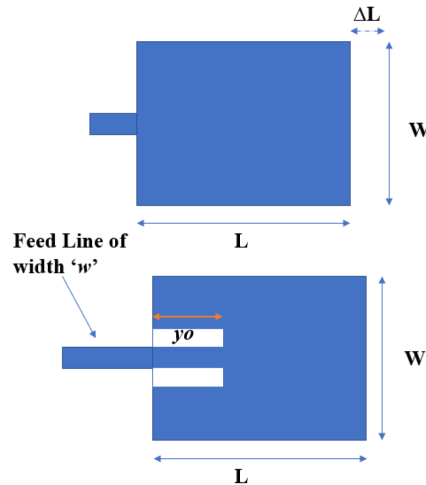

Figure 73. Rectangular Patch Antenna

The inset feed is an important thing for an antenna to be resonating at the desired frequency, which is dependent on the factors R_{in} (input resistance at radiation edge from feed line) and the Z_o characteristic impedance of the feed line (in this case a microstrip). R_{in} can be found either by the equation 26 manually or there is an option in CST for de-embedding the port and finding the input impedance just at the edge of the radiating element.

$$R_{in}(y = y_o) = R_{in}(y = 0)cos^2\left(\frac{\pi}{L}y_o\right) \tag{26}$$

Inset feed gap choice may varies but as starting point it can typically chosen to be $W/10$, $W/15$, $W/20$, $W/25$ etc., where W is width of the patch [39].

From equations (22)-(26), the values of L, W, and y_o, were calculated manually and the desired frequency resonance was not achieved. Even the patch started radiating at lower frequency range around 140-145 GHz, the results within this range show low gain, low radiation efficiency and directivity which was discouraging. After the simulation for 140-150 GHz range, the next frequency was simulated for 160 – 170 GHz range. Some useful online sources were then used to verify hand calculations, the values were chosen for 170 GHz and later tuned to get the required frequency around 165 GHz with 42-ohm feed line (quite challenging as it not 50 ohm). The dimensions for f_r = 166 GHz based on hand calculations, and two online sources [40], [41] (for cross verification) along with the ground size, which can be of the size: L:6h + L (length of the patch), W:6h + W (width of the patch) – short edge [42], but not in this simulated case are given in Table 7

Table 7. 166 GHz Antenna's dimensions

Antenna (f_r)	166 GHz
Patch Length (*L*)	467 µm
Patch Width (*W*)	592 µm
Inset feed (y_0)	130 µm
Length of feed	501 µm
Ground size (*L*x*W*)	1469 x 1591 µm

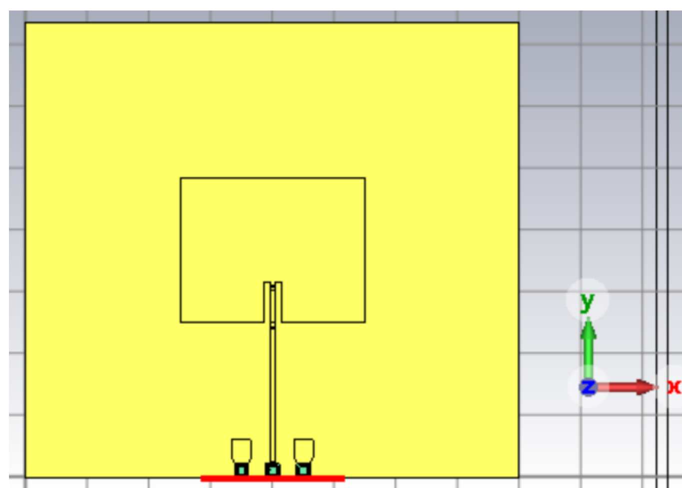

Figure 74. Rectangular Patch Antenna – 166 GHz

The 3D metal stack (antenna patch, ground and inset feed) is shown in Figure 74. After simulation the antenna started resonating at 166 GHz with a narrow bandwidth which was expected for a patch antenna. Important factors after simulation in CST for antenna's performance point of view can be regarded as antenna efficiency, antenna's directivity, and gain. Antenna's matching in terms of S_{11}, efficiencies and gain from CST simulations are visible in Figures 75, 76 and 77, respectively.

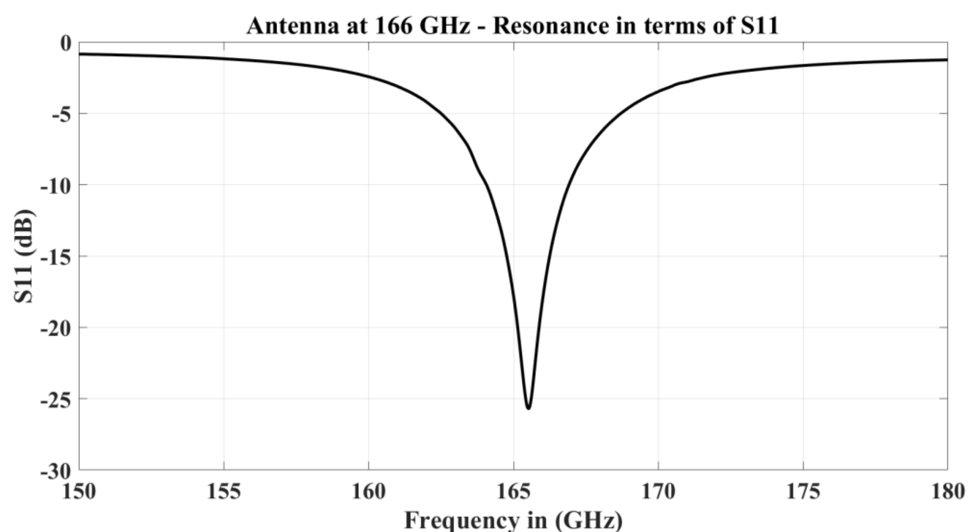

Figure 75. 166 GHz Antenna Matching in Terms of S_{11} (dB)

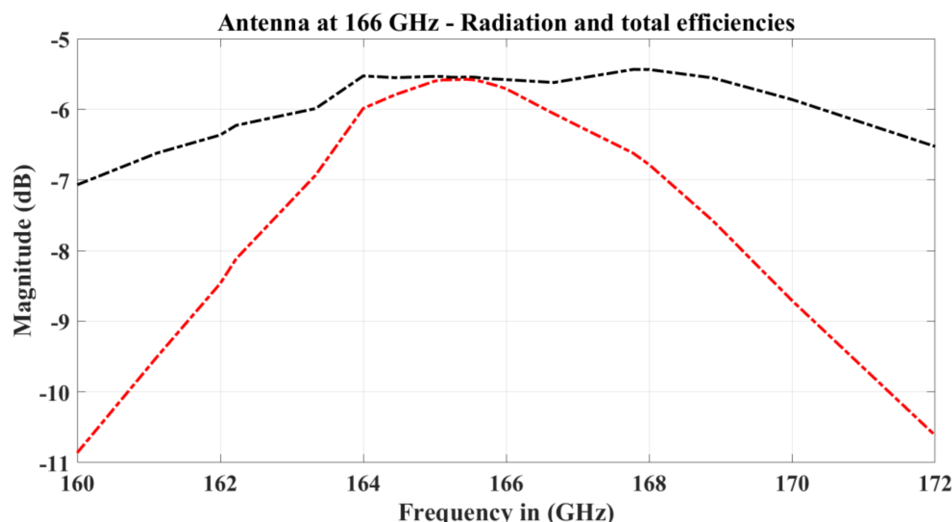

Figure 76. 166 GHz Antenna Radiation & Total Efficiencies

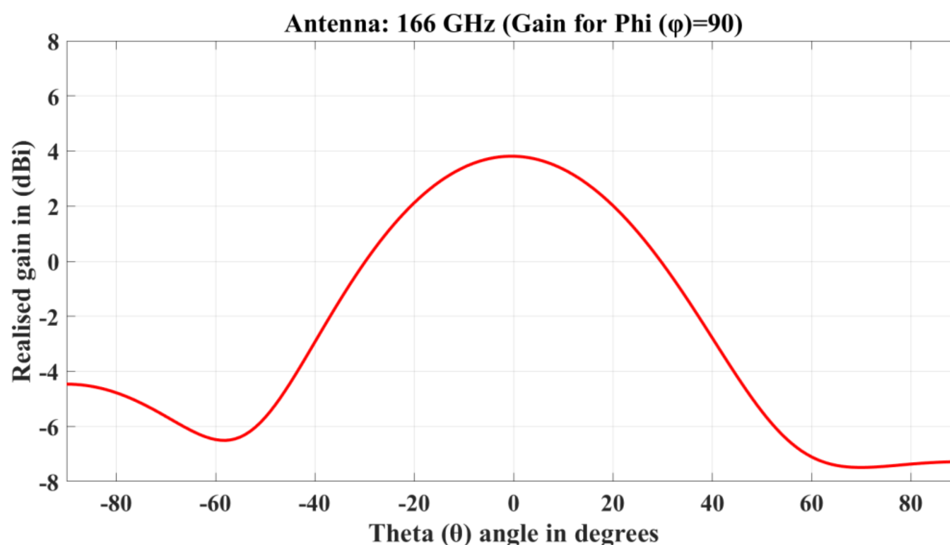

Figure 77. 166 GHz antenna gain

4.1.2 G-Band Antennas

A reasonable gain as compared to lower side of D-band at 165 GHz gave a ground to push forward antennas in the higher frequency range and see the effect of shifting in the higher end in this IPD. The starting frequency selected for the G-band antennas was for frequency range 240-250 GHz. The dimensions *L*, *W*, feed length and inset feed were calculated with the same set of equations for 166 GHz antenna case, these values were also cross verified from the online sources in a similar fashion like for D-band. After tuning (several simulations run), the dimensions for the patch antenna resonating at 234 GHz are shown in the Table 8

Table 8. 234 GHz Antenna's dimensions

Antenna (f_r)	234 GHz
Patch Length (*L*)	325 µm
Patch Width (*W*)	406 µm
Inset feed (y_0)	104 µm
Length of feed	354 µm
Ground size (*L*x*W*)	1028 x 1105 µm

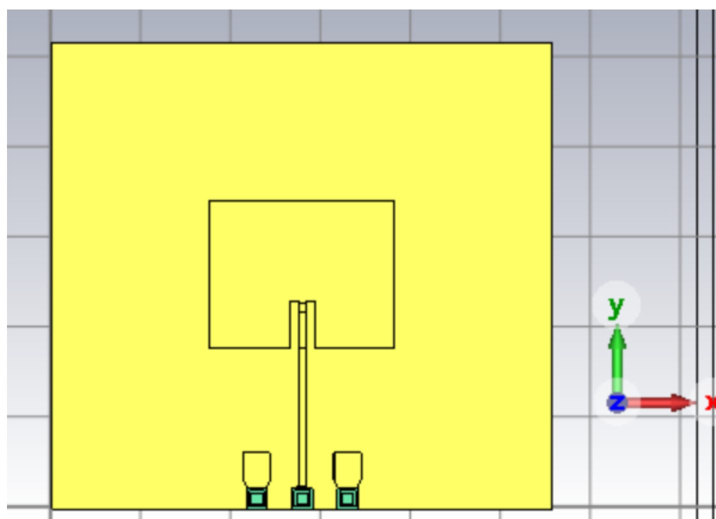

Figure 78. Rectangular Patch Antenna – 234 GHz

A significant rise was observed in terms of directivity and gain as compared to D-band, after simulation. The radiation efficiency was not as much improved which can be seen in Figure 80. The resonance frequency plot with narrow fractional bandwidth can be seen in Figure 79. The 3D model and gain can be seen in Figures 78 and 81, respectively.

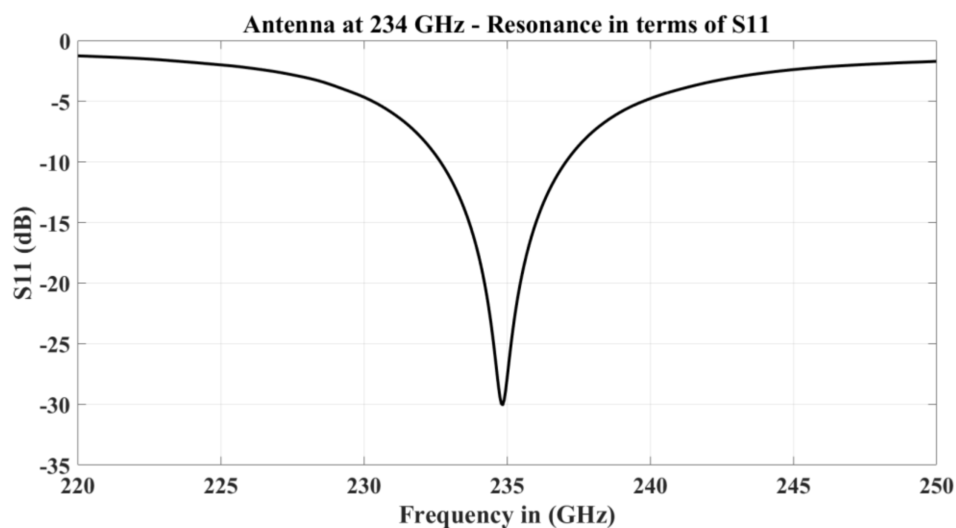

Figure 79. 234 GHz Antenna Matching in Terms of S_{11} (dB)

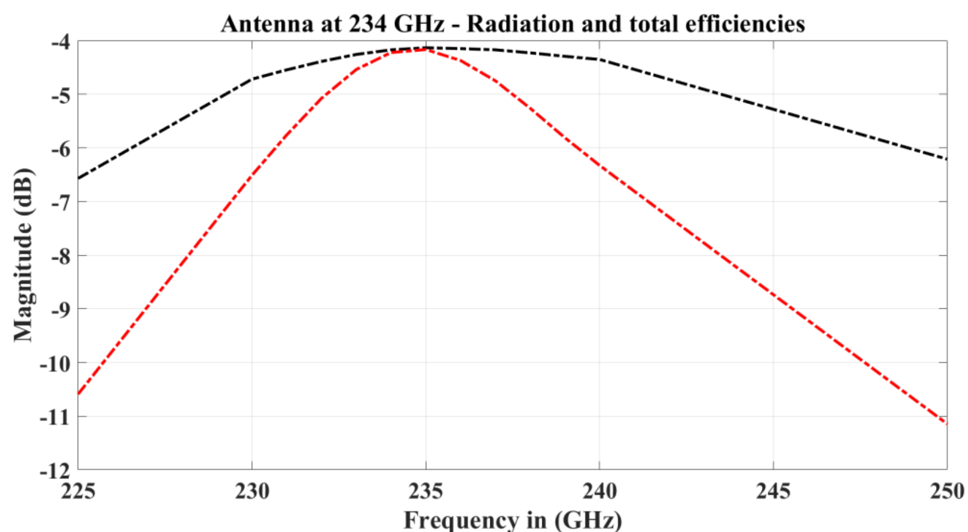

Figure 80. 234 GHz Antenna Radiation & Total Efficiencies

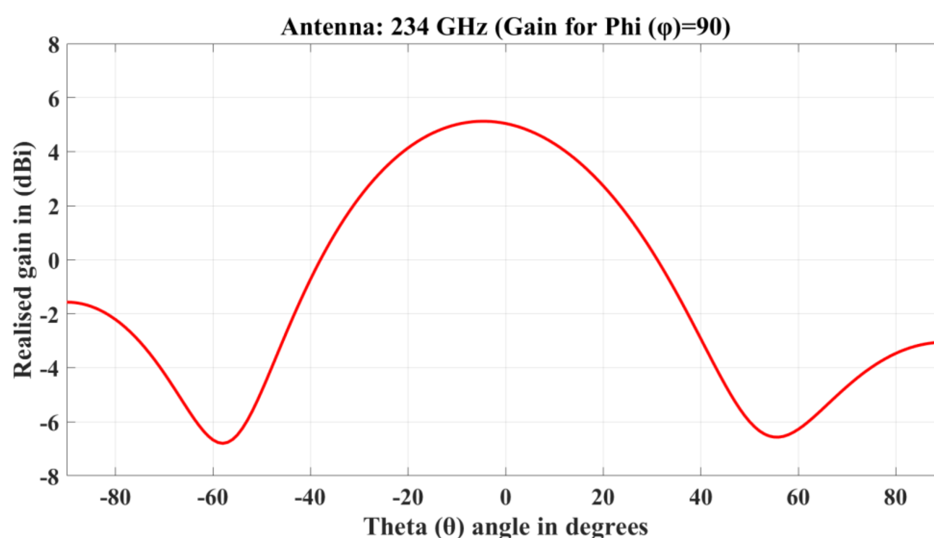

Figure 81. 234 GHz antenna gain

With an ongoing demand of the increased data rates, there is an obvious demand for broader bandwidth for radio access technologies. From 22 MHz channels in IEEE 802.11–1997 to a demand now in several GHz range, this demand can only be fulfilled if we go beyond 100 GHz, as there is no possibility of getting a bandwidth broader than 10 GHz and it has been comparatively unexplored region as compared to mmWave and infrared range [44]. This limitation gives a push to go for THz (from 100 to 10,000 GHz) range [45]. Due to high free space losses in the range going beyond 100 GHz [47], some highly directional antennas are needed for communications systems with good coverage range. There can be many available options to implement antennas for THz communications, but majority of THz antennas can be obtained by modifying mm-Wave antennas, but they need further improvement and optimization.[43]

In the lower THz frequency range (252 - 325 GHz) [43] depending upon the facility to measure up to 330 GHz in the EMC lab of University of Oulu, the dielectric type THz antennas can be simulated above 300 GHz (to see the trend in gain and directivity increase) in comparison with the previous ones. The next planar antenna was for 302 GHz, the dimensions for this patch are shown in Table 9.

Table 9. 302 GHz Antenna's dimensions

Antenna (f_r)	302 GHz
Patch Length (L)	249 µm
Patch Width (W)	323 µm
Inset feed (y_0)	70 µm
Length of feed	276 µm
Ground size (LxW)	796 x 864 µm

Figure 82 shows the simulated 302 GHz antenna with same boundary conditions and re-normalized to 50 ohms form center of the probe pads. The graphs in Figures 83, 84 and 85 show us the resonance frequency in terms of S_{11}, radiation efficiencies and gain. The gain appears to be lower than 234 GHz antenna but there can be seen an improvement in the radiation efficiency for this range.

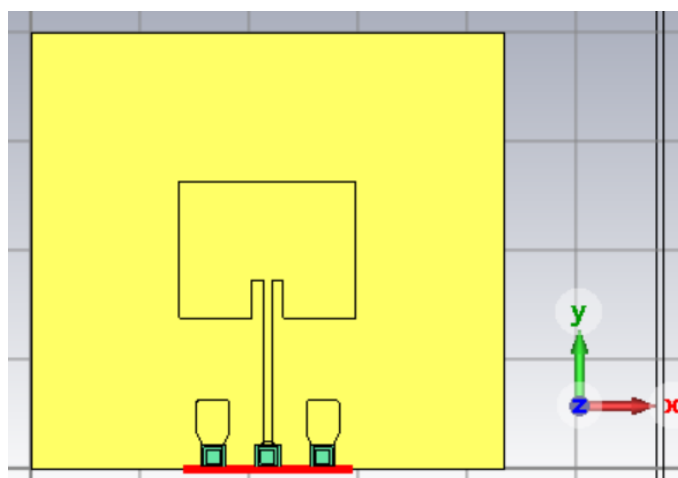

Figure 82. Rectangular Patch Antenna – 302 GHz

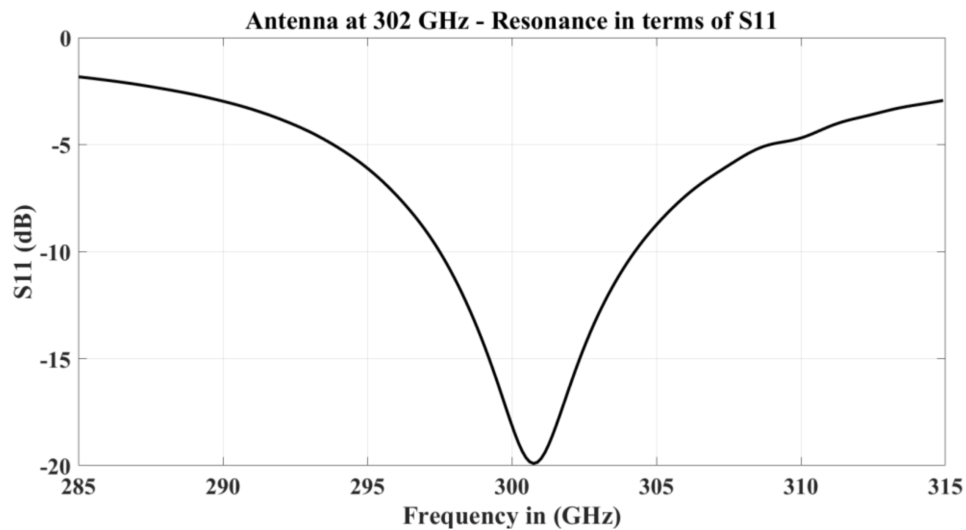

Figure 83. 302 GHz Antenna Matching in Terms of S_{11} (dB)

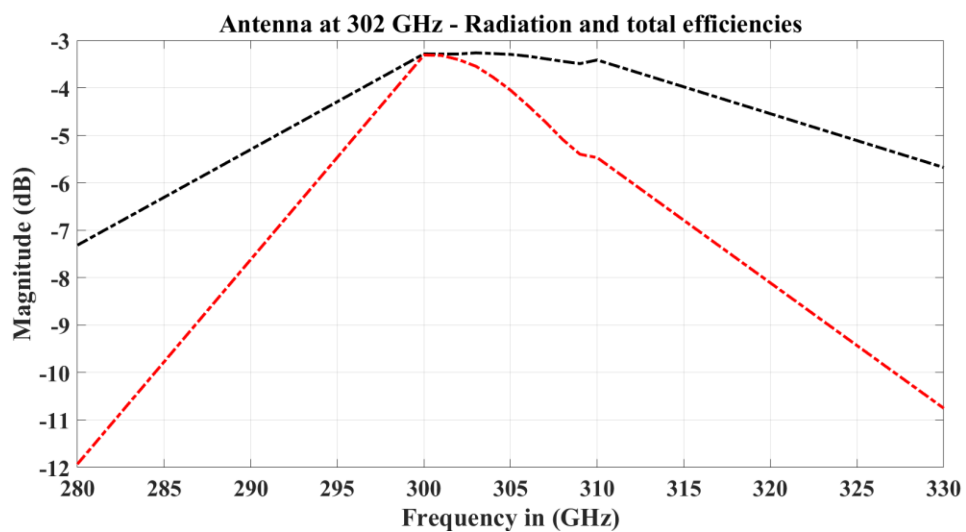

Figure 84. 302 GHz Antenna Radiation & Total Efficiencies

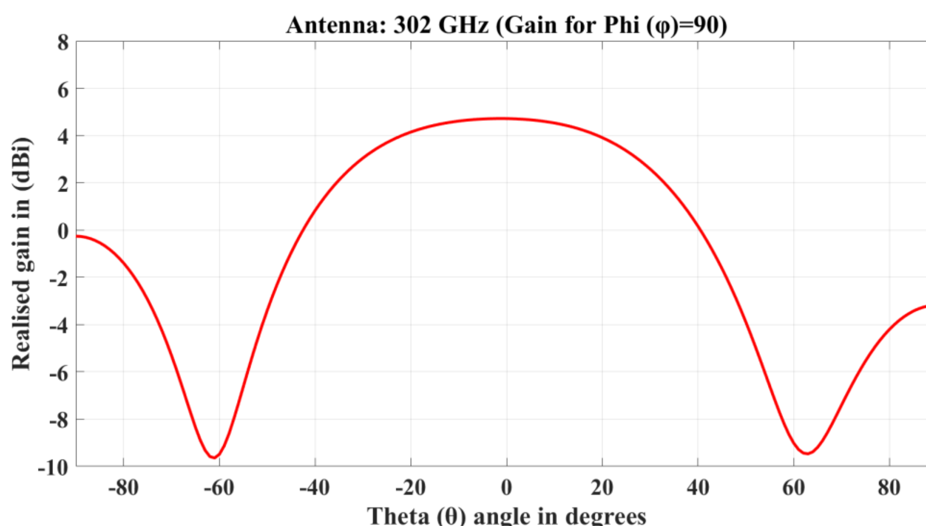

Figure 85. 302 GHz antenna gain

Gain comes up with a decreasing manner when the 302 GHz antenna is simulated. To verify this decreasing trend in terms of gain, the next simulated planar antenna was at frequency higher than 302 GHz (10 GHz higher), so another simulation was carried out for 312 GHz frequency. The width *W*, length *L*, and the feed length along with other dimensions are presented in Table 10.

Table 10. 312 GHz Antenna's dimensions

Antenna (f_r)	312 GHz
Patch Length (*L*)	239 µm
Patch Width (*W*)	310 µm
Inset feed (y_0)	67 µm
Length of feed	268 µm
Ground size (*L*x*W*)	770 x 836 µm

The metallic structure of the antenna surrounded by the polyimide layers is visible in Figure 86 with ground. After simulation, we can see that the gain was not increased and also there was no change in terms of radiation efficiencies. The resonance frequency plot, radiation efficiencies and gain plot are shown in Figures 87, 88 and 89, respectively.

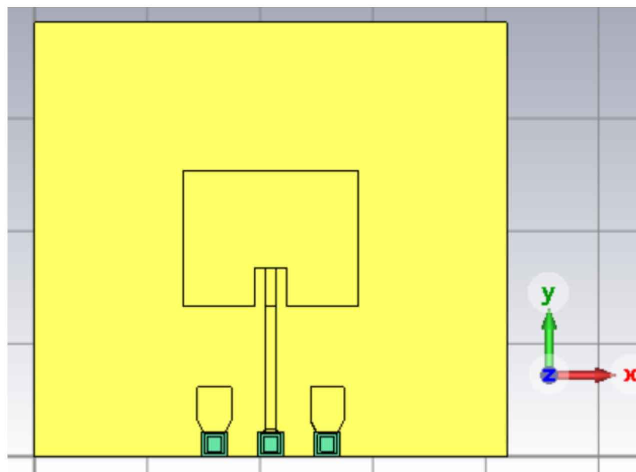

Figure 86. Rectangular Patch Antenna – 312 GHz

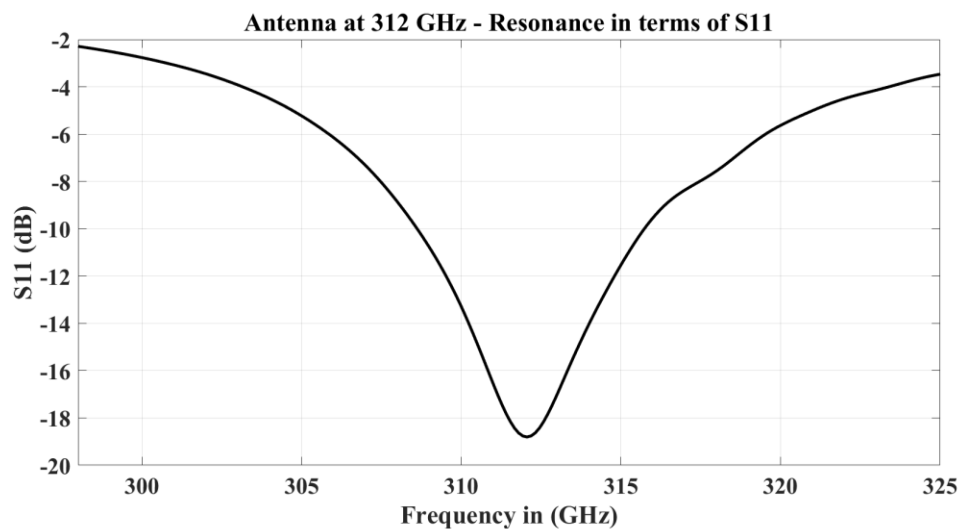

Figure 87. 312 GHz Antenna Matching in Terms of S_{11} (dB)

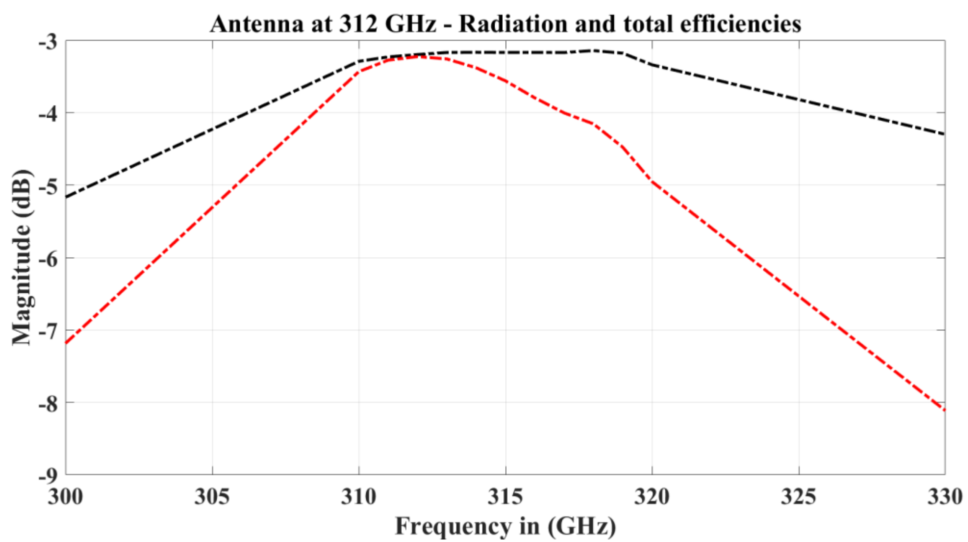

Figure 88. 312 GHz Antenna Radiation & Total Efficiencies

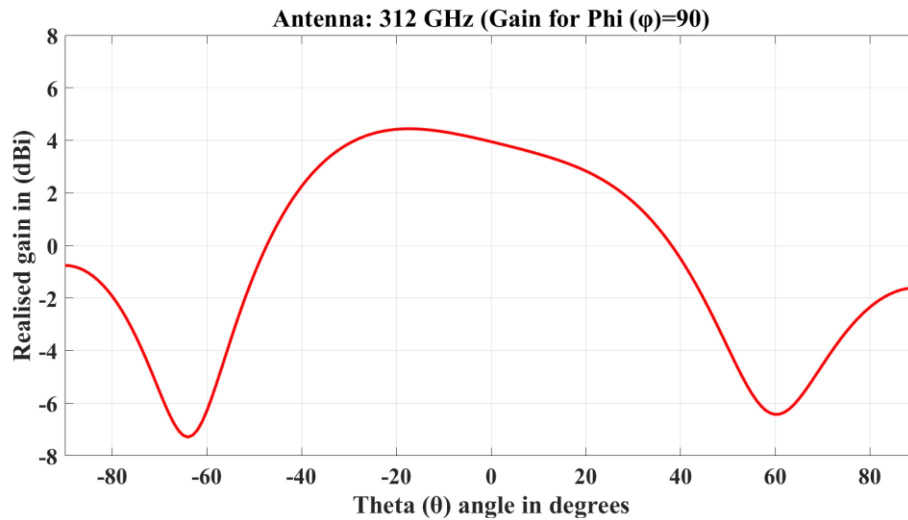

Figure 89. 312 GHz antenna gain

4.1.3 Antennas comparisons

Covering the frequency range from 165 GHz to 312 GHz at five distinct single frequencies, we have seen the changes in terms of gain, radiation efficiency, directivity and fractional bandwidth from single patch antenna point of view. Substrate material, height (*h*), and thickness of top metal 3 layer can be regarded as main factors for antennas performance. Modifying the substrate height affects the antenna properties. For example an increment in *h* may cause decreased radiation efficiency, gain and reduction in the impedance of antenna but it can cause increase in antenna's directivity and bandwidth [46]. The selection of substrate material also reflects on the antenna's gain, taken as an example at 39 GHz for a material – Teflon with $\mathcal{E}_r$ (2.0) shows highest antenna gain – 7.037 dBi as compared to other two materials: Duroid 5880 with $\mathcal{E}_r$ = 2.2 showing gain of 6.52 dBi and a common printed circuit board (PCB) material FR4 having $\mathcal{E}_r$ = 4.6 with a gain of 2.76 dBi [48].

With all the design rules to be followed, designed and simulated single rectangular patch antennas at the frequencies: 166, 234, 302 and 312 GHz can be compared in different terms: gain, directivity, radiation efficiencies and FBW (fractional bandwidth) as represented in Table 11. For all these antennas, when the ground dimensions – length and width were enlarged ($\lambda/2$) from the patch in all directions, a significant enhancement in the gain was observed, especially for the antenna resonating at 166 GHz showed 1.6 dBi initially. After changes made in the ground size, its directivity turns out to be around 3.8 dBi.

Table 11. Antennas Comparison

f_r (GHz)	Gain (dBi)	Directivity (dBi)	Radiation efficiency (dB) at f_r	FBW (%)
166	3.81	9.51	-5.57	1.81%
234	5.12	9.34	-4.17	2.13%
302	4.71	8.15	-3.29	2.64%
312	4.42	7.65	-3.19	2.24%

At D-band, based on the dielectric material used as substrate we can have look at some other materials and technologies as compared high resistivity silicon used in for the IPD technology used in this thesis work. Based on substrate material, a single element patch antenna at 146 GHz on a quartz glass substrate without any vias presence shows a gain of 6.6 dBi [49]. In terms of different technologies like PCB and LTCC, when the single element of cavity-backed aperture-coupled patch antenna type is implemented using 4 metal layers PCB with Megtron 7N (ε_r = 3.20) as substrate at 143 GHz gives a gain of 7 dBi [50]. By using LTCC, at 170 GHz with dielectric as substrate- polyimide (ε_r = 3.10), metal as gold (3 µm thick) – single metal layer, the CPW-fed planar bow-tie dipole antenna shows a high antenna gain of 14 dBi [51].

At G-band, we have witnessed with simulation results the trend of increasing the antenna gain and directivity with increasing frequency up to 234 GHz, after that gain doesn't increase even up to 312 GHz using the IPD technology. Unlike silicon used as substrate, an elevated microstrip patch antenna with Si-GaS substrate (ε_r =12.9) fabricated with III-V PA air-bridge technology at 206 GHz offers broader bandwidth of 12.5 GHz and a realized gain of 5.5 dBi [52]. For 300 GHz range, a dipole planar antenna with a reflector simulated with gold as metal and a polymer BCB (Benzocyclobutene) (ε_r = 2.5) based substrate shows a gain of 5.14 dBi and an impedance bandwidth of 116 GHz [53]. Another single patch antenna at 300 GHz quartz-based substrate separated by BCB layer of thickness 4 µm with two metal layers of gold can be mentioned here as a comparison to 302 GHz antenna mentioned in Table 7, showing a gain of around 10 dBi and bandwidth of 30 GHz [54].

4.2 Multiple Elements Antenna Array

The use of antenna arrays rather than single element patch antenna is more diverse in various applications. Antenna arrays help to get some specific patterns, cause enhancement in gain, directivity and some other functions which are not achievable with single element antennas. Common ways to have an antenna array are either series feed or corporate feed network [9]. A series fed array is shown in Figure 90. In both D and G bands, simpler arrays of two to three elements were simulated, which are discussed in detail in the following subsections.

4.2.1 D-Band Antenna Array

At this band, a single patch antenna was already simulated at 166 GHz, so an array comprising of two patches as starting point can be made to see the effect of multiple elements. To adopt either of the ways: series or corporate was not a choice with this IPD, because of the highest achievable impedance with the technology used was 42.5 ohms. Implementing a corporate type of array may require changes in the impedance usually from lower to higher in terms of power division. The only option to implement an array of two elements was to use series feed.

The feed line length for the patch was same as used for 166 GHz single element but there was an addition of another patch with the same feed line *λ/2* apart from first element, and this array is shown in Figure 90. The variations lie in terms of patch length used for 166 GHz, which was slightly changed to get rid of the main-lobe splitting, and there was an extension of the ground plane unlike a single element ground.

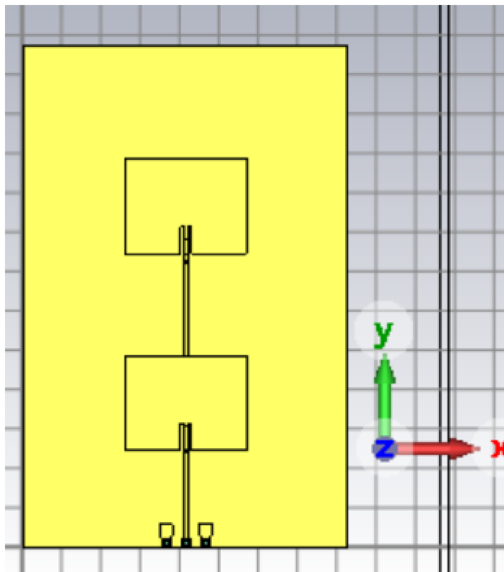

Figure 90. 2-Element series feed 166 GHz array

After getting the simulation results from CST, Figure 91 shows the combined effect of two elements in terms of resonance we get. There was an increase in the gain and directivity of which gain is presented in Figure 92.

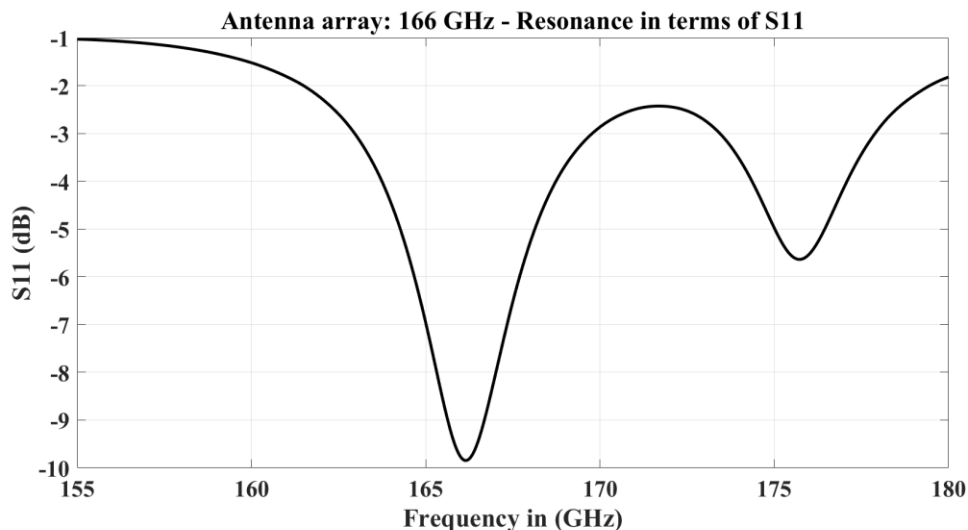

Figure 91. 2 element array at 166 GHz antenna matching - S_{11} (dB)

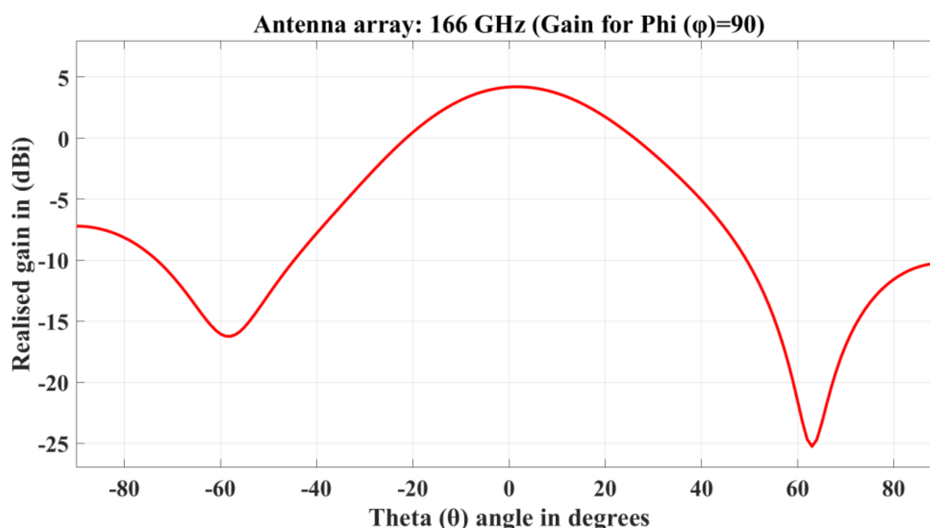

Figure 92. 2 element array combined gain at 166 GHz

4.2.2 G-Band Antenna Array

Within the D-band frequency range, the idea to use the series feed with three antennas doesn't seem to be promising or useful as expected. Depending upon the technology constraints, and from series feed simulation results, there seem to be a need of some other approach different from both series and corporate feeds. At the G-band, the single element already being tested by simulation was at 234 GHz. So, the three-element array was made of 234 GHz antenna, the approach for this type of array was to use the parasitic patches around the main central radiating patch. The idea to have this approach is inspired from the paper [55], in which a 300 GHz on-chip antenna comprising of three elements using passive coupling approach between the main and parasitic patches to get a broad matching bandwidth of 26 GHz is presented.

To have an array of 3 elements at 234 GHz through capacitive coupling, we can have the same structure for the central patch, the other deciding factors were the dimensions (length and width) of the parasitic patches around the central patch and the coupling gap between them. Some slightly different sizes as compared to the central patch were tried out and after few simulations, a size was selected shown in Figure 93, because of the useful outcomes in terms of gain and directivity increment (though not achieving the broader bandwidth).

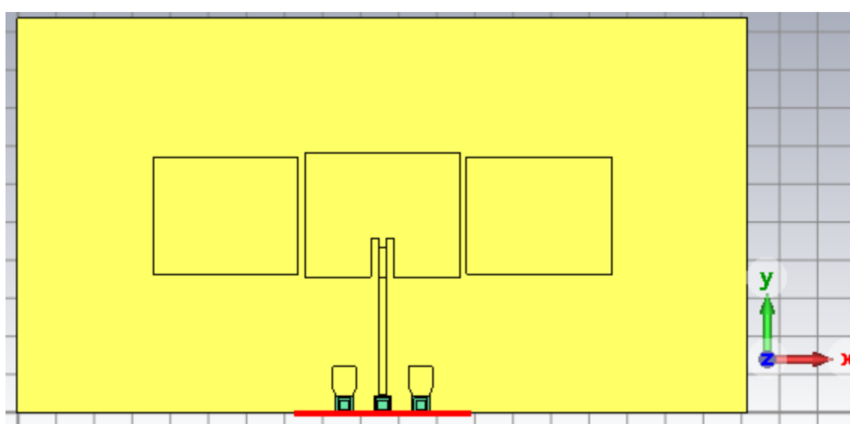

Figure 93. 3 – element capacitive coupling 234 GHz

With the simulation of this array, we can see the matching in terms of S_{11} (dB) in Figure 94. There was an enhancement of both directivity and gain but the gain is shown in Figure 95.

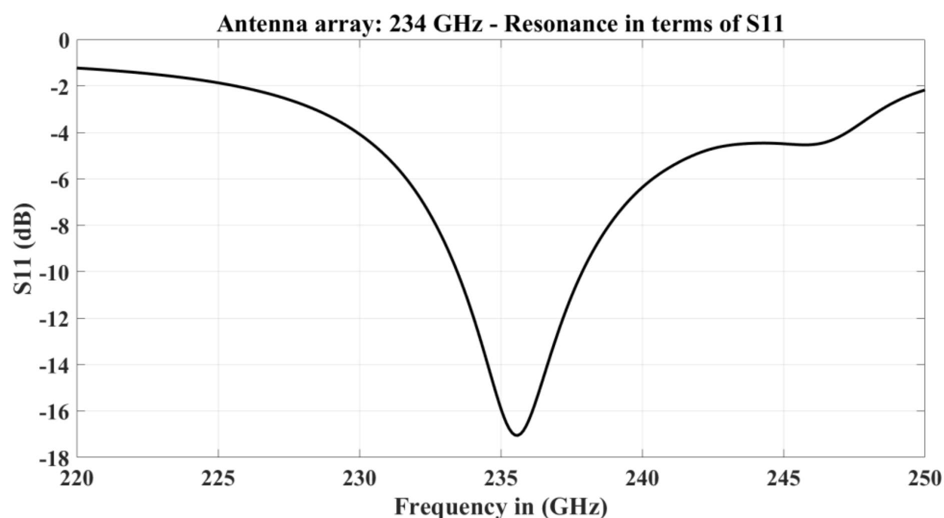

Figure 94. 3 element array at 234 GHz antenna matching - S11 (dB)

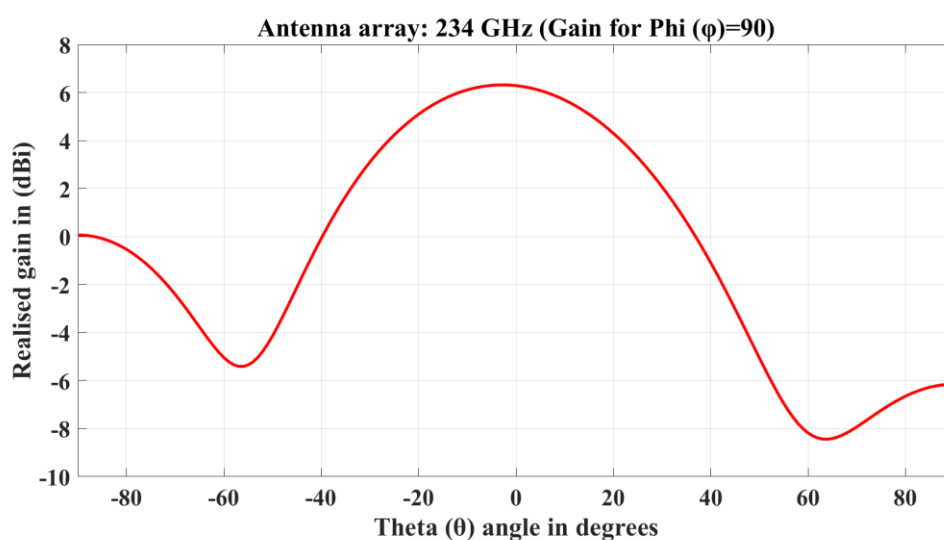

Figure 95. 3 element array combined gain at 234 GHz

4.2.3 DRC – Design Rule Check (Antenna Structures)

Like the transmission lines and all other passive structures to successfully implemented using IPD technology must obey the design rules and pass the DRC check in KLayout. So, the antennas at the frequencies: 166, 234, and 302 GHz with the metal layers involved and vias with probe pads were checked for DRC. All the structures were checked separately and there comes no DRC error after running the test. Figures 96, 97 and 98 show these antennas, respectively.

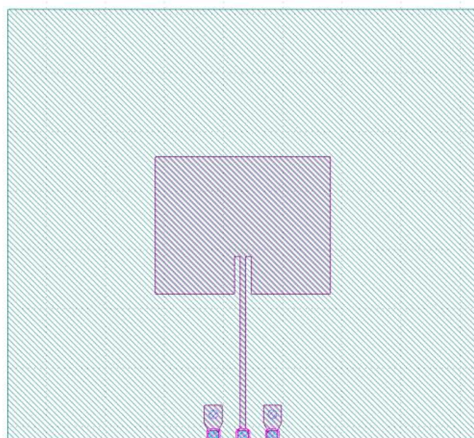

Figure 96. DRC check for 166 GHz antenna (KLayout)

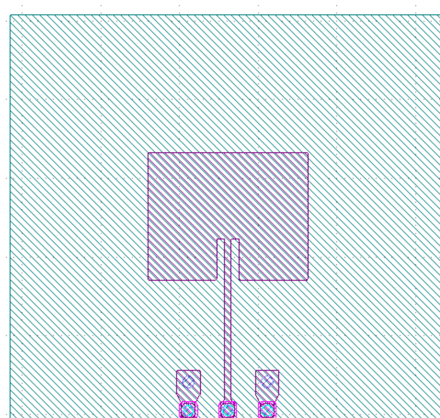

Figure 97. DRC check for 234 GHz antenna (KLayout)

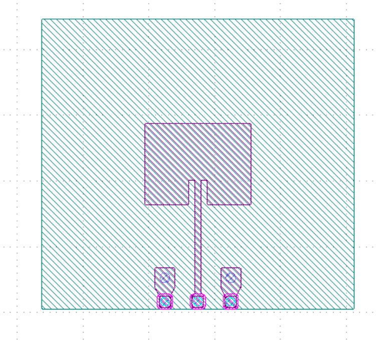

Figure 98. DRC check for 302 GHz antenna (KLayout)

The arrays for D-band were also checked for the DRC errors, as the 2-element array found to be good as both directivity and gain were increased. Therefore, Figure 99 shows a DRC clean two-element array at 166 GHz. The array of 3-elements with parasitic patches, vias and probe pads was checked for the DRC and there were no conflicts found with the set of rules defined by the technology. Figure 100 shows the DRC free structure of this 3-element array.

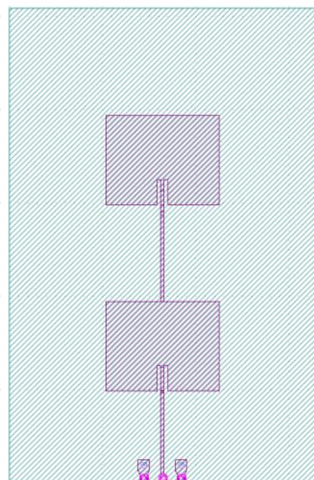

Figure 99. DRC check for 2-element 166 GHz array (KLayout)

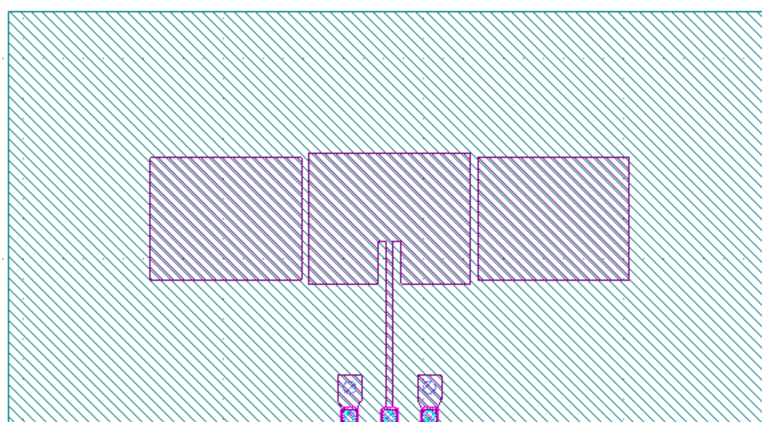

Figure 100. DRC check for 3-element 234 GHz array (KLayout)

4.2.4 Antenna arrays observations

While there can be any number of antenna elements that can be combined to get a desired output out of antennas, the minimum number of elements combined taken as 2 or 3 antennas can be regarded as an initial estimation of how antennas will behave when joined together as an array. This number can further be increased for the type of application used.

Both numbers of antenna elements (2 and 3) implemented in terms of an array at 166 and 234 GHz frequencies respectively, shows us an idea of array implementation. When looking at Figure 91 we see that there are some notches above the desired f_r for 166 GHz, and with some more tuning and optimization this may help to increase the bandwidth. This case applies to the 234 GHz 3-element array as well, as there is an additional resonance with a matching of -4.5 dB above 245 GHz as seen in Figure 94. There was a clear increment for both directivity and gain for both scenarios: 0.38 dBi enhancement in terms of gain and 0.95 in terms of directivity for 166 GHz array; and 1.16 dBi was raised in terms gain and 0.92 dBi for directivity in 234 GHz array. When the number of elements increases in series feed type implementation, the main beam becomes split, and this problem was observed when implementing 3 elements.

5 RF Filters

RF filters can be regarded as broad term, but the ranges of frequency were implied in filters. As the technology used for filter implementation is same as for antennas and other passive elements in previous simulations in this thesis, which is two-dimensional and planar. So, the options for planar filters were considered. Microstrip filters can be called a good choice for planar filters realization, though there are possibilities using CPW, strip line or cavity-based resonators. Using microstrip, there is a freedom to choose the type of filter we want to get out of microstrip, the decision must be made among edge coupled or end coupled configurations. Considering the single line microstrip's behavior, and dimensions, edge-coupled filter was chosen.

5.1 Edge-Coupled Bandpass Filters

Not going beyond the allowed area by the technology, and the targeted band (110-170 GHz), the starting point was getting a filter at a frequency above 120 GHz. Going in the higher range in terms of frequency aid to have miniaturization which eventually helped in obeying the area constraints. Among low-pass, high-pass, band-pass and band-stop types, a band-pass filter is chosen to get out of edge-coupling between microstrip. Because the relevancy of the band-pass filters related research specially – multiband type in modern wireless networks and almost in every transmitter or receiver front ends band-pass filters find their application [56].

The design specifications of the band-pass filter at a frequency above 120 GHz are: 4th order 0.1 dB ripple Chebyshev type. To get the dimensions: length of microstrip line, the spacings between coupling elements, we need to calculate the even-odd impedances from the equations 27 and 28 taken from the book [4]:

$$Z_{0e} = Z_0[1 + J.Z_0 + (J.Z_0)^2] \quad (27)$$

$$Z_{0o} = Z_0[1 - J.Z_0 + (J.Z_0)^2] \quad (28)$$

where Z_0 is the characteristic impedance of the microstrip line, and J being called admittance inverter constant based on the order of filter selected can be calculated with the following equations 29, 30 and 31 defined in the book [4]:

$$Z_0.J_1 = \sqrt{\frac{\pi.\Delta}{2.g_1}} \quad (29)$$

$$Z_0.J_n = \frac{\pi.\Delta}{2.\sqrt{g_{n-1}.g_n}} \quad (30)$$

$$Z_0.J_{N+1} = \sqrt{\frac{\pi.\Delta}{2.g_N.g_{N+1}}} \quad (31)$$

In the above-mentioned equations (29)-(31), the value of elements: low pass prototype values (g_n) and (Δ) being the fractional bandwidth based on the type of filter's response we want can be calculated from the graph for 0.1 dB ripple Chebyshev, and the table is available in the book [3].

With even and odd impedances calculated, we can have the dimensions of microstrip length based on the frequency we want as central one and the coupling gaps between microstrip lines, the calculator in Advanced design System (ADS) was used which gives us the values based on substrate we want, the central frequency, even odd impedances and the phase shift we want, in this case a 90° or *λ/4* transformation.

The values taken from ADS line calculator when shifted into modeling the filter in CST, the value of central frequency shifted in the higher end rather than being exactly at 137 GHz as we want. After tuning the values of transmission lines widths and gaps, with several simulations done, it was shifted to the desired central frequency. Figure 101 is showing CST – only metal without dielectric materials filter model.

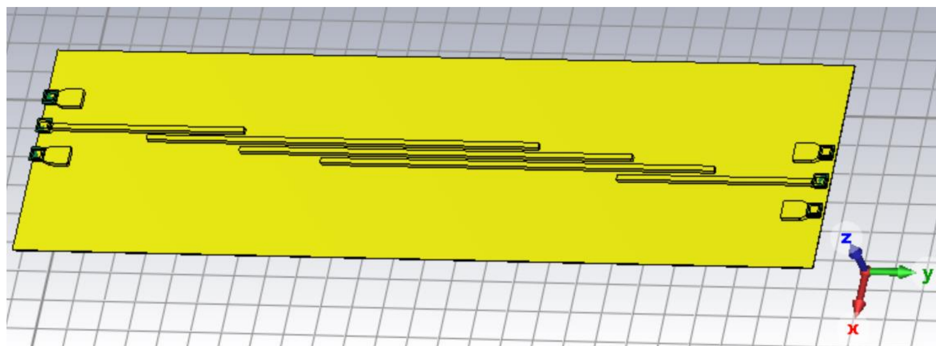

Figure 101. 137 GHz - Central frequency bandpass filter

Re-normalized to 50 ohms, and de-embedded to the center of the probe pads, we can get the response of the bandpass filter. The visualities of behavior of the filters is possible in terms S_{11}, and S_{21} parameters plots are shown in Figures 102 and 103, respectively.

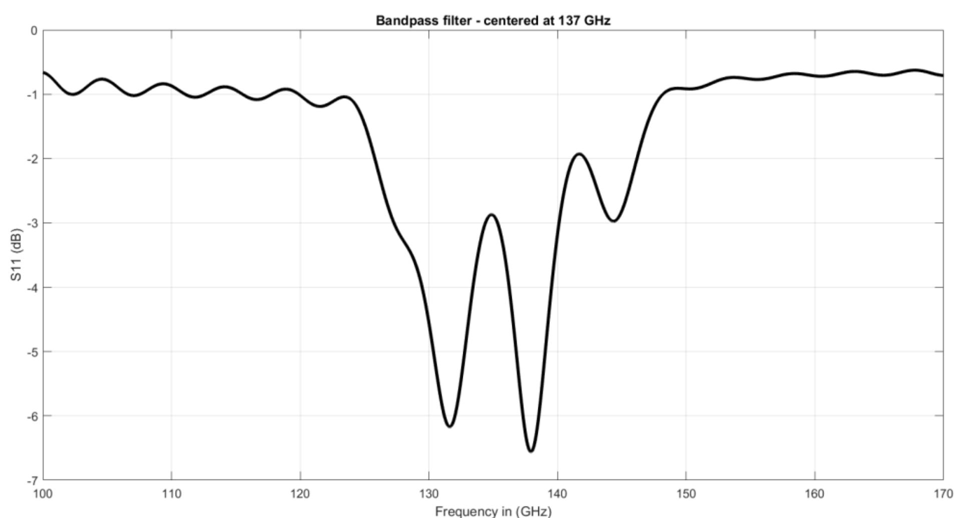

Figure 102. S_{11} (dB) for 137 GHz centered bandpass filter

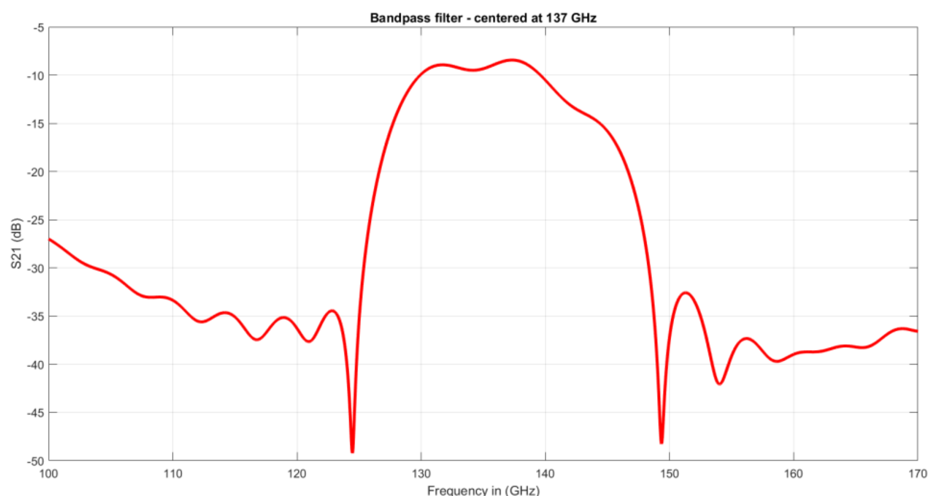

Figure 103. S_{21} (dB) for 137 GHz centered bandpass filter

In order to get the idea of frequency shifting within the constraints of the technology used, there was another filter simulated. Roughly half of the value we get as central frequency, the frequency was downgraded to lower value of 75 GHz. The values for even-odd impedances were calculated from the set of equations used for high frequency filter. The values of the lengths of lines and gaps were calculated form the same ADS calculator, and the trend of frequency shifting from the values obtained by the using the calculator was kept in consideration in modeling the filter's structure and later simulating it. The optimized CST structure along with filter's response (S_{11} and S_{21} plots) centered at 75 GHz is shown in Figures 104,105 and 106, respectively.

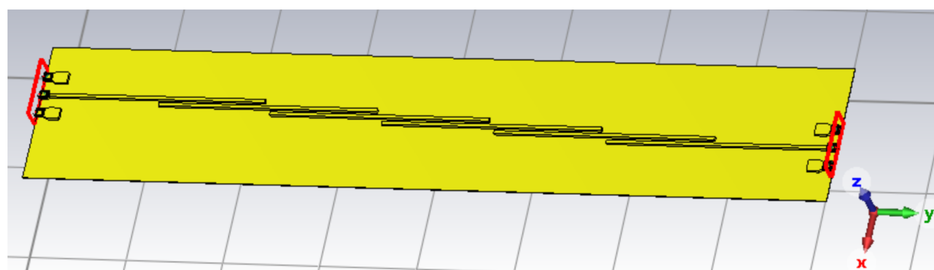

Figure 104. 75 GHz - Central frequency bandpass filter

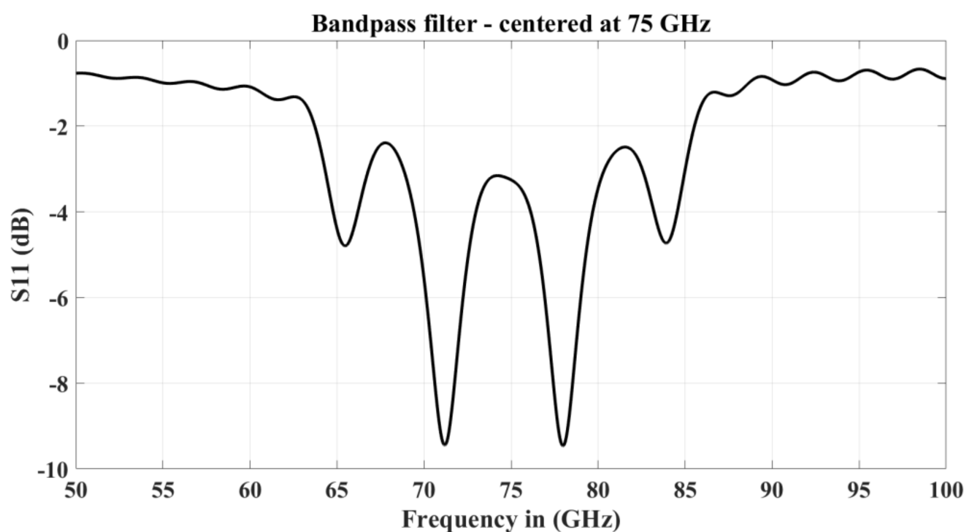

Figure 105. S_{11} (dB) for 137 GHz centered bandpass filter

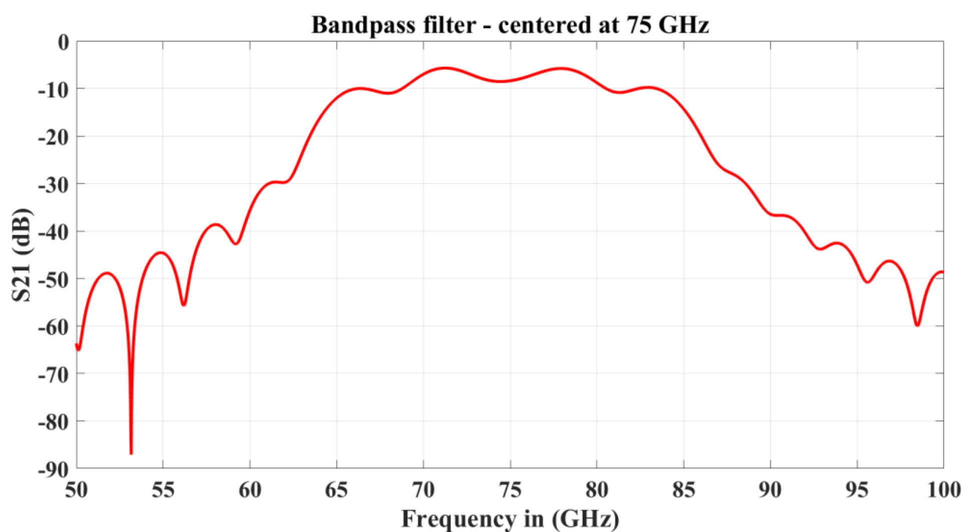

Figure 106. S_{21} (dB) for 75 GHz centered bandpass filter

5.1.1 DRC runs for filters

In a similar fashion to antennas, the structures for both frequencies at 135 and 75 GHz, respectively were checked in KLayout in order to get them error free in terms of all the metal layers including vias and the grounds. After the DRC check, both filters were considered to be errors free, and the filter structures in KLayout are shown in Figures 107 and 108.

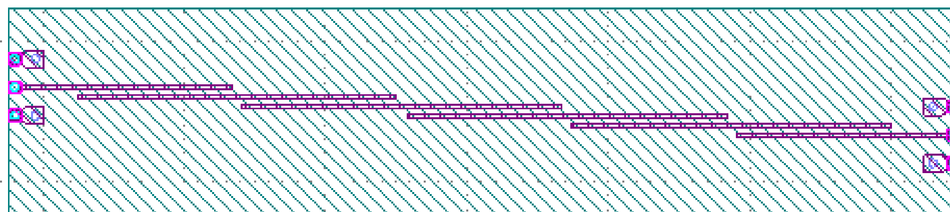

Figure 107. DRC check for 137 GHz centered filter

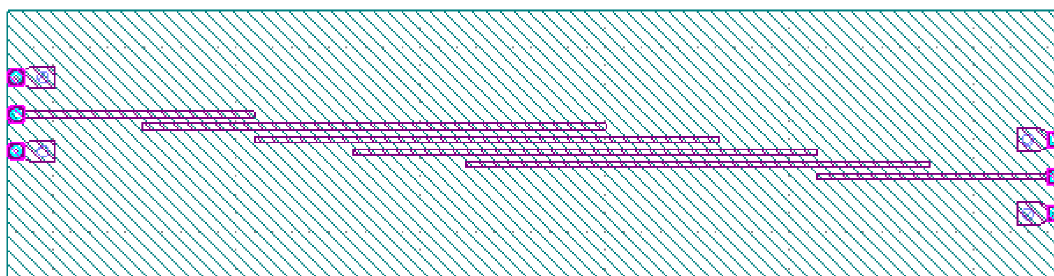

Figure 108. DRC check for 75 GHz centered filter

5.1.2 Observations in filters simulated

Fulfilling the typical 3-dB insertion loss criterion, both filters at D-band and lower band when simulated do not fulfill this criterion but give a high insertion loss (nearly 8.4 dB for both cases). The side suppression (S_{21}) in terms of dB for the filter centered at 137 GHz was good which shows us a fractional bandwidth (-3 dB criterion) of 8.17%. The lower frequency filter centered at 75 GHz gives an insertion loss of 8.4 dB and a fractional bandwidth of 24.32 % but doesn't show as better side suppression as the former case. More optimization would be needed. The matching in terms of S_{11} for both filters shown in Figures 102 and 105 didn't go beyond -6 dB.

To validate the root cause of not achieving the better results for both return and insertion loss, there was another simulation done for lower frequency filter. This simulation was done deliberately to go beyond the IPD technological restrictions and see the effect, CST model of this filter is shown in Figure 109. When simulated this shows a huge difference as compared what has been simulated earlier. There is a clear improvement for both S_{11} and S_{21} shown in Figures 110 and 111, and even the bandwidth increased drastically.

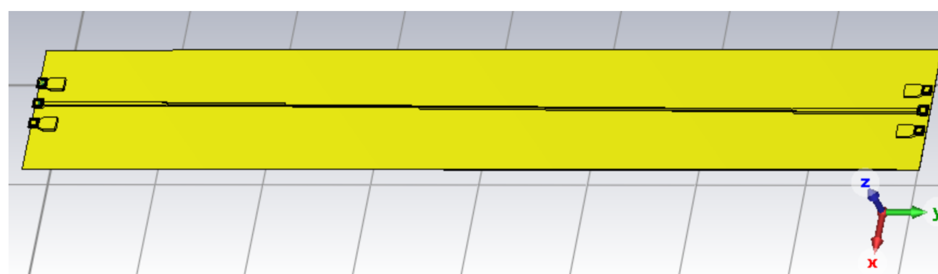

Figure 109. Bandpass filter centered at 75 GHz – different configuration

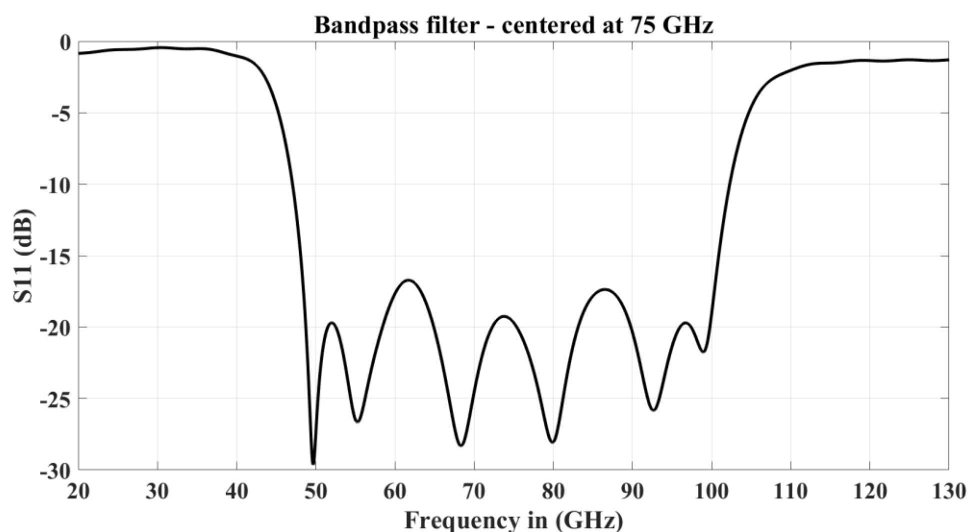

Figure 110. S_{11} (dB) for 75 GHz centered bandpass filter – different configuration

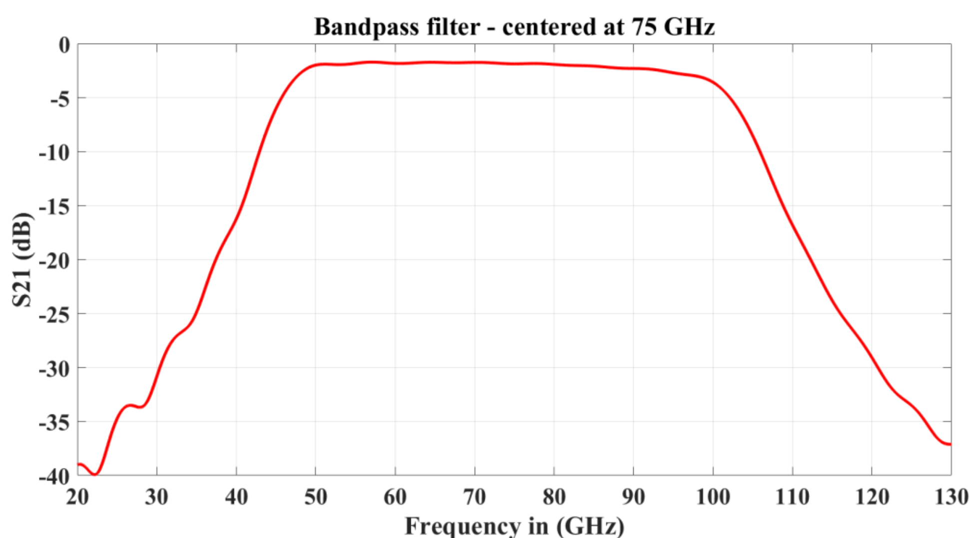

Figure 111. S_{21} (dB) for 75 GHz centered bandpass filter – different configuration

Simulations were done by varying the technology definition for both the metals and dielectrics. When observations were made after trying out different cases varying in terms of dielectrics and metals, the main contributor towards high insertion losses and bad matching of this IPD technology turns out to be the metal layers and not the type of substrate or dielectrics used in the technology definitions. These observations only can be defined for the edge-coupled filter type and the simulated frequency ranges (75 -137 GHz). They cannot be generalized to the overall behavior of this technology as there can be some other ways to implement a bandpass filter out of the various available techniques by using three available metal layers of this technology to get an RF filter.

6 SUMMARY

This thesis topic was related to the IPD technology consisting of 3 metal layers designed by VTT. The IPD technology uses silicon as a substrate and among metal layers polyimide as dielectric layer. With an ongoing trend of shift towards high frequency range, the IPD comes up to a sensible choice in achieving miniaturization and compactness as compared to discrete RF components. The miniaturization in terms of RF front end can also be achieved with some other available options like: LTCC and PCB technologies which are varying in both type of substrate used and the number of metal layers. But the main focus of this research was to check for the potential which IPD technology offers especially providing AiP solutions, and all the work is based on CST simulations.

Frequency range initially proposed for this thesis was from 110 GHz to 170 GHz range, and later it was extended to 330 GHz for transmission lines and antennas. The first RF components to be simulated were transmission lines: microstrip, CPW with and without ground and via transitions from one type of transmission line to another implemented in different layers. The effect of adding via fencing in a CPW with a ground was also observed. Within the IPD technology restrictions, very high impedance above 50 ohms was not possible. In a comparative manner, the transmission lines were judged based on insertion loss or return loss, the latter criterion can be more considerable.

For antenna simulations, patch antennas of rectangular shape with inset feeding were made. The frequency range covered for antennas is from 166 – 312 GHz. Simulations show us the trend of increasing gain and directivities with increasing frequency up to 234 GHz with having the highest gain and directivity within the mentioned frequency range, but it shows a decline when extending the frequency up to 312 GHz. There was another trend of radiation efficiency improvement as we go in the high frequency range with a short electrical length. The comparisons were made by mentioning of the gain achieved with single patch antennas by using different technologies and the type of substrates used. Antenna arrays simulations with series feed, and capacitive coupling technique with 2 and 3 radiating elements respectively gave us an idea of implementing arrays and how much increase in terms of gain and directivity can be expected with the mentioned number of elements.

The last structures simulated were edge-coupled filters with central frequencies at 75 and 137 GHz. Results show us that the insertion loss cannot be improved, and this can be attributed to the metallic technological constraints, rather than varying the frequency. Though the side suppressions and fractional bandwidth were not discouraging with filters.

Simulations from this work can be taken as an overview and starting point for implementing complex RF components by using the IPD technology. There is a possibility for extension of the existed simulated structures or even some more complex structures which are not considered in this work and yet to be explored.

7 REFERENCES

[1] ST Microelectronics, “Integrated passive devices (IPD) for RF applications” (accessed 06.06.2023). URL:https://www.st.com/resource/en/product_presentation/integrated-passive-devices-ipd-for-rf-applications.pdf

[2] Watanabe A. O. et al., “A review of 5G front-end systems package integration,” *IEEE Transactions on Components, Packaging and Manufacturing Technology,* vol: 11, no: 1, January 2021.

[3] Pozar M. D. (2011) Microwave Engineering, fourth edition. John Wiley & Sons. Hoboken, New Jersey.

[4] Steer M. (2019) Fundamentals of Microwave and RF Design, third edition. NC State University. Chapel Hill, NC.

[5] Iulian Rosu I., “Microstrip, Stripline, CPW, and SIW Design”, (accessed 06.06.2023). URL: https://www.qsl.net/va3iul/Microstrip_Stripline_CPW_Design/Microstrip_Stripline_and_CPW_Design.pdf

[6] Nguyen C. (2001) Analysis Methods for RF, Microwave, and Millimeter-WavePlanar Transmission Line Structures. John Wiley & Sons. Hoboken, New Jersey.

[7] C. P. Wen “Coplanar Waveguide: A Surface Strip Transmission Line Suitable for Nonreciprocal Gyromagnetic Device Applications,” in *G-MTT International Microwave Symposium, IEEE*. Dallas, TX, 1969.

[8] Balanis A. C. (2005) Antenna theory: Analysis and Design, third edition. John Wiley & Sons. Hoboken, New Jersey.

[9] S. Mahon “The 5G Effect on RF Filter Technologies,” *IEEE Transactions on Semiconductor Manufacturing,* vol: 30, issue: 4, pp 494 – 499, Nov 2017.

[10] Pramanick P. & Bhartia P. (2016) Modern RF and Microwave Filter Design. Artech House. Norwood, MA

[11] Caspers F. “RF engineering basic concepts: S-parameters” CERN Yellow Report CERN-2011-007, pp. 67-93, June 2010. (accessed 08.06.2023).URL:https://cds.cern.ch/record/1415639/files/p67.pdf

[12] Dr. Choma J. (2002), “Scattering Parameters: Concept, Theory, and Applications” (accessed 06.06.2023). URL:https://www.ieee.li/pdf/essay/scattering_parameters_concept_theory_applications.pdf

[13] Räisänen A. V. & Lehto A. (2003) Radio Engineering for Wireless Communication and Sensor Applications. Artech House. Norwood, MA

[14] O. Zinke & H. Brunswig. (1999) Hochfrequenztechnik 1, sixth edition. Springer. Berlin/ Heidelberg.

[15] Collin E. R. (2001) Foundations for Microwave Engineering, second edition. Wiley-IEEE Press. Hoboken, New Jersey.

[16] PacketMicro, “RF Probing WithRohde & Schwarz ZNB VNA” (accessed 06.06.2023). URL: https://www.packetmicro.com/documents/RF_Probing_with_Rohde_VNA.pdf

[17] A. Rumiantsev & R. Doerner “RF Probe Technology: History and Selected Topics,” *IEEE Microwave Magazine,* vol: 14, issue: 7, pp: 46 – 58, Dec 2013.

[18] Alpern P. et al. “On the Way to Zero Defect of Plastic-Encapsulated Electronic Power Devices—Part III: Chip Coating, Passivation, and Design” *IEEE Transactions on Device and Materials Reliability*, vol: 9, issue: 2, pp: 288 – 295, June 2009.

[19] Panigrahi K. A. et al. "Metal-alloy Cu surface passivation leads to high quality fine-pitch bump-less Cu-Cu bonding for 3D IC and Heterogeneous Integration applications" in *IEEE 68th Electronic Components and Technology Conference (ECTC),* San Diego, CA, USA, 2018.
[20] S. Bulja & D. Mirshekar-Syahkal "Novel Wideband Transition Between Coplanar Waveguide and Microstrip Line," *IEEE Transactions on Microwave Theory and Techniques*, vol: 58, issue: 7, pp: 1851 – 1857, Jul 2010.
[21] R. S. Beeresha, A. M. Khan & H. V. M. Reddy "CPW to Microstrip Transition Using Different CPW Ground Plane Structures," in *IEEE International Conference on Recent Trends in Electronics, Information & Communication Technology (RTEICT),* Bangalore, India, 2016.
[22] Z. Zhou & K. L. Melde (2008) "Development of a Broadband Coplanar Waveguide-to-Microstrip Transition with Vias," *IEEE Transactions on Advanced Packaging,* vol: 31, issue: 4, pp: 861 – 872, Nov 2008.
[23] Rehman M., Ravichandran S., Erdogan S. and Swaminathan M. "W-band and D-band Transmission Lines on Glass Based Substrates for Sub-THz Modules" in *IEEE 70th Electronic Components and Technology Conference (ECTC),* Orlando, FL, USA, 2020.
[24] A. Sain & L. K. L. Melde "Impact of Ground Via Placement in Grounded Coplanar Waveguide (GCPW) Interconnects," *IEEE Transactions on Components, Packaging and Manufacturing Technology,* vol: 6, issue: 1, pp: 136 – 144, Jan 2016.
[25] Marković D. and Ljuština D. "The Role of Post-Layout Verification in Microprocessor Design" in *Proceedings of MIPRO 2004 27th International Convention,* MEET & HGS / Biljanović, Petar, 2004.
[26] Synopsys Home Page, "What is Design Rule Checking (DRC)?", (accessed 06.06.2023) .URL:https://www.synopsys.com/glossary/what-is-design-rule-checking.html
[27]Semiconductor Engineering, "Design Rule Checking (DRC)", (accessed 06.06.2023). URL:https://semiengineering.com/knowledge_centers/eda-design/verification/design-rule-checking-drc/
[28] Espenshade J. and Romero M., (11.12.2008) "CUDA (Compute Unified Device Architecture) Independent Study Final Paper", (accessed 06.06.2023). URL:https://halogenica.net/bin/tools/cuda-design-rule-checking/CUDA_DRC_Paper.pdf
[29] Chen N. Z. and Chia W. Y. M (2006) Broadband Planar Antennas: Design and Applications, 1st edition. Wiley-IEEE Press. Hoboken, New Jersey.
[30] Nayna A. F. T, Baki M. K. A. "Comparative Study of Rectangular and Circular Microstrip Patch Antennas in X Band" in *IEEE International Conference on Electrical Engineering and Information & Communication Technology,* Dhaka, Bangladesh, 2014.
[31] Koul K. S. and Singh K. R. (2022) Reconfigurable Active and Passive Planar Antennas for Wireless Communication Systems. Springer, Singapore.
[32] Toh K. W., Chen N. Z., and Qing X. "A Broadband Planar Antenna" in *IEEE Antennas and Propagation Society International Symposium,* San Diego, CA, USA, 2008.
[33] Joerg S. and Pablo H. (2010). "Planar Antenna Technology for mm-Wave Automotive Radar, Sensing, and Communications", Radar Technology, Guy Kouemou (Ed.)
[34] Zwenger C. and Chaudhry V. "Antenna in package (AiP) technology for 5G growth" *Chip Scale Review,* vol:24, issue:2, April 2020. [Online] Available: https://c44f5d406df450f4a66b1b94a87d576253d9446df0a9ca62e142.ssl.cf2.rackcdn.com/2020/09/Antenna-in-Package-AiP-Technology-For-5G-Growth-CSR-April-2020-Article-EN.pdf

[35] Kok de M., Smolders B. A., and Ulf Johannsen U., "A Review of Design and Integration Technologies for D-Band Antennas" in *IEEE Open Journal of Antennas and Propagation,* vol: 2, pp: 746 – 758, June 2021.
[36] Frecassetti et al "D-Band Radio Solutions For Beyond 5G Reconfigurable Meshed Cellular Networks" in *16th International Symposium on Wireless Communication Systems (ISWCS),* Oulu, Finland, 2019.
[37] Anderson J. A. and Genschow D. "Adaption of a Low Power 122 GHz Radar Transceiver for Long Range Communications" in *German Microwave Conference (GeMiC),* Cottbus, Germany, 2020.
[38] Li S., "D-Band Wafer-Scale IF beamforming Transmit and Receive Phased-Array Systems with On-Chip Antennas", Ph.D. dissertation, EE Dept., UCSD Univ, San Diego, SD, USA, 2021. [Online]. Available:https://78cholarship.org/content/qt5m69361x/qt5m69361x_noSplash_3f6fbcca910d7503cdd1800002ec961c.pdf
[39] Matin A. M., Sayeed I. A. "A Design Rule for Inset-fed Rectangular Microstrip Patch Antenna" in *WSEAS Transactions on Communications,* 2010.
[40] Em: talk, "Microstrip Patch Antenna Calculator", (accessed 06.06.2023). URL:https://www.emtalk.com/mpacalc.php
[41] Altium, "Microstrip Patch Antenna Calculator for RF Designers", (accessed 06.06.2023). URL:https://resources.altium.com/p/microstrip-patch-antenna-calculator-rf-designers
[42] Pranathi P. V. G., Rani D. N., Satyanarayana M. and Rao T. G. "Patch Antenna Parameters Variation with Ground Plane Dimensions" *International Journal of Advanced Research in Electrical, Electronics and Instrumentation Engineering,* vol: 4, issue: 8, August 2015.
[43] He Y., Chen Y., Zhang L., Wong S. and Chen N. Z. "An Overview of Terahertz Antennas", *China Communications*, vol: 17, issue:7, pp**:** 124 – 165, July 2020.
[44] Petrov V., Pyattaev A., Moltchanov D., and Koucheryavy Y. "Terahertz Band Communications: Applications, Research Challenges, and Standardization Activities" in *International Congress on Ultra-Modern Telecommunications and Control Systems and Workshops (ICUMT),* Lisbon, Portugal, 2016.
[45] Nissan U. and Singh G."Beamforming D-band phased array microstrip antennas" in *Sensors International,* vol: 3, July 2022.
[46] Kara M. "Effects of Substrate Thickness on the Properties of Rectangular Microstrip Antenna Elements" in *AMPC Asia-Pacific Microwave Conference,* Adelaide, SA, Australia, 1992.
[47] Ma C., Ma S., Dai L., Zhang Q., Wang H., and Yu H. "Wideband and High-Gain D-Band Antennas for Next-Generation Short-Distance Wireless Communication Chips" *IEEE Transactions on Antennas and Propagation*, vol: 69, issue: 7, pp: 3700 – 3708, July 2021.
[48] Jugurnauth A. R., and Vythee E. "Microstrip Patch Antenna Design and Analysis with Varying Substrates for 5G" in *3rd International Conference on Emerging Trends in Electrical, Electronic and Communications Engineering (ELECOM),* Balaclava, Mauritius, 2020.
[49] Zhou L., Tang M., Gao Z., Mao J., Yue H. "Design and Fabrication of Patch Antenna Array on Quartz Glass Substrate at 146 GHz" in *International Conference on Microwave and Millimeter Wave Technology (ICMMT),* Shanghai, China, 2020.
[50] Lamminen A.,1, Säily J., Ala-laurinaho J., De cos J., and Ermolov V. "Patch Antenna and Antenna Array on Multilayer High-Frequency PCB for D-Band" *IEEE Open Journal of Antennas and Propagation,* vol: 1, pp: 396 – 403, June 2020.

[51] Göttel B., Beer S., Pauli M., Zwick T. “Ultra wideband D-band antenna integrated in a LTCC based QFN package using a flip-chip interconnect” in *European Microwave Conference,* Nuremberg, Germany, 2013.
[52] Emhemmed S. A., Elgaid K. “Broadband micromachined microstrip patch antenna for G-band applications” in *European Microwave Conference (EuMC),* Rome, Italy, 2009.
[53] Vettikalladi H., Sethi T. W., Fauzi Bin Abas A., Ko W., Alkanhal A. M.,1 and Himd M. “Sub-THz Antenna for High-Speed Wireless Communication Systems” in *2nd International Conference on Computer Applications & Information Security (ICCAIS),* Riyadh, Saudi Arabia, 2019.
[54] Dyck A. et al, “A 300 GHz microstrip multilayered antenna on quartz substrate” in *International Workshop on Antenna Technology (iWAT),* Nanjing, China, 2018.
[55] Pfähler T., Vossiek M., Schur J. “Compact and Broadband 300 GHz Three-Element On-Chip Patch Antenna” in *IEEE Radio and Wireless Symposium (RWS),* Las Vegas, NV, USA, 2023.
[56] Wu Y., Fourn E. and Besnier P. “A Planar Quad-band Band-Pass Filter Employing Dual-Mode Band-Stop Resonators” in *International Microwave Filter Workshop,* Perugia, Italy, 2021.